Magnetic Flux Leakage techniques for detecting corrosion of pipes

Nagu Sathappan

School of Engineering, London South Bank University

A thesis submitted in partial fulfilment of the requirements for the degree of Doctor of Philosophy

2022

Abstract

Oil and gas pipelines are subjected to corrosion due to harsh environmental conditions as in refinery and thermal power plants. Interesting problems such as internal and external corrosion, emerging from the increasing demand for pipeline protection have prompted this study. Thus, early detection of faults in pipes is essential to avoid disastrous outcomes.

The research work presented in this thesis comprises investigations into the use of magnetic flux leakage (MFL) testing for pipe in extreme (underwater and high temperature)conditions. The design of a coil sensor (ferrite core with coil) with a magnetic circuit is carried out for high temperature conditions. The sensor thus developed lays the ground for non-destructive evaluation (NDE) of flaws in pipes through the MFL technique. The research focusses on the detection and characterization of MFL distribution caused by the loss of metal in ferromagnetic steel pipes.

Experimental verifications are initially conducted with deeply rusted pipe samples of varying thicknesses in air. AlNiCo magnets are used along with Giant Magneto Resistance (GMR) sensor (AA002-02). The experiment is further repeated for saltwater conditions in relation to varying electrical conductivity with radiofrequency identification (RFID) technique.

A further study carried out in the research is the correlation between magnetic and underwater data communication. The study has resulted in the development and experimental evaluation of a coil sensor with its magnetic response at room and high temperatures. This makes the system effective under high temperature conditions where corrosion metal loss needs to be determined.

Declaration

I declare that the thesis has been composed by myself. The thesis submitted for examination in consideration of the award of a higher degree of Doctor of Philosophy in Electronics and Electrical Engineering is my personal effort and that the work has not been submitted for any other degree or professional qualification. Furthermore, I have taken reasonable care to ensure that the work is original and to the best of my knowledge, does not breach copyright law, and has not been taken from other sources except where such work has been cited and acknowledged within the text.

Acknowledgement

First and foremost, I would like to thank the Almighty for giving me such wonderful ever-loving parents and sister for their good wishes and prayers. I am grateful to them for supporting me in all fields of life and helping me in achieving the set goal.

I would like to express my sincere gratitude to my academic supervisor Prof. M. Osman Tokhi and industrial supervisor Liam Penaluna and Dr John Rudlin for the continuous support for my Ph.D. study. He had been continuously motivating, encouraging me to strive more with his immense knowledge. His guidance helped me in all the time of research and writing of this thesis. Also my gratitude goes to all the members of LSBU, NDT department of TWI and plant Integrity for their help and cooperation where I was instilled in research in pioneering and niche technologies. Second, I would like to thank the committee head and the members: Dr. Ebad Banissi, Dr. Fang Duan, Dr. ZhanFang Zhao and Dr. Gholamhossein Shirkoohi for their helpful comments and suggestions.

I acknowledge with gratitude the full scholarship provided by Lloyd's Register Foundation to make this PhD possible.

I would like to present this simple and humble work as a gift to my country India and all my family members.

Contents

List of Tables

List of Figures

List of Publications

[P1] Nagu Sathappan, Mohammad Osman Tokhi, Liam Penaluna, Zhanfang Zhao, Fang Duan, Gholamhossein Shirkoohi and Aman Kaur (2021), "**Development of an MFL Coil Sensor for Testing Pipes in Extreme Temperature Conditions**". *Sensors, Women in Sensors- special issue*, Vol.21, Issue 9.

[P2] Nagu Sathappan, Mohammad Osman Tokhi, Liam Penaluna, Zhanfang Zhao, Fang Duan, Gholamhossein Shirkoohi and Aman Kaur (2021), "**A Literature Review on Data Transmission Using Electromagnetic Waves Under Different Aquatic Environments**". *Marine Technology Society Journal*, Vol.55, Number 5, pp. 138-149(12).

[P3] Nagu Sathappan, Mohammad Osman Tokhi, Liam Penaluna, Zhanfang Zhao, Fang Duan, Gholamhossein Shirkoohi and Aman Kaur (2021), "**Properties of GMR based sensor for Magnetic field measurement at increasing Temperature Conditions**". *Journal of Non-Destructive Evaluation*, Indian Society for NDT (ISNDT) (NDE-India 2020).

[P4] Nagu Sathappan, Mohammad Osman Tokhi, Liam Penaluna, Zhanfang Zhao, Fang Duan, Gholamhossein Shirkoohi and Aman Kaur (2022), "**Application of Radio Frequency Identification Underwater with Magnetic Flux Leakage Testing Technique"**, Volume **530**, **Lecture Notes in Networks and Systems** series.

Conference Presentations

[P5] Nagu Sathappan, Mohammad Osman Tokhi, Liam Penaluna, Zhanfang Zhao, Fang Duan, Gholamhossein Shirkoohi and Aman Kaur (2019) "**Development of an underwater and high temperature sensor for corrosion monitoring system**", LRF Conference ,9-10 October 2019, Northumberland Avenue, London, UK.

[P6] Nagu Sathappan, Mohammad Osman Tokhi, Liam Penaluna, Zhanfang Zhao, Fang Duan, Gholamhossein Shirkoohi and Aman Kaur (2020) "**3D FEM and analysis of defect in steel plates using magnetic flux leakage testing**", NSIRC Conference, 2-3 July 2020, TWI Ltd, Cambridge.

[P7] Nagu Sathappan, Mohammad Osman Tokhi, Giorgos Asfis, Zhanfang Zhao, Fang Duan, Gholamhossein Shirkoohi and Aman Kaur (2020) **"Development of an underwater and high-temperature sensor for permanently installed corrosion monitoring system"**, British Institute of Non-Destructive Testing -Virtual Conference(Webinar), Sep 2020, London, UK.

[P8] Nagu Sathappan, Mohammad Osman Tokhi, Liam Penaluna, Zhanfang Zhao, Fang Duan, Gholamhossein Shirkoohi and Aman Kaur (2021), "**Properties of GMR based sensor for Magnetic field measurement at increasing Temperature Conditions**". *NDE 2020 - Virtual*

Conference & Exhibition, 10-12 Dec 2020 by Indian Society for NDT (ISNDT) (NDE-India 2020).

[P9] Nagu Sathappan, Mohammad Osman Tokhi, Liam Penaluna, Zhanfang Zhao, Fang Duan, Gholamhossein Shirkoohi and Aman Kaur (2022), "**Underwater GMR sensor data storage using RFID tags**"**,** *IEEE***,** *Prognostics and Health Management Conference (PHM-2022 London),* **DOI:** 10.1109/PHM2022-London 52454.2022.00036

[P10] Nagu Sathappan, Mohammad Osman Tokhi, Liam Penaluna, Zhanfang Zhao, Fang Duan, Gholamhossein Shirkoohi and Aman Kaur (2022), "**Application of RFID transponders underwater in MFL NDT**", CLAWAR 2022:25th International Conference on Climbing and Walking Robots and the Support Technologies for Mobile Machines, University of the Azores, S. Miguel, Açores, Portugal, September 12-14, 2022.

Nomenclature

Symbol	Quantity	Unit
PHMSA	Pipeline and Hazardous Materials Safety Administration	
API	American Petroleum Institute	
B	Magnetic Flux Density	T
H	Magnetic Field Strength	A/m
μ_0	Magnetic Permeability of free space ($4\pi \times 10^{-7}$)	H/m
μ_r	Relative Permeability	No unit
ε_r	Relative permittivity	F/m
f	Frequency	Hz
ω	Angular frequency	rad/s
σ	Conductivity	S/m
MOT	Maximum Operating Temperature	ºC
T_C	Curie temperature	ºC
ΔT	Temperature increase	ºC
FEA	Finite Element Analysis	
FEM	Finite Element Modelling	
NDT	Non-Destructive Testing	
NDE	Non-Destructive Evaluation	

QNDE	Qualitative Non-Destructive Evaluation	
MFL	Magnetic Flux Leakage	
MPI	Magnetic Particle Testing	
PIG	Pipeline Inspection Gauges	
ROV	Remotely operated Vehicle	
RFID	Radio Frequency Identification	
OPT	Optical signal Transmission	
ACFM	Alternating current field measurement	
UT	Ultrasonic Testing	
AE	Acoustic Emission	
GWUT	Guided Wave Ultrasonic Testing	
ECT	Eddy Current Testing	
EMAT	Electro-Magnetic Acoustic Transducer	
MR	Magneto Resistance	
GMR	Giant Magneto Resistance	
Nd-Fe-B	Neodymium-Iron-Boron	

Chapter 1

Introduction

1.1 Motivation

Pipes and pipelines used in the petroleum, natural gas, and petrochemical industries need attention because they work in severe environments such as underwater and high temperatures, requiring greater protection, durability, and maintainability of equipment. Pipeline monitoring is crucial nowadays because petroleum and natural gas, which are vital for energy and chemical raw materials, play a critical role in people's lives, industrial and agricultural development, and national defence [1-2]. Corrosion is a problem, as a result, a corrosion monitoring system is needed for early detection of corrosion and also determines patterns, processing parameters. As a result, the author conceived this study with an aim of detecting the effect of corrosion metal loss on pipe samples under extreme conditions.

Pipelines must be monitored on a regular basis to ensure that transportation for longer distances is reliable and safe within the environment [1]. Traditional non-destructive inspection and advanced sensor techniques for condition monitoring are among the technologies used to avoid pipeline failures. Despite the use of numerous NDE techniques, the MFL methodology remains the most commonly used, and effective NDE technique, according to a literature review [2].

As a result, in order to resolve the challenges of transporting petrol and petroleum products in pipelines under extreme conditions, a fundamental understanding of the entire MFL phenomenon and a comprehensive magnetic circuit is strongly needed.

1.2 Thesis overview

Chapter 2 contains the main literature survey in this thesis. It focusses on the context of the research undertaken, giving an overview of the Non-Destructive Testing (NDT) techniques, its general processes and typical requirements used in corrosion monitoring of pipes and, giving an overview of the magnetic sensors used under extreme conditions. The aim of this is to summarise the fundamental principles of each technique, as well as give a balanced overview of their advantages and limitations in corrosion monitoring of pipes.

Chapter 3 describes the design and development of MFL coil sensor for high temperature conditions. In this section, the underlying theory of the MFL coil sensor will be explored, along with their attributing performance, as well as identifying the factors affecting their performance. Also modelling and simulation of the magnetic circuit using COMSOL Multiphysics is described. The aim of this is to give an overview of the different magnetic sensors as a context from which it can be able to compare the MFL coil sensor and associated NDT techniques that use the various sensors outlined.

Chapter 4 focusses on the finite element modelling of the magnetic circuit using Finite Element Analysis (FEA) COMSOL Multiphysics software. The aim of this is to provide a summary and provide an explanation of the key behaviours which make them suitable for high-quality MFL NDT.

Chapter 5 focusses on the underwater experiments with respect to data communication. The features and specification of apparatus that are common to both underwater and high temperature experiments performed are described, and the results obtained using Radio Frequency Identification (RFID) technique compared in different conditions are presented.

Chapter 6 describes about the performance of the MFL coil sensor under high temperature condition, the procedure followed and the experimental setup involved in detail. Advantages and limitations of the MFL coil sensor are discussed.

Chapter 7 summarizes and draws conclusions from the results obtained using high temperature and underwater experiments. Also the recommendations for future work is discussed.

1.3 Research background

Corrosion that is not detected will result in failure, causing the leakage of dangerous substances from pipelines, which is the failure lowering the efficiency and reliability of equipment [3]. As a result, corrosion damage can jeopardise the general public's safety and well-being, as well as cause operations to shut down. Since 1987, the US Department of transportation Pipeline and Hazardous Materials Safety Administration (PHMSA), a US Department of transportation agency responsible for natural gas, has collected data on more than 3,200 minor or significant incidents [4]. One of the most recent major pipeline incidents occurred in Oakland in 2018 [4], when a natural gas and oil explosion occurred, resulting in 1.4 million dollars' loss due to a break in a weld link at one of the pumps in the plant. The crude oil was leaking from pump stations, which are positioned along pipelines to keep the commodity flowing and track its movement, due to “excessive vibration” [4].

The corrosion of metal products and machinery accounts for around 1/3rd of global annual metal scrap demand [5]. The direct economic loss from earthquakes, floods, typhoons, and other natural disasters accounts for 2% to 4% of each country's Gross Domestic Product(GDP) [6]. Pipeline monitoring is limited by detection equipment and means, resulting in a loss of manpower, materials, and financial resources and all of this emphasises the value of pipeline monitoring [7].

Consequently, there is a vital need to ensure safe operation, and there are several maintenance and condition control approaches that can be used. In general, pipe condition assessment involves assessing the current state of a pipeline, as well as tracking its structural health or fitness for purpose. The first and most important step in detecting and monitoring critical conditions to avoid or minimise catastrophic failures is to collect and analyse relevant data and information [8,96]. It is now essential to comply with the hazardous industries directorate's pipeline requirements for both offshore and onshore pipelines (IGE/TD/1, BS EN 14161, BS EN 1594). Steel pipelines must be tested using NDT methods, according to the American Petroleum Institute (API) [6-8].

Steel materials are produced more than any other industrial metal per year. In the year 2015, the global output of crude steel and iron production totalled 1599×10^6 tonnes and 59×10^6 tonnes, respectively, with 66 countries accounting for nearly all of the world's crude steel production and 14 countries accounting for nearly all of the world's total iron production [9]. Steel is thus known as one of the most significant manufacturing goods in terms of economics. Furthermore, steel grades such as P91, P96, and DP steel 600 are commonly and extensively used as a constructional commodity for large-scale designs and projects such as storage tanks, rail lines, bridges, and pipelines [8,9,96], as well as manufacturing high-strength structures and assemblies. As a result, there is a rising demand for steel part condition assessment and estimation of defects and irregularities to prolong their service life.

NDE is a collection of techniques for examining and evaluating components, structures, and assemblies for flaws or variations in characteristics without affecting their re-use ability [1-3].

The challenge with NDT&E is that these tests must be performed in such a way to be non-destructive to the sample being inspected without causing damage or restriction of its applications and lifespan of the sample [3]. In general, the NDE method of testing uses a probing process to classify material properties, and the technique measures physical properties to show the existence of irregularities in a material (surface, far surface, or obscured) [1]. That is, NDE is a tool for detecting variations in the material's physical properties. A technique may be used to evaluate a material or component in a manufacturing quality control system on a sampling basis, for a specific inspection or for a full assessment of a material or component [1].

Visual inspection, ultrasonic testing (UT), eddy current testing(ECT), MFL testing, and radiography testing are all examples of NDE techniques. The environment, the temperature of the substance transported in the pipeline, and the type of defect are all factors to consider when selecting a NDT technique [1,2].

1.4 Project aim

Many researchers have previously investigated both the theoretical (modelling) and experimental methods of examining ferromagnetic industrial components using the MFL NDE technique. Even though previous models were well-equipped to represent complex industrial activities under room temperature, the aim was to develop a magnetic circuit with a coil sensor that works efficiently under high temperature conditions. However, by first creating an optimised 3D finite element (FE) simulation model to predict the leakage field signal induced by metal loss due to corrosion, followed by an experimental validation of the predicted effects, this work will provide a link between both theoretical and experimental techniques.

The aim of the study is to look at and reflect on the factors that affect the probe and magnet under extreme conditions in order to detect corrosion metal loss using the MFL technique.

1.5 Specific project objectives

(i) To conduct a current state-of-the-art literature review on non-destructive techniques in general, and MFL technique in particular, as well as investigate recent research on pipeline condition monitoring using MFL.

(ii) To examine and critically evaluate the factors that affect the magnet and sensor at high temperatures.

(iii) To create a holder for mounting the sensor on pipes so that a magnetic circuit device can be developed to make it function in harsh environments.

(iv) To study the methods of communication that can be used with the magnetic sensor underwater.

1.6 Contributions to knowledge

The following issues are addressed by this project:

(a) A systematic analysis of the literature on improvements in metal thickness assessment, as well as corrosion metal loss detection and characterization in extreme environments.

(b) 3D FE computation of the MFL magnetic circuit in order to increase the detection sensitivity of the feeble leakage field from metal loss under extreme conditions. This will be achieved by acquiring the field response and distribution pattern of the leakage fields (*Bx*, *By*, *Bz*) developed.

(c) It will also be determining the magnitude of the leakage flux needed to accurately detect, classify, and measure corrosion metal loss.

(d) Using the information gathered to make a quantitative assessment of the defect's orientation, shape, and position inside the specimen.

(e) Comprehensive knowledge of data transmission methods for addressing data communication weaknesses in underwater pipeline condition monitoring.

(f) Application of RFID for data communication underwater in order to collect data from the magnetic circuit.

Chapter 2

Literature Review

This chapter examines the literature on the most widely used and well-established NDT techniques, with a special emphasis on steel pipes and the MFL technique. The principles, standard implementations, merits, and drawbacks of different approaches are also discussed.

2.1 Introduction

Various NDE methods are available for pipeline monitoring and evaluation, and numerous steel structures need extensive and comprehensive inspection during manufacturing and service. MFL testing, liquid penetration testing, and radiographic testing are the most commonly used NDT techniques under extreme conditions [9-10]. Each approach has advantages and disadvantages, so the best NDT technique to use depends on the material's structure and properties, as well as the type of defect being investigated. For pipelines, the test is normally performed from the inside of the pipe due to the length of the pipeline using pipeline inspection gauges (PIG) [9].

MFL testing is one of the most effective and commonly used techniques for crack detection and characterization in pipelines, both circumferentially and axially [10,11]. Pipeline control is very important nowadays because petroleum and natural gas transported by this means plays a critical role in people's lives, industrial and agricultural development, and national security [10]. Long-distance natural gas and oil transportation became conceivable with the introduction of high-strength steel pipes. Steel pipe with welded joints make up the majority of high-pressure pipes today [11].

Pipelines can, however, have different bends and inclination angles depending on the nature and physical features of the ground [12,13]. [12,13]. Many cross country pipelines, on the other hand, are buried underground for security (intentional damage) and safety, where they are susceptible to deformation and corrosion due to strain and humidity [13].

External corrosion was responsible for 65 percent of oil transmission pipeline failures, while internal corrosion was responsible for 35 percent [13,14]. Gas delivery pipelines operate at low pressure, so faults in these pipelines would result in leaks rather than ruptures like those seen in natural gas transmission pipelines that operate at high pressure [14].

Various methods to identify, measure, and compute the degree of degradation in terms of the duration, width, and depth of defects, and also to track the life expectancy of materials over time are provided in qualitative non-destructive evaluation(QNDE) [15]. QNDE can also be used as a quality management tool for material evaluation and to collect information on the interrelationship between corrosion rates and operating variables [14]. For an effective assessment, any element of the measurement system and defect geometries that have a direct or important impact on the inspection performance should be considered [15].

Progress in NDE method accuracy is needed in a number of applications, such as pipeline investigation, where high accuracy in defect detection and characterization will reduce the need for costly pipe replacement [14,15]. It is essential to consider pipe wall losses due to corrosion.

2.2 NDT techniques for high temperature corrosion monitoring

NDT approaches for pipeline corrosion measurement under extreme conditions are complicated by a variety of environmental factors. ECT, magnetic particle inspection (MPI), and MFL testing are all based on electromagnetism or electromagnetic effects [18] induced by the interaction of electricity and magnetism.

Corrosion typically increases with the rate of external factors in extreme environments, such as underwater and high temperatures, since greater surface areas of the metal are in contact with the external environment [16]. Under the normal temperature of NDT methods currently applied widely, but the high temperature of NDT methods and its applications are relatively less.

Acoustic Emission (AE) is the identification and conversion of high frequency elastic waves produced by mechanical vibrations to electrical signals. Pipelines are often subjected to harsh environments such as high pressure, temperature, and mechanical stress [30,35]. As a result, over time, the structures begin to develop cracks and corrosion products. Using AE from these defects by directly coupling piezoelectric transducers on the structure's surface, the transducers can detect the waves based on the obtained wave patterns. Thus the location of the defect can be calculated [19,34]. Since the AE technique has been used to identify corrosion pitting in steel plates, it is now being used to detect cracks in general.

MPI is the most widely used NDT&E method for ferromagnetic materials worldwide. It is based on MFL principles, which can produce a high magnetic field strength (0.72 T rms), often low frequency (DC or 50 Hz) magnetic field into the sample [130]. MPI techniques are widely utilised in industry because they are rapid to run, adaptable to sample geometry (particularly when employing an MPI bench for small samples and an electromagnet yoke for big samples), and produce an image of the identified defect [130]. Under high temperature conditions, magnetic particles can’t survive due to its characteristics.

A pulsed electromagnet for both generating and detecting ultrasound that is effective up to 250°C on ferromagnetic low carbon steel [19,20,33], and an EMAT system that can generate shear waveforms successfully at temperatures up to the curie point of ferromagnetic low carbon steel [18-21] are two systems that have previously been proposed for use at high temperatures [19,33]. Although this is a relatively costly type of NDT, laser interferometry has been successfully used for ultrasonic thickness measurements on various steel grades at temperatures up to 1200°C [18-22,33].

The techniques used for high temperature conditions are described in the sections below:

2.2.1 Acoustic Emission

AE transducers have been successfully used at high temperatures, in particular piezoelectric transducers, such as Yttrium Calcium Oxyborate and Aluminium Nitride, which have been used in AE up to 700°C and 1200°C, respectively [33,37,38]. These acoustic waves are passively produced by the structure during defect detection, particularly corrosion, and the rate of growth of the defect is directly proportional to the amplitude of the emitted acoustic waves, allowing for a more precise assessment of the situation and its urgency [19].

The problem with this technique is that the creation of the acoustic waves only occurs with change of stress and cannot be confirmed by repeated measurements, as a defect can grow in a matter of hours or days or years, emitting acoustic waves, but once its growth is inhibited, no acoustic waves are emitted from the static state [37]. Unfortunately, AE Systems can only be used for qualitative research, and environmental noise can interfere with the AE signals that are to be received [34]. As a result, in real-world applications, signal discrimination and noise reduction techniques are critical [33,34].

2.2.2 Electromagnetic Acoustic Transducers

Electromagnetic Acoustic Transducers (EMAT) and laser ultrasound are two of the common non-contact techniques used for NDE at elevated temperatures [33]. High-temperature EMAT’s have only been developed so far for measuring the thickness of metal blocks [33-35]. It is still important to design and test an EMAT that can be used in guided wave testing(GUWT) and can withstand high temperatures for both inspection and monitoring.

In an oil and gas industry, EMAT’s may be used for high-temperature GUWT inspection of long pipelines or tanks that hold flammable liquids, and structural integrity evaluation is critical [33]. In that case, MFL technique can be used for evaluating structural integrity of pipes as it is suitable for condition monitoring.

2.2.3 Magnetic Flux Leakage Testing

The MFL method remains the powerful NDE technique used for pipelines, due to its effective detection and characterization of flaws in very long structures such as steel pipes [23]. Large magnets are used to build a saturated magnetic field around the wall of a ferrous pipe in the MFL process [24,25]. A homogeneous and uniform distribution of magnetic flux is obtained in the pipe if it is in good condition, while a defect such as a crack or corrosion metal loss, will cause a change in the magnetic flux distribution. Since damaged areas cannot support as much magnetic flux in undamaged areas, the flux field at the damaged areas increases [24].

Damaged areas cause a change in magnetic flux inside the closed magnetic circuit, which results in a change in flux leakage into the atmosphere [11]. A magnetic sensor detects such flux leakage. MFL has been successfully used in a number of applications, including tubing and piping inspection in gas and oil pipelines, tank floor and rail line inspection [24]. In addition, the latest improvements in MFL technology have aided in the prevention of significant losses such as pipeline breaks.

The MFL technique is quick and simple to use [25,26]. Curie temperature of permanent magnets is an important factor to consider in high-temperature settings, as the permanent magnet loses its magnetism when the surrounding temperature reaches the curie limit, and corrosion resistance of permanent magnets is also important to consider for long-term use underwater [26-28]. The magnetic circuit, which includes both the permanent magnet, and the magnetic sensor must be shielded from both extreme conditions because they have a greater effect on the MFL mechanism. Apart from MFL, other techniques for condition monitoring includes:

2.2.4 Eddy Current Testing

ECT is an electromagnetic non-contact technique that is frequently utilised. It was originally created for the NDT of mixed metals. They are susceptible to changes in the specimen's electrical conductivity and magnetic permeability measurement with lift-off variations [33-35]. ECT techniques have advanced significantly in the last 70 years to handle a variety of industrial NDT&E difficulties, including surface-breaking crack detection, fault length and depth measurement, and insulative coating thickness measurement [33].

For inspection of corroded areas, ECT-based techniques have been used, which involve only a small probe and no physical contact with the specimen [5,30]. Eddy current methods have been used to detect the presence of corrosion on the surface or near the surface of metal samples and have proven to be very accurate [32]. There are commercial high-temperature EC probes operating up to 280ºC and 380ºC (continuously) [67, 68]. as [30]. Urayama et al. have also developed and tested a dual EMAT/EC probe for high-temperature monitoring (300ºC) of pipe wall loss thickness [69]. It is subjected to skin effect so it can only be utilized on electrically conductive materials for surface and subsurface defects, since [70].

2.2.5 Pulsed eddy current testing

Pulsed eddy current is an external inspection technique for determining the wall thickness of insulated and non-insulated steel pipelines [30,31]. A transmitter coil produces a wave shape of rectangular eddy current, with each loop consisting of one positive and a negative pulse [32,33]. The response of the system is determined by quantifying the magnetic field reaction picked up by the receiver coil at a distance from the pipe wall (e.g., due to lift off or insulation thickness) [32-34]. The magnetic field strength measured is inversely proportional to the pipe wall thickness.

By comparing the transient time of such signal features with similar calibrated signals, the average thickness of the metal can be determined [5]. The magnetic field's interaction with the inspected portion creates an image that reflects the inspected region for wall thickness measurement. The diameter of the coils which varies between 25 and 150mm depending on wall and insulation thickness, and sensor size, is a factor to consider during measurements [19,33]. The inspection tool is small and portable, making it easy to deploy from a remote vehicle.

Alternating Current Field Measurement (ACFM) and is a relatively new NDT&E technology. It is exclusively commercially available through one company, TSC Inspection Systems, unlike other approaches (Eddyfi) [32,33]. It is an electromagnetic therapy that has concepts that are similar to both MFL and ECT but is very different. The illuminating coil (or coils) in ACFM probes are normally oriented tangentially to the sample surface, generating a low intensity (1 mT rms) high frequency (commonly 5 kHz and 50 kHz) applied magnetic field that is parallel to the sample surface [33].

Electromagnetic wave signals are transmitted through the ground by ground penetrating radar (GPR) antennae, which spread through the ground and bounce off of sub-surface boundaries [7]. A receiving antenna detects the reflections, which are then interpreted [32-35]. GPR can detect voids or defects in the pipe as the radar propagation velocity increases due to soil contamination with leaking water, suggesting the possibility of defects in underground water pipes [35,36]. This high-resolution ground penetrating imaging radar can be capable of detecting pipelines of various materials. It penetrates the ground to a depth of up to 200 cm, achieving an image resolution of less than 50 mm, and surveying at a speed of 0.36 km/h [35-37]. As a dis-advantage, GPR could be interrupted by external factors through unwanted signals.

2.3 Ultrasound methods

NDT using UT methods uses short-wavelength, high-frequency mechanical waves (vibrations) emitted from a small probe and detected by the same or other probes. Such mechanical waves, in the form of compression and shear waves, can travel a certain distance through metal and detect internal and hidden defects [44]. While UT can detect corrosion, if the metal surface changes it can be difficult to tell the difference between reflections from surface/near-surface corrosion and reflections from multiple material surfaces [33-37]. Another drawback is that they require acoustic coupling media such as water or gel to acoustically couple pulses from the transducer to the material, which makes standard UT unsuitable for some circumstances due to the surface preparation requirements [43-45].

2.3.1 Guided wave ultrasound pipeline inspection

The GUWT technique is based on the ability to spread a torsion or longitudinal wave which can propagate along the length of the pipe section [40,42,46]. The number of transducers will vary between two and four, depending on the form of guided wave.

In case of torsional wave system, when four transducers of the same kind are used, a wide range of frequencies can be applied, resulting in a better inspection performance [46,47]. Laminar waves mirror back to the transducer's original position when these guided waves encounter an anomaly or pipe feature [19,33]. Each signature's time-of-flight is calculated to determine its distance from the transducer, and the amplitude of the signature determines the defect's size significance [33]. The horizontal axis represents pipe length, while the vertical axis represents signal magnitude, which can be used to describe corrosion-related metal loss and shows up the welds [33].

The inspection for a pipe can be performed for a range of up to 30 m in either direction from a specific spot where the probe is positioned since this method is ideal for pipes over 50 mm in diameter and wall thicknesses up to 40 mm [44]. GWUT has been used to inspect buried pipes, but due to the rapid attenuation of the signals, the range of inspection would be limited [44,45]. This is a long-range inspection technique that uses reflections created by changes in cross-sectional areas (e.g., thickness, welds, pipe features, etc.) to detect problems like cracks or corrosion [46]. This technique has the advantage of allowing a remote location to scan long lengths of pipe for estimated size and location of flaws or corrosion [46].

Magnetic sensors play an important role in the magnetic circuit along with the methods used for condition monitoring at high temperature conditions.

2.4 Magnetic sensors for high temperature corrosion monitoring

For decades, magnetic sensors have aided mankind in analysing and monitoring thousands of functions [21,56]. Computers, for example, have a memory storage thanks to magnetic sensors where they have a role in magnetic storage discs, tape drives, and aircraft for higher safety requirements and also to the high efficiency of non-contact switching with magnetic sensors [13]. Magnetic sensors have a more durable, reliable, and maintenance-free technology than other sensor technologies, allowing factories to improve efficiency due to their precise stability and low cost [13].

Fluxgate sensors, Giant Magneto Resistive (GMR) sensors, Anisotropic Magneto Resistive (AMR) sensors, and Hall Effect sensors are some of the sensor types that can be used to test magnetic fields in extreme conditions (underwater and at high temperatures). However, one of these sensors' main disadvantages is their inability to detect large areas of a specimen. The inherent capability with temperature, and the signal voltage are two critical factors to consider when using magnetic sensors at high-temperature environments [11,13].

2.4.1 Hall sensor

The Hall effect sensor tests the normal portion of the magnetic field and offers accurate information about the magnetic poles as well as the magnitude of the magnetic field [13]. A hall effect sensor's output signal is a function of the magnetic field density around the instrument [6]. The sensor senses when the magnetic flux density around it reaches a certain threshold and produces the hall voltage [6]. The output voltage increases as the magnetic field gets near and hence stronger, and vice versa. Offset voltage and sensitivity makes it less suitable under high temperature conditions.

2.4.2 Fluxgate sensors

The main (excitation coil) and the secondary (pickup coil), along with the ferromagnetic core form part of the magnetic sensor [13]. When the ferromagnetic core is not saturated, it provides a low-resistance direction for the flux lines of an externally applied magnetic field [6]. The magnetic resistance of the core increases as the core becomes saturated, and the excess magnetic flux lines are ejected from the core. The flux gate sensor has a drawback in that it has a lower sensitivity.

2.4.3 Magneto resistance sensors

Magnetic field measurement at high temperatures and compatibility of MR sensors with high temperature fabrication processes poses a challenge in the context of MR sensors [13]. Thermal stability of a multilayer thin film sensor is limited on one hand by diffusion and on the other hand with loss of pinning [13-15], e.g., in the case of exchange bias. Diffusion creates mixed interfaces between the functional layers of the sensor, which is detrimental to the MR effect [13].

2.4.3.1 Giant magneto resistance sensor

GMR Sensors are made up of multilayer structures that are a few nanometers thick and have ferromagnetic layers separated by non-magnetic layers, such as Fe/Cr/Fe and Co/Cu/Co [25]. Based on the GMR effect, there is a significant change in electrical resistance in response to an applied magnetic field [25]. When positioned parallel to the chip plane of the sensor, GMR sensors are more sensitive. GMR sensors have a high sensitivity at low magnetic fields and a high spatial resolution, and they can be used to scan surfaces in precise [26].

However, they suffer from hysteresis and a low saturation field [23,26]. Many investigations dealt with the realization of robust GMR sensors with reliable thermal stability in the range of over 200°C, comprising of spin valve systems with IrMn, PtMn or NiMn due to their high blocking temperatures [134-138].

Tunneling Magneto Resistance (TMR) sensors have advantages such as high resistance and low power consumption, which ranges from a few Ohm to MOhm, as well as large signal amplitude. However, there are risks associated with TMR technology, which includes critical resistance specifications for which a deposition tool with high uniformity and repeatability is needed, otherwise the final resistance specification would be compromised.

On the other hand, there are few magnetic sensors being considered for corrosion monitoring underwater which are as described below

2.5 Magnetic sensors for corrosion monitoring under water

There are a few sensors that are used to track corrosion underwater, and they are described below.

The electrical resistance (ER) technique is used by the corrosion rate sensor, and it is one of the most widely used methods for measuring metal loss due to corrosion [18,59]. Only one section of the pipe will be exposed, which is the ferric portion, which loses metal due to corrosion and experiences a change in electrical resistivity as a result [17]. This shift is compared to a sealed reference part using the ER process [17]. The probe is mounted in close proximity to the exposed pipe section, exposing it to the same temperature as the reference component (metal resistivity is influenced by temperature) [59,60]. The use of an entire pipe as the exposed feature is impractical, which is a drawback.

The monitoring sensors are mounted inside or on the pipe to monitor acoustic activity, and the sensor location and monitoring period are two significant variables for acoustic monitoring [32,60]. The acoustic sensor should be located close enough together to ensure that two sensors detect the acoustic event and have enough acoustic data to identify the source [32]. For rapid screening of long stretches of pipelines for corrosion and other defects, directed wave UT has been commonly used [32]. Data communication underwater is a challenging task as factors such as frequency, attenuation needs to be considered.

2.6 Data communication techniques for underwater conditions

For underwater pipelines, if oxygen is not adequately removed, corrosion would be greatly accelerated [16]. In that case, duplex stainless steels corrode at a lower rate than other stainless steels in conditions with high CO_2 levels, as well as combustion gases (oxygen, organic acids, carbon dioxide, sulphides and chlorides), steam, and temperature [16]. During the pipelining of crude oil, the thermal characteristics turn to be the first concern.

Some environmental conditions, such as freezing cold temperatures, may cause hydrate formation in gas pipelines, as well as the deposition of certain chemicals in oil pipelines, such as paraffins, wax, and asphaltenes [16]. Currently, inspection results are interpreted manually, although computer vision techniques are likely to be introduced in the future to aid in the coding of defects and the assessment of the pipe's overall condition [17].

Safety and efficiency in operating at offshore production sites are critical in the oil and gas industry, especially for pipelines. The adoption of an efficient and cost-effective inspection technique, which includes the pipeline inspection of offshore facilities is a crucial factor in achieving the above [17]. Since pipelines stretch over long distances, such as miles or thousands of kilometres, in both shallow and deep waters, inspecting and controlling them for maintenance and repair is a complex activity requiring the use of numerous resources [17,62].

In the Gulf of Mexico, for example, there are approximately 45310 miles of underwater pipelines that carry oil and gas, and the majority of pipeline failures are caused by corrosion [35]. Pipeline damage or leakage cause a large portion of oil spills, which can result in multiple environmental hazards such as oil contamination and production loss. According to a recent study, the number of accidental spills in the transportation of oil into the marine environment is about 600 tonnes per year out of a total of 20000 tonnes [16]. More technologies are being used nowadays to track and manage pipelines under water, both internally and externally, and examples of these technologies include sensors, mobile robots, algorithms, autonomous underwater vehicle (AUV) [35]. The deployable technologies were created with the aim of detecting and identifying pipeline leaks, corrosion, and underwater data processing in mind.

For pipeline monitoring, there are a variety of inspection methods available, including the ones mentioned below:

2.6.1 Intelligent pigs and robotic systems

PIGs are used to measure the geometry and diameter of pipelines, as well as to detect metal loss and corrosion. Apart from that, the data these instruments may provide covers a much broader range of inspections, including curvature monitoring, pipeline profile, temperature/pressure recording, metal loss/corrosion detection, photographic inspection, crack detection, wax deposition measurement, leak detection, product sampling, mapping in terms of images out of a single inspection run [33,49,50].

PIG’s have become more intelligent as a result of technological advancements with one or more sensors inside of large pipelines. Using MFL technique, they can detect internal leaks, corrosion, or flaws. [49,50]. PIG’s were designed to solve deposit removal problems because contaminants can block the flow through a pipeline. Routine line cleaning and inspection with intelligent PIG’s can be used to take care of the pipe internally in most installations.

External corrosion is more serious in general because it can shorten the pipeline's life and compromise its protection [51]. As a result, it is critical to build an innovative corrosion sensing device for external monitoring, with the ability to traverse the entire pipe in a reasonable amount of time without being stuck [19,52]. It is necessary for the system to have the ability to inspect the pipe with appropriate accuracy and resolution, as well as the ability to report on the inspection data or save it locally for later retrieval [6,51].

The majority of underwater robotic systems are tethered for control and communications [19,52]. While not all platforms are designed for pipeline monitoring, it is still a useful resource for the creation of robotic platforms for underwater pipeline defect detection [53. In addition, ultrasonic intelligent pigs are used to calculate the wall thickness of the entire pipe surface directly [53]. They are best suited to liquid pipelines and cannot be used without a liquid couplant in gas pipelines, which is a drawback. External inspection with sonar or Remotely Operated Vehicles(ROV) has historically been used to locate pipeline lengths.

ROV can hold a variety of inspection tools and record a vast number of data collected from on-board sensors [19]. In comparison to what a diver would do, this allows for a more thorough examination [17,54]. For example, ECA ROVING BAT-INS offshore ROV are capable of performing quantitative measurements for cathodic protection surveys and thickness measurement using UT are equipped to work on underwater pipeline environments [54,55]. As a result, combining multiple inspection technologies on a single inspection method may be an effective approach. This approach is used for obtaining a more comprehensive picture of the asset's condition and integrity.

Underwater wireless communication is a novel approach to Under Water Communication (UWC) that has been chosen for data investigation and observation [61-64]. Sensor network architectures are currently one of the methods used to transfer data underwater.

Electromagnetic (in RF ranges), optical, and acoustic wireless carriers are used to envision UWC techniques in underwater wireless signal transmission. With EM waves (in the form of radio frequencies) being the first and foremost technology to be specified, adapt a function of high data rate over short distances [60,61]. Second, the underwater optical signal transmission (OPT) technique, which requires a line attenuating location during signal propagation over moderate distances in order to achieve high bandwidth and data rate. The third and most commonly used technology, acoustic waves, which are used for the longest range of contact distances [61,63].

2.7 Wired and wireless communication techniques

Apart from the approaches described above, there are other sensor network architecture designs that can be used to transmit data underwater. They're a mix of wired and acoustic wireless sensor networks, as well as wired and radio frequency wireless sensor networks. [62] Compare and contrast the reliability problems, features, benefits, and drawbacks, as well as methods that can be adapted for these network architectures. The network reliability assessment took into account some factors such as network access, network power supply continuity, and physical network security [62].

In general, wired sensor networks are favoured over wireless sensor networks. Multiple wires can be connected to sensor nodes in a wired sensor network, and power is not a concern because it flows through the wires. Also if one wire is also cut, the remaining wires can manage data transmission and save the data. However, its limitations include protecting the wires from water, including the power supply, which plays a major role when considering sea water as RF waves lose energy slowly.

In this case, the Internet of underwater Things (IoT) makes use of light's influence as well. Subsea radio frequency, which transmits large amounts of data in short distances underwater wirelessly, is changing the face of underwater communication. In the offshore oil and gas industry, subsea radio frequency is replacing traditional acoustic systems and the need for cables with its efficient transmitting capability. All WFS sea tooth-enabled devices, including a variety of subsea modems that transfer data and video through water, can be wirelessly communicated with by ROVs [142]. This is especially important for individuals working in a sector that is mostly developing and that struggles with a lack of connectivity and sensors in harsh environments.

Wireless sensor networks have the potential to fix some of the existing wired sensor network's reliability problems in pipeline monitoring [62,64]. Table 2.1 shows the different types of sensor network architectures.

Table 2.1 Comparison of sensor networks

Sensor network architecture	Design	Properties	Advantages and disadvantages	
Acoustic communication	1.Can travel up to a long distance of 20 km [64].	1.Acoustic bandwidth is up to 20 kbps, and attenuation is dependent on distance and frequency (0.1-4 dB/m) [64-66]. 2.The permeability of seawater is almost the same for fresh water. As a result, there is no distinction in the magnetic field.	1.Acoustic signals have a very long and variable propagation delay underwater [66]. 2.Consumed battery power.	1.The bandwidth between nodes is very small, and it is determined by the distance and frequency of acoustic channels [66].
Integrated wired/acoustic wireless sensor network	1.Each node is connected to a device that includes a transceiver, memory, and storage unit, as well as a wired network interface that has the same configuration as the above [67], and the nodes are connected through wireless acoustic and wired links.	2.Each node regularly tracks the network's status on both sides by sending echo messages to its neighbours [67,68].	1.One to the major drawbacks of this architecture is that if a single wire is broken, the network's average bandwidth (data rate) drops to the bandwidth of the replacement acoustic communicatio n path [68].	
Integrated wired/RF wireless sensor networks	1. The buoy is connected to the nodes and floats on the surface while the transceiver within the floating buoy is enabled to provide contact and synchronisation between them, effectively replacing the broken connection underwater [62,68].	1. When a wire connecting two nodes is cut or faulty, a buoy fitted with a radio transceiver is released in this architecture [62].	1.Since the buoy will not appear unless there is an issue with the wired link, this architecture will provide better physical security protection for the network than the RF wireless sensor network [62,68].	

2.7.1 RF communication technique underwater

Despite the fact that underwater radio links were tested in the early days of radio, they were unable to meet the requirements of the time [67]. When compared to acoustic and optical wave technologies, Radio Frequency (RF) EM technology offers great potential for underwater sensor communications [67]. [67] examine the emergence and future of engineering implementations for efficient data transmission. The exchange of information is in the form of signals through wireless communication using physical waves as the carrier, among nodes in an underwater sensor network [65-68,100]. The advantages and disadvantages of using different communication technologies (acoustic, radio, and optical), as well as possible consequences, are contrasted [65]. Dealing with densely and widely dispersed poznodes, as well as improving communication efficiency in complex underwater environments, would be a possible gap [65,100].

2.8 Radio frequency identification

In the last 15 years or so, the idea of a "smart pipe" has been circulating. It's a loosely described term in which a pipe sample is outfitted with a variety of sensors to provide a comprehensive monitoring system for the pipe's condition and output [35,37]. In Europe, a smart pipe project for deep-sea pipelines began in 2006 and was scheduled to be completed in 2012 [37]. The aim is to create a comprehensive pipeline monitoring system that integrates sensor technology, data collection, data analysis, and decision support for online, real-time asset management. Sensors will be mounted along the entire length of each pipeline for the remainder of its life, with expected benefits including improved decision-making, residual life estimation, and reduced need for onsite inspection [37-40].

One of the essential components of a ship are the pipes, which are found in great quantity and in many different types. A potential cyber-physical system would involve monitoring these pipes. The efficiency and safety of the shipyard can be increased by their improved identification, traceability, and indoor placement from manufacturing through their life. The fundamental hardware and software technological requirements are established from this analysis [141]. The concept of a "smart pipe," which is defined as a piece with periodic signal transmission capabilities that facilitates the provision of improved services at a shipyard, is then introduced.

Different technologies are chosen and assessed in order to establish a smart pipe system, and it is determined that passive and active Radio Frequency Identification (RFID) are now the best technology to do so. Additionally, some encouraging indoor positioning findings from a pipe workshop are shown, demonstrating how kalman filtering and multi-antenna algorithms can assist and stabilise received signal strength (RSS) and boost the system's overall accuracy.

RFID is a recent advancement in radio frequency that enables almost any entity to be wirelessly identified with data transmitted through radio waves [69]. It is a technology that uses radio waves to transmit power and data between a reader and a tag [70]. RFID technology is now widely used in a range of industries for a variety of applications ranging from item tracking to personal identification. Few studies have explored and explained the possibilities and risks of using RFID systems in marine or other aquatic environments for underwater monitoring operations [69], as well as with the technical limitations [62,69].

While the electrical conductivity of water, a significant parameter to consider, is a factor that cannot be adjusted or improved and the only factor that can be modified to enhance underwater efficiency is the RF spectrum [65,69,70]. This aspect has already been adapted by using the EM field for typical radio transmissions of different frequencies. Very Low-Frequency radio waves (VLF – 3-30kHz) have shown to be able to penetrate under seawater to a depth of up to 20 metres, while Extremely Low-Frequency radio waves (ELF – 3-300Hz) range varies, allowing them to travel hundreds of metres in seawater [70,71].

In general, these frequency ranges have significant technological limitations. First, their exceedingly long wavelengths necessitate antennas of immense dimensions with frequencies lower than 100Hz and wavelengths of thousands of kilometres, requiring antennas to reach wider and broader areas. Second, due to their limited bandwidth, these frequencies can only transmit text signals at slower data speeds [71].

Components of RFID system are

- Transponder (attached with an object, unique identification).
- Antenna (tag detector, creates magnetic field).
- Reader (receiver of tag information, manipulator).
- Communication infrastructure (enable reader/RFID to work through IT infrastructure).
- Application software (user database/application/ interface).
- Reader-transponder read distances in different fluids.

2.8.1 Applications of RFID technology underwater

When it comes to applications, RFID technology has been used to monitor pebbles underwater, with displacement being a key factor in order to measure the movement [72]. Three types of transponders were used to read the range of the pebbles in the system [72]. To determine the reading range, tests were performed under various conditions, and passive transponders were inserted into pebbles, with a core 125 kHz reader selected to transmit EM waves to the transponder [72]. When a pebble is detected, an acoustic signal is produced, which causes the identification code of the pebble to be shown on the screen of a laptop connected to the reader [72].

The location of the pebbles was measured using a complete station, and the best results were obtained using a 125 kHz system rather than a 13.56 MHz system due to the latter's higher attenuation [72]. The disadvantage of this method is that the underwater transponder range is usually restricted with regards to frequency.

2.8.2 Limitations of RFID technology

The reduction in range is up to a certain limit, based on its frequency that brings the transponder in contact and within the range of the reader antenna. Application of rewritable RFID tags is a potential development in RFID. Data can be stored on rewritable RFID tags depending on the range and limit of the RFID reader. The other benefits of RFID are its cost-effectiveness and off-the-shelf (commercially available) hardware. The disadvantage of RFID-based sensing is that when checked with near metal in the marine environment, the reading distance between the tag and reader is of short range [71,72].

2.9 Related standards of defect detection methods

It's crucial to define appropriate standards or requirements in addition to developing techniques for detecting defects in oil and gas pipelines. According to a literature review, there are 16 standards in all, which are divided into three categories: operating procedure (it is used to direct the application and planning specifications of testing technology in the field), technical issues related (introduce the concept of related technology), and management related (requirements for detection management) [22,73]. The statistics are based on the year, the country (or organisation) that created the standard, and the key functions for these 16 standards related to oil and gas pipeline leakage detection. Table 2.2 shows standards related to oil and gas pipeline defect detection

Table 2.2 Related standards of oil and gas pipeline detection [73]

Standard Code	Name	Issuance department	Latest version	Main function
SY/T 4109	NDT standard of oil and gas steel pipeline	National Development and Reform Commission (China)	2013	Specifies about four non-destructive methods for long distance oil and gas pipelines and their quality grading.
API SMART	Smart Leak Detection and Repair (LDAR) for Control of fugitive emissions	API	2004	Focuses on locating and repairing the most leaking components in a more cheaper and quicker way than existing LDAR practices.
API RP 1130	Computational pipeline monitoring for liquids	API	2007	Focuses on the design, implementation, testing and operation of computational pipeline monitoring systems that uses an algorithmic approach to detect hydraulic anomalies in pipeline operating parameters.
API 1175	Pipeline leak detection program management	API	2015	Establishes a framework for Leak Detection Program(LDP) management for hazardous liquid pipelines.
API TR 1149	Pipeline variable uncertainties and their effects on leak detectability	API	2015	Describes the procedures for predicting uncertainties in the detection of leaks in pipelines using computational methods based upon certain measurements.

API PUBL 346	Results of range-finding testing of leak detection and leak location technologies for underground pipelines	API	1998	Reviewed the current leak detection and leak location methods for pressurized underground piping.
API PUBL 4716	Buried pressurized piping systems leak detection guide	API	2002	Identify and evaluate reliable leak detection technologies for potential application.
API RP 1175	Recommended practice for pipeline leak detection-program management, and companion guide bundle	API	2017	Focuses on selecting the right leak detection methods, maintaining the leak detection systems and their supporting components and on making sure the systems are optimized in order to minimize the pipeline accidents.
ISO 20,486	NDT – Leak testing – calibration of reference leaks for gases	ISO	2017	Specifies the calibration of those leaks that are used for the adjustment of leak detectors for the determination of leakage rate in everyday use.
ISO 20,485	NDT– Leak testing – Tracer gas method	ISO	2017	Describes the techniques to be applied for the detection of a leak using a tracer gas and a tracer gas specific leak detector.
ISO 20,484	NDT – Leak testing- Vocabulary	ISO	2017	Technical issues related
ISO 18,081	NDT – Acoustic emission testing (AET) – leak detection by means of acoustic emission	ISO	2016	Specifies the general principles required for leak detection by AE testing which is addressed to the application of the methodology on structures and components.

ASTM E432	Standard guide for selection of a leak testing method	ASTM	2017	The selection of the appropriate leak testing method for either leak measurement or location for a particular system being tested, which may consist either of open or sealed units.
ASTM E479	Standard guide for preparation of a leak testing specification	ASTM	2006	Factors to be considered in preparing a definitive specification for maximum permissible gas leakage of a component, device, or system.
SY/T 6889	In-line inspection of pipelines	National Energy Administration (China)	2012	Operating procedure
DNVGL-RP-F302	Offshore leak detection	DNV	2016	Provides recommendations for successful planning, design, integration and operation of leak detection technology in offshore fields for hydrocarbon production.
ASTM E 570-97	Standard practice for flux leakage examination of ferromagnetic steel tubular products	ASTM	2020	Covers the application and standardization of equipment using the flux leakage test method for detection of subsurface discontinuities in ferromagnetic steel tubular products of uniform cross section such as seamless and welded tubing.
ASTM E 1571-11	Standard practice for EM examination of ferromagnetic steel wire rope	ASTM	2016	To examine ferromagnetic wire rope products in which the magnetic flux and MFL methods are used.

IS 11655	Procedure for stray flux testing of ferrous magnetic seamless steel tubular products	Bureau of Indian Standards	1986	Capable of detecting the presence and location of longitudinally oriented defects, scabs, cracks, holes in tubes.
ISO 10893-3:2011	NDT of steel tubes — Part 3: Automated full peripheral flux leakage testing of seamless and welded (except submerged arc-welded) ferromagnetic steel tubes for the detection of longitudinal and/or transverse imperfections	ISO	2016	Specifies requirements for automated full peripheral MFL testing of seamless and welded ferromagnetic steel tubes.
API 5L	American piping products for seamless and welded steel pipes	American piping products	2018	Specifies the manufacture of two product levels of seamless and welded steel oil and gas pipelines and for offshore service applications

2.10 Summary

Successful management of oil and gas pipelines necessitates condition assessment, which entails gathering information about their condition, analysing it, and finally transforming it into expertise, which leads to informed decisions about renewal. To summarize,

a. In terms of sensitivity and positioning precision, exterior methods usually have an advantage over interior methods. The current high cost of various technologies justifies their use primarily on massive water transport pipelines with high failure implications.
b. Prices are expected to fall as new technologies emerge and competition increases, allowing non-destructive inspection to be justified even for pipes with relatively minor failure consequences [16].
c. Multi-sensor systems and array sensors have given us a lot of versatility in terms of multipoint detection and positioning accuracy [13,16]. As a result, sensor fusion or the use of an array of sensors is a potential development path [16].

Chapter 3

Design of MFL Coil Sensor for Extreme Conditions

3.1 Introduction

The research work presented in this thesis makes use of both finite element (FE) numerical modelling and experimental techniques to address the research questions posed. For metal loss due to corrosion characterization, the former method is used. With the resultant leakage field arising from the interaction between the induced magnetic field in the specimen and the geometries, this is modelled in COMSOL Multiphysics 5.4 using 3D representation. The identification of magnetic field signatures corresponding to various thicknesses of the test specimen are focused on the interpretation of the simulation results obtained through numerical modelling. In addition to modelling of various thicknesses of the test specimen under investigation, the accuracy of the MFL inspection results generated by the simulation is confirmed by experiment.

MFL coil sensor plays an important role in determining the integrity of structures and structural health monitoring (SHM) of metal members, such as pipelines in the oil and gas industry, load carrying cables in bridges, lifts, and cranes. SHM is an important task that must be performed on a regular basis to prevent structural failure and economic loss [1]. For example, the most common oil/gas product transportation system is a pipeline, which needs regular inspection due to atmospheric corrosion and underground pressure, as any metal failure, crack, or internal or erosion corrosion could result in an accident. As a result, pipelines must always be operational while remaining sound and intact [2,3].

3.1.2 Theoretical background

From a magnetic standpoint, the toroidal ferrite core is the best possible form. Ferrites are ceramic materials made by sintering a mixture of iron oxide with oxides or carbonates of either manganese and zinc or nickel and zinc [140]. The advantage of the toroidal shape is that, due to its symmetry, the amount of magnetic flux that escapes outside the core (leakage flux) is low, therefore it is more efficient and thus radiates less electromagnetic interference (EMI). MnZn ferrites are used in applications up to l or 2 MHz [140]. Saturation flux density in ferrite is much less than with the tape-wound or powdered metal cores. Ferrite transforms from paramagnetic to ferromagnetic when cooled below curie temperature, due to the formation of magnetic domains. The small domain magnetic moments in ferromagnetic material will be aligned into larger domains and produce a strong magnetisation, if applied an external field [7,140]. The relationship between steel microstructure and the EM properties of the material is complex, depending on both phase fraction and morphology. In [7], the relationship between phase fraction and EM properties is investigated using both theoretical and 3D FEM methods.

The hysteresis loops of the core material represent the core overdriven by a sinusoidal waveform from + to - saturation. Inside the magnetic system, the magnetic flux path is completely enclosed. The toroidal structure completely utilises the ferrite material's capabilities. Equation (1) shows the relationship between the induced voltage in the coil sensor (V_c), and magnetic flux(ϕ) as [74,140]

$$\mathbf{V_c} = -\boldsymbol{N d\phi(t)/dt} \qquad (3.1)$$

where, $\mathbf{N}$ denotes the number of wire loops, $\boldsymbol{\emptyset}$ denotes magnetic flux, and $\boldsymbol{V_c}$ denotes the induced voltage inside the multi-turn coil [74].

3.1.3 Basic design of system

Based upon the faraday's law of electromagnetic induction, an inductor develops a magnetic field when current flows through it. Alternatively, a current will flow through a circuit containing an inductor when the magnetic field through it changes [74]. This effect can be used to detect metallic objects that interact with a magnetic field. Non-metallic substances such as liquids or some kinds of dirt do not interact with the magnetic field, so an inductive sensor can operate in wet or dirty conditions.

The number of wire loops in a MFL coil sensor is another significant parameter. Reducing the amount of wire wound in a sensing coil not only results in a much more compact coil with less occupied space, but it also reduces the thermal heat generated in the sensing coil [74,140]. When a DC current passes through an electromagnet, too many twists, a powerful current flowing through the circuit, and longer inspection times are the most common causes of excessive heat [140]. Continuous inspection is frequently needed when using magnetic sensors (especially coil sensors) to detect damage in pipes. As a result, reducing the number of wire loops in the coil sensor is one way to minimise the aforementioned heat [140].

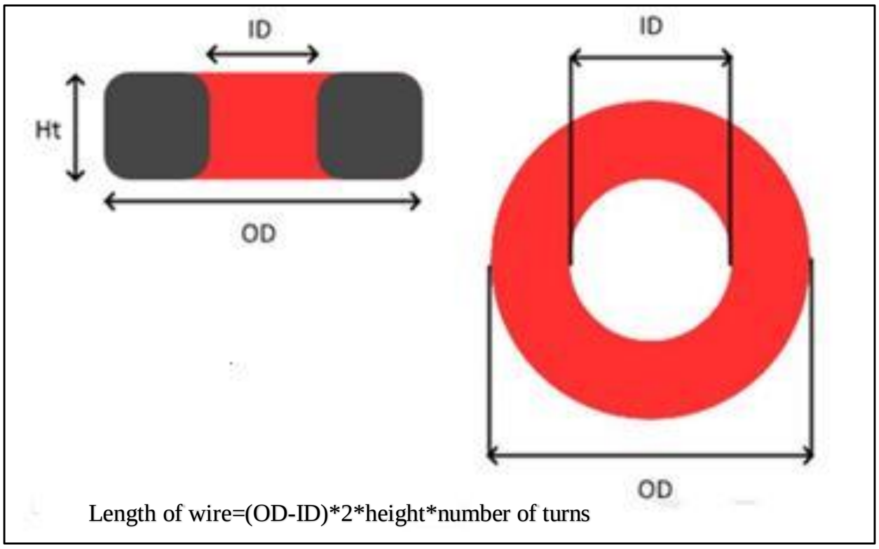

Figure 3.1. The toroidal cylindrical core [140]

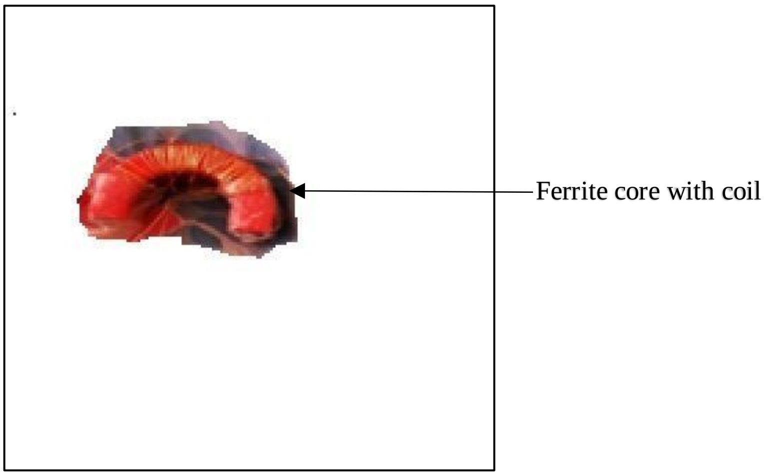

***Figure 3.2**. showing the half cut cylindrical core wound with coil*

Figure 3.1 shows the cylindrical toroidal ferrite core. A grinding machine was used to break the toroidal ferrite core into two halves as in **Figure 3.2.** The cylindrical part was cut in such a way that the core could be put over the cylindrical component avoiding lift off factor. The virtue of the air gap is that; it does not suffer any change of reluctance with flux level.

3.1.4 Mechanical design (room temperature system)

The magnetising and sensing units are the two key components of a MFL sensor setup which are critical for optimising the magnetic apparatus. Any change in the values of the parameters such as the magnitude of the magnetic flux density, can have a major effect on the output signal in the magnetising device. The number of wire turns and lift-off from the specimen's surface are two critical parameters in the sensing device that are supposed to have a significant effect on the output signal [73,74].

The signal amplitude increases if the lift-off value is considered to be reduced. However, due to the small distance between the specimen and the sensor, the probability of collision increases as well. As a result, the best values for critical parameters in both sensing and magnetising units must be determined.

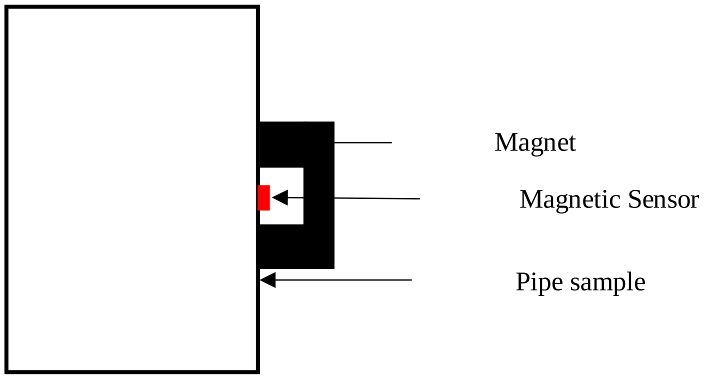

Figure 3.3. *showing the magnetic circuit designed for room temperature*

3.2 Selection of equipment for extreme conditions

All the components in the sensor magnets, wires, insulation, joints etc considered priority or the sensor will breakdown. The choice of magnet and sensor for extreme conditions must be given top priority because it is critical to the experimental setup as in **Figure 3.3**. For example, permanent magnets capable of operating at temperatures higher than 400°C are needed in the power system of a new generation of aircraft, and engines and the optimal maximum operating temperature for some applications is above 450°C [139]. Three rare earth transition metals are considered among the permanent magnets used to work under extreme conditions. Iron, nickel, and cobalt, in general, can generate a magnetic field.

The most important thing to note about permanent magnets is that they can preserve their physical integrity even when subjected to harsh operating conditions. Second, after exposure to corrosive conditions, the magnet's magnetic properties can remain relatively stable [139]. The maximum energy product (BH_{max}), which is a measurement for the maximum amount of magnetic energy contained in a magnet, defines its power [76,139]. When magnets are corroded, their magnetic properties are greatly affected. Since marine and industrial environments are highly corrosive, it's important to know how magnets hold up under these conditions [139].

3.2.1 Permanent magnet

In extreme situations, the following permanent magnets should be considered:

- The magnets are made of neodymium iron boron, aluminium nickel cobalt, and samarium cobalt respectively. Rare-earth (RE) metals are prone to oxidation, and Neodymium-Iron-Boron (Nd-Fe-B) magnets can begin to oxidise at high temperatures in the air if not properly shielded, resulting in irreversible magnetization loss. The curie temperature (T_c) of Nd- (Fe, Co)-B is about 900°C, making it the strongest permanent magnet. Since neodymium has a negative coefficient, its coercivity and magnetic energy density (BH_{max}) decrease with increasing temperature. It has a lower corrosion resistance and a higher coercivity than AlNiCo magnets (which has lower coercivity) [76,139].

- AlNiCo magnets are thermally stable. Nickel has a high corrosion resistance, while cobalt has the highest curie temperature (the maximum operating temperature above which the magnet loses its magnetic properties).

- As compared to the other two magnets, AlNiCo magnets have a higher remanent flux density (when the magnetic field is reduced to zero, some magnetic flux remains in the material even if the magnetizing force is zero). Magnetic field strength at the poles of AlNiCo 5 magnets can exceed 1500 gauss (0.15T) [75,76,139]. It has a high corrosion resistance and is used in applications that do not need coatings or plating. It's perfect for corrosive and high-heat applications up to 500°C [139].

- There are two types of samarium cobalt magnets: Sm_1Co_5 and Sm_2Co_{17}. The 1-5 series' energy product range is 15 to 22 MGO_e, while the 2-17 series' range is 22 to 32 MGO_e. Magnets made of samarium cobalt have the best thermal stability (up till 550°C and strong resistant to demagnetization) [139]. These magnets are very fragile.

- Standard samarium cobalt (Sm_2Co_{17}) magnets will not undergo irreversible losses before the temperature reaches 350°C, and oxidation will not be a concern until that temperature is reached [62,76].

- With increasing temperature and time, losses due to surface oxidation and metallurgical changes become more significant. Samarium cobalt magnets are used in applications where high temperature and corrosion resistance are needed due to the high cost of the material samarium. The high anisotropy field of Sm_2Co_{17} grades aids in preserving magnetization. The properties of the permanent magnets (reversible temperature co-efficient, curie and maximum service temperature) are as in Table 3.1.

Table **3.1** showing the properties of the permanent magnets [62].

Magnetic Material	α (percent/ °C) (20 – 150 °C) °C	Curie Temperature °C	Maximum Service Temperature °C
Alnico 5–7	−0.02	720	520
Sintered ferrite	−0.2	450	400
$SmCo_5$	−0.045	725	250
$Sm_2Co(CuZr)_{17}$	−0.035	825	300
NdFeB	−0.11	310	150

The corrosion rate of $SmCo_5$ permanent magnetic alloy in 3.5 percent NaCl and 0.5M Na_2SO_4 conditions at room temperature, which simulates marine and industrial environments, is revealed by a study of the literature [62]. They demonstrated the long-term stability of the permanent magnets in their tests. The corrosion behaviour of the permanent magnetic alloy $SmCo_5$ is investigated in two separate environments: marine and agricultural.

As opposed to marine environments, the findings indicate that the corrosion rate of the alloy nearly doubles in industrial environments. In both environments tested, the alloy was unable to form protective oxide scale on its surface, according to the study. In both marine and industrial conditions, the alloy was found to be corrosive in case of Samarium Cobalt [64].

3.2.2 Magnetic sensor

Sensors are essential components in the operation of most engineering devices, and they are built on a diverse set of physical concepts. The selection of the most appropriate sensor for a new application is the responsibility of the design engineer, considering the large number of sensor types available on the market. When selecting the best sensor for a given application, a systematic approach should be used. The combination of mechanical and electrical characteristics is used in many current magnetic field sensors. The sensitivity, accuracy, operating temperature, drift, sensing frequency, resolution, operating environment, reliability, and size of the most suitable magnetic field sensor for a particular application are all dependent on the sensor's operating characteristics meeting the application's unique specifications [61].

Furthermore, the choice of a suitable sensor type would be based on the sensor's ability to convert the power of a stimulus (leakage field) into the power of an electrical signal with high stability and gain in modern electronics. This includes the sensor's ability to convert the power of a stimulus (leakage field) into the power of an electrical signal efficiently [61]. Since each magnetic sensor has a different shape, location, and orientation, there is a different optimal crossing point between the sensor scan path and the linear defect. This is found for each sensor to optimise its detection sensitivity.

The final selection criteria will be determined after further analysis and considerations such as sensor size, impedance matching, cost, and working space are taken into account.

3.3 Specific requirements in designing MFL coil sensor

The sensing elements that define cross-sectional loss and surface defect, respectively, are coil and hall-effect sensors. Magnetic flux would not leak from the surface of a defect-free specimen when examined using this process because the specimen has a higher relative permeability than air [8]. When inspecting a damaged specimen [23], on the other hand, magnetic flux will leak from a defect (e.g., crack or discontinuity). This flux leakage can be detected by coil or hall-effect sensors, depending on the type of defect.

A permanent magnet or a solenoid may also produce magnetic flux. A specimen must also be saturated, according to the MFL method's principles [2,8,23]. Both the number of coil turns and the amplitude of the current (either AC or DC) must be high enough to provide a good magnetic field for magnetising a specimen [23]. Despite the fact that the coil sensor can produce a uniform magnetic field, a permanent magnet is a good choice because it is a self-sustaining source of strong magnetic field.

3.3.1 High temperature application

External heat sources, as well as internal energy losses, can be used to heat components. Understanding the behaviour of magnetic cores at elevated temperatures is critical for designing the ferrite core, since inductors and transformers are often designed for significant temperature rise in order to maximize cost, size, and performance [85,139]. Magnetics offer seven different materials for their ferrite cores. The five power materials (L, R, P, F, and T) have low core losses and core loss minimums at favourable temperatures and frequencies. The highest temperature of all eight magnetics powder core materials is 200°C. The stumbling block is the epoxy coating, which is rated for 155°C or 200°C [139].

There is no ageing effect when (ferrites) magnetics powder cores are used at high temperatures. This is frequently an advantage as opposed to iron powders [140]. Magnetics powder core materials do not undergo the thermal ageing that iron powder materials do because they do not contain an organic binder.

Magnetics powder cores have a significant advantage over iron powder cores in terms of core losses. They are more immune to changes in temperature, frequency, and drive level. Powder cores' magnetic properties change slightly at high temperatures. Both improvements in permeability, DC bias reaction, and core loss is reversible [140]. When the goods are returned to room temperature, their magnetic properties return to their original values, no matter how many times the loop is repeated. Excessing the curie point does not damage ferrites, even if it is done repeatedly or over long periods of time. When the core cools down, the magnetic properties return to normal [85,140].

Similarly, ferrites exhibit no ageing or structural deterioration when subjected to high temperatures for long periods of time. The thermal stability of the ceramic material is excellent. Magnetic properties, not physical structure, change at the curie point [8]. Ferrites can quickly crack if subjected to rapid temperature changes because they are ceramic (thermal shock.) When the temperature is increased from 4°C to 8°C or more every minute, the material becomes vulnerable. A temperature rise of 2°C or 3°C per minute is usually considered safe [140].

Ferrites have a low thermal conductivity, which is advantageous in terms of thermal shock. A brief exposure to high temperatures (such as when soldering) is often inadequate to induce core heating or cracking [140]. Ferrite toroids are available in two standard coatings: Z and Y. Both present a smooth winding surface. Very large and very small cores are coated with an epoxy finish rated at 200ºC. The relationship between core loss and temperature is an important consideration.

Power materials are designed to have consistent core loss curves as a function of temperature. When the materials are returned to room temperature, the magnetic properties return to their initial values, no matter how many times the cycle is repeated. T materials have their lowest losses at 60℃-100℃ respectively. The relationship of permeability vs. temperature is taken into consideration.

In all ferrites, permeability is sensitive to temperature. The temperature-dependency of permeability is predictable for each material, and it can be used to the designer's advantage [140]. (Of course, permeability is sensitive to other factors as well, especially flux density). Power materials are typically used at flux levels and temperatures that increase the permeability. Ferrites lose their magnetic properties while above the curie temperature but are not damaged. Effect is completely reversible. It was intended as part of the "safe life" design that a structure should not develop macroscopic defects during its lifespan [139,140], with the discovery of such defects requiring the device to be removed from operation. Increasingly sophisticated techniques, such as ultrasonics, eddy currents, x-rays, dye penetrants, magnetic particles, and other types of interrogating energy, arose in response to this need.

Second, new technical advances allowed the identification of smaller defects, resulting in the rejection of more components, despite the fact that the risk of component failure remained unchanged. Refining and petrochemical, power generation (nuclear and fossil fuel), aerospace and gas turbine, heat treating, mineral and metallurgical processing, chemical processing, automotive, pulp and paper, and waste incineration are just a few of the industries where high-temperature corrosion is a concern [139]. Temperatures of about 90 or 150°C are often referred to as "high temperature" (for example, in heated oil pipelines).

Decades of pipeline corrosion and the presence of a buried log led to a June 2020 sewage spill of approximately 14.7 million gal (55,645.6 m^3) in Manatee County, Florida, USA ,according to a newly released investigative report by Berkeley Research Group(BRG)(Emeryville, California, USA) [128].It's important to note that most corrosion rates are expressed as a weight loss over time (mils per year, millimetres per close to that of many other pure metals).In many cases, pure iron has considerably higher corrosion resistance than many of its alloys, such as mild steels and unalloyed cast irons. Pure iron, on the other hand, has little to no resistance to attack by hostile chemicals including stronger acids.

To begin, I have decided to use AlNiCo 5 grade permanent magnets under severe conditions. The explanation for this is that AlNiCos are extremely stable over a broad temperature spectrum. Both above and below room temperature, and based on the following facts and figures, AlNiCo may be the material of choice in many applications. AlNiCo magnets have an irreversible flux loss of $1.1O_e$ at 300°C, which is higher than that of other permanent magnets [140]. AlNiCo magnets can be used in harsh environments due to their high corrosion resistance and temperature properties (curie temperature of 720°C and irreversible temperature co-efficient of -0.02%) [76,77]. While samarium cobalt appears to be a safer choice for high-temperature applications, it has a history of chipping and breaking due to its brittleness, and it cannot be used for long-term use.

The probe is made up of an enamelled wire coil wrapped around a ferrite core. Induction coils, as opposed to hall elements, may prevent saturation under a strong magnetic field. The experimental setup with the MFL coil sensor is shown in **Figure 3.4**. An induction coil, a ferrite yoke, a magnetic sensor, a function generator, a current source, and a lock-in amplifier made up the magnetic measurement probe. An induction coil and a ferrite yoke were used to apply an alternating-current magnetic field to a metal sample. With 200 twists, the induction coil was wound as a single loop around the ferrite core. For a 5 volt power supply, a DC power source is used. An oscilloscope is a piece of electronic test equipment that records varying signal voltages over a wide frequency range [77,78]. A thermocouple needs to be put inside the furnace in order to obtain the temperature readings of the pipe sample along with time.

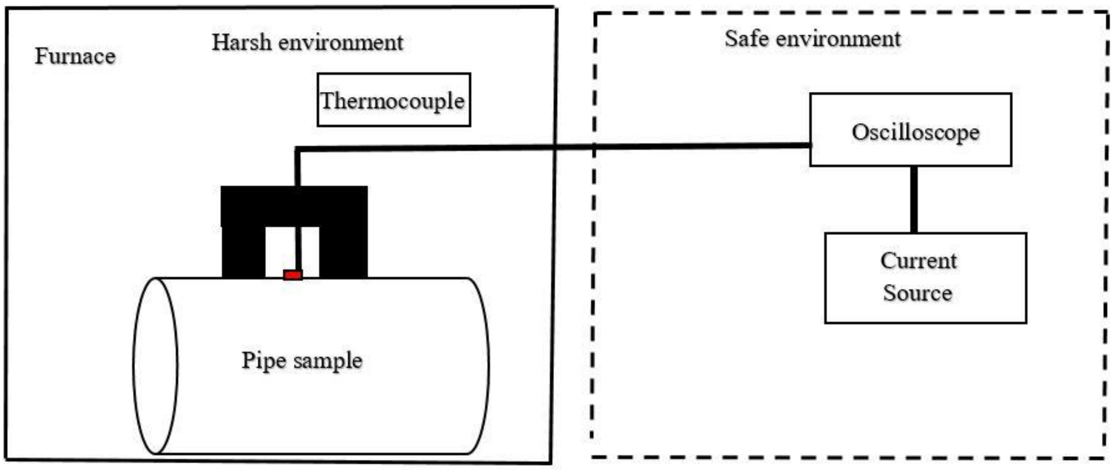

Figure 3.4. *Schematic diagram of the experimental setup for high temperature*

Figure 3.5. *Experimental testing: Comparison of GMR and coil sensor (up to 130°C)*

3.4 Effect of temperature on MFL coil transduction

The MFL coil is more sensitive to temperature than other coils. Material properties such as electric conductivity and magnetic permeability, as well as operating conditions such as frequency and magnetic field, affect various transduction phenomena. Magnetization are of similar amplitude and out of phase with those generated by lorentz force when the bias magnetic field is tangential to the sample surface [77,78

3.4.1 Magnetic flux density

The magnetic circuit is the area around the coil where the flux flows. The product of the current, I, and the number of turns, N, in the coil determines the magnitude of the flux. The magneto motive force, NI, is necessary to generate the flux (mmf). For an air-core, the relationship between flux density, **B**, relative permeability of air, $\boldsymbol{\mu_0}$ and magnetising power, **H**, is as follows in equation 3.3 [77]. The permeability is defined as the ratio of B to H, which for this air-core coil is unity in the CGS system, where it is expressed in gauss per oersteds [78].

$$\mu_0 = 1$$

$$\boldsymbol{B} = \mu_0 \times \mathbf{H} \tag{3.3}$$

The key benefit of air-core coils is the linearity of the relationship between B and H. Since the relationship is linear as in **Figure 3.5**, increasing H increases B, and thus the flux in the coil, allowing for the creation of very large magnetic fields with very large currents. There is, of course, a practical limit to this, which is determined by the conductor's maximum permissible current and the resulting increase. Only flux that is perpendicular to the apertures is detected by coil sensors.

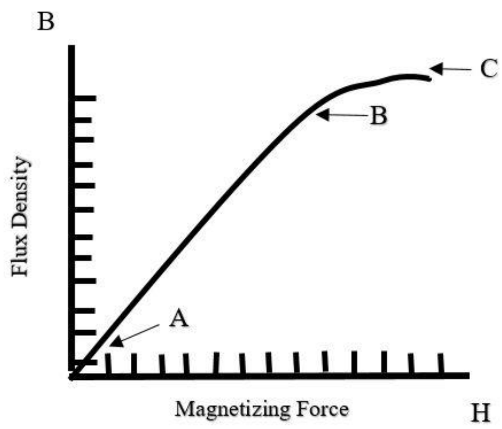

***Figure 3.6**: Typical magnetization curve*

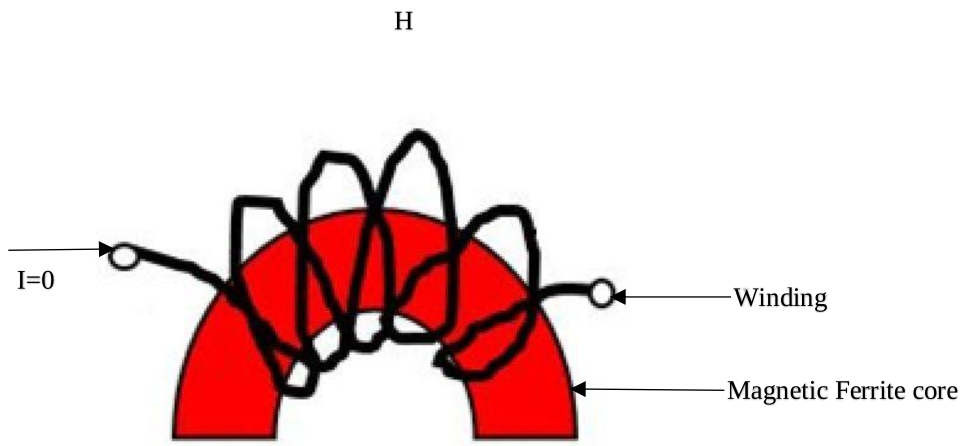

Figure 3.7: *Magnetic core with zero excitation*

The coil winding wound around the ferrite core is depicted in the **Figure 3.6**.

3.5 Summary

In this chapter, a prototype magnetic circuit has been designed along with a MFL coil sensor. The idea behind the design of the MFL coil sensor(magnetic ferrite core and coil) has been briefly described. Lorentz force, magnetizing force, and magnetic flux density have been addressed in depth in relation to coil sensors. Electrical circuit behind the MFL coil sensor has been designed with reference to the magnetic circuit to complete the process.

The maximum operating temperature of the torroidal ferrite core is 200°C upto which the coil sensor survived.After that limit,the ferromagnetic core started cracking up eventually.Further a encasing is required which can protect the magnetic circuit from getting affected with higher temperatures above 200°C.

Chapter 4
Finite Element Modelling and Simulation

4.1 Introduction

The magnetic sensor in traditional pipeline design and condition monitoring, is focused primarily on the sensor design intended for but not limited to pipe inspection. A mathematical model is based on the physical principles of the design. These models can be more or less accurate, but in general, model accuracy can only be checked when the model is put to the test in real life. It's crucial to be able to anticipate and/or track emerging pipeline failures so that any appropriate maintenance can be prepared for and carried out during normal outages [79,80].

There are appropriate direct measurement methods that can provide details about the actual state and condition of the piping. As a result, to get good agreement between computational and experimental outcomes, an iterative process is frequently needed [79]. Special purpose software designed to update FEA models with experimental data can be used to accomplish this. It should be noted, however, that pipes rarely corrode in a uniform manner due to material heterogeneity and soil variability [79,80]. Since the sensor is mainly designed for detecting internal corrosion or erosion, the main variable is the location. Therefore, a single sensor is not likely to provide a good representation for the condition of long pipes. In that case, array(multiple) sensors should be placed in long pipes.

4.2 Selection of software and development of the modelling system

COMSOL Multiphysics 5.4, a general-purpose simulation programme for modelling designs, devices, and processes in all fields of engineering, manufacturing, and scientific research, was used in this study. The models can be converted into simulation software for use by other design teams, manufacturing departments, research laboratories, clients, and more, in addition to multiphysics modelling. The platform product can be used on its own or with add-on modules for electromagnetics, structural dynamics, acoustics, fluid flow, heat transfer, and chemical engineering simulations. As engineering features and modelling techniques advance, the number of applications for COMSOL Multiphysics increases almost every year.

COMSOL Multiphysics includes a selection of protocols for dealing with a wide range of engineering issues.

4.3 FEA model overview

The following equations as in figure 4.1 and 4.2 can be used to treat the MFL problem as a magneto static problem. The following are Maxwell's equations to express it [14]:

$$\boldsymbol{\nabla} \times \{\boldsymbol{H}\} = \{\boldsymbol{J}_s\} \tag{4.1}$$

$$\boldsymbol{\nabla} \cdot \{\boldsymbol{B}\} = \mathbf{0} \tag{4.2}$$

where **H** denotes magnetic field power, $\mathbf{J_s}$ denotes applied source current density, and **B** denotes magnetic flux density. The constitutive relation describes the behaviour of electromagnetic materials and is used to complement the field equations [14].

$$\{\boldsymbol{B}\} = \{\mu\}\{\boldsymbol{H}\} + \mu_0\{\boldsymbol{M}_0\} \tag{4.3}$$

In other region

$$\{\boldsymbol{B}\} = [\mu]\{\boldsymbol{H}\} \tag{4.4}$$

where $\boldsymbol{\mu_0}$ is the permeability of free space. where $\mathbf{M_0}$ is the remanent intrinsic magnetization vector and $\boldsymbol{\mu}$ is the magnetic permeability matrix.

4.3.1 Geometry, material properties, and boundary conditions

The basic model in this study is a low carbon steel pipe (**Figure 4.1**) that has been subjected to stationary analysis (a pipe(mesh) with a defect) as in **Figure 4.2**. The model's basic geometry, with structural parameters L = 148 mm, OD = 80 mm, and T = 8 mm, reflects the pipe's length, outside diameter, and thickness, respectively. The defect measures 8 mm in diameter [125].

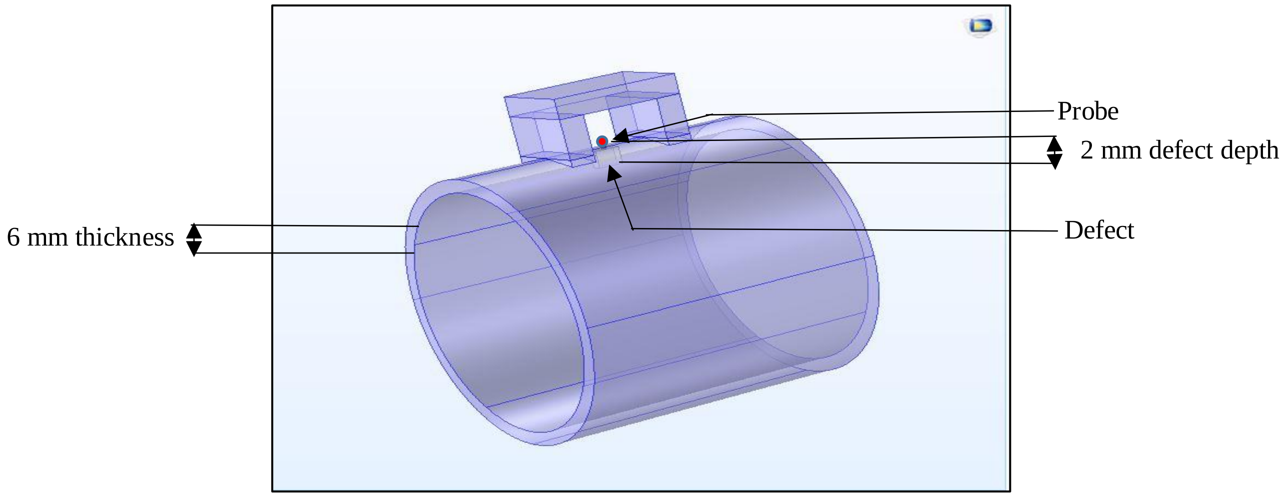

All Dimensions are in mm

Figure 4.1. *COMSOL Multiphysics basic pipe model simulation*

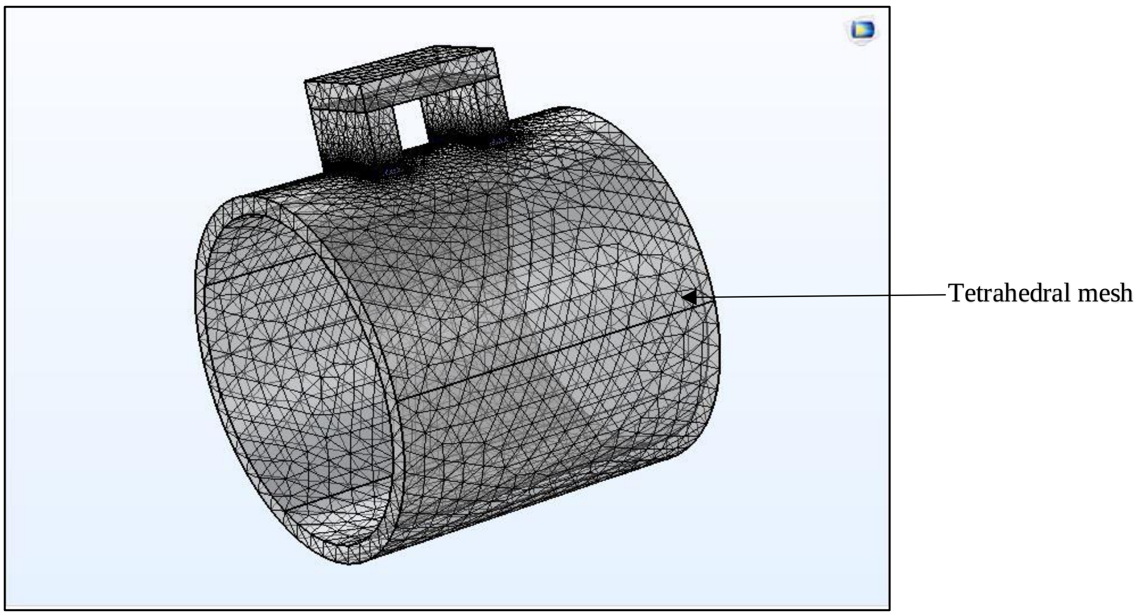

Figure 4.2. *Basic pipe model simulation with mesh*

The specimen properties and model parameters that are given as input in COMSOL model are listed in the Table 4.1.

Table 4.1 Specimen properties and parameters of the model

Model Configurations	
Pipe material	Low Carbon Steel 1002
Permanent magnet	AlNiCo 5 grade (70x41x57 mm)
Metal pieces	Soft iron
Length of the pipe (L)	148 mm
Outside diameter of the pipe	80 mm
Thickness of the pipe (T)	8 mm
Material Properties	
Stiffness (Young's Modulus)	E = 200
Poisson's ratio (v)	0.3 Pa
Density	7850 kg/m^3
Variables' Parameters	
Relative Permeability	100

The relative permeability value was considered based upon the steel grade material used for experiments accordingly.

4.4 FEA model simulations

A contour plot was used to clearly display the magnetic flux density in order to clarify the modelling outcomes and effects, as shown in the following **Figure 4.3(a)** and **(b)**. The magnetic field lines are shown by the arrow lines in the contour map.

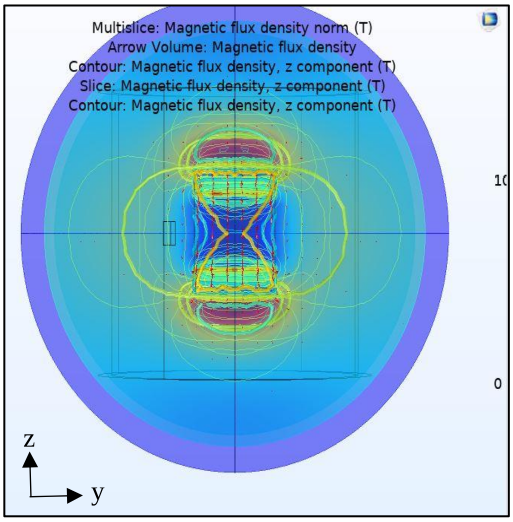

(a)

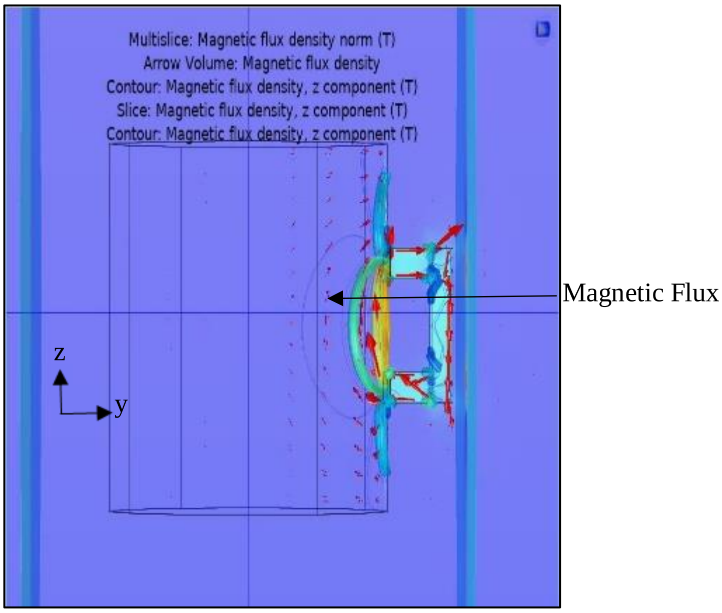

(b)

Figure 4.3. *Top view(a) and the side view(b), of the contour plot showing the magnetic flux density*

The line graphs in **Figures 4.4** and **4.5** show the plots for the (B_x) and (B_z)component with defect. Arc length signifies the distance from the start point along the line of the line plot

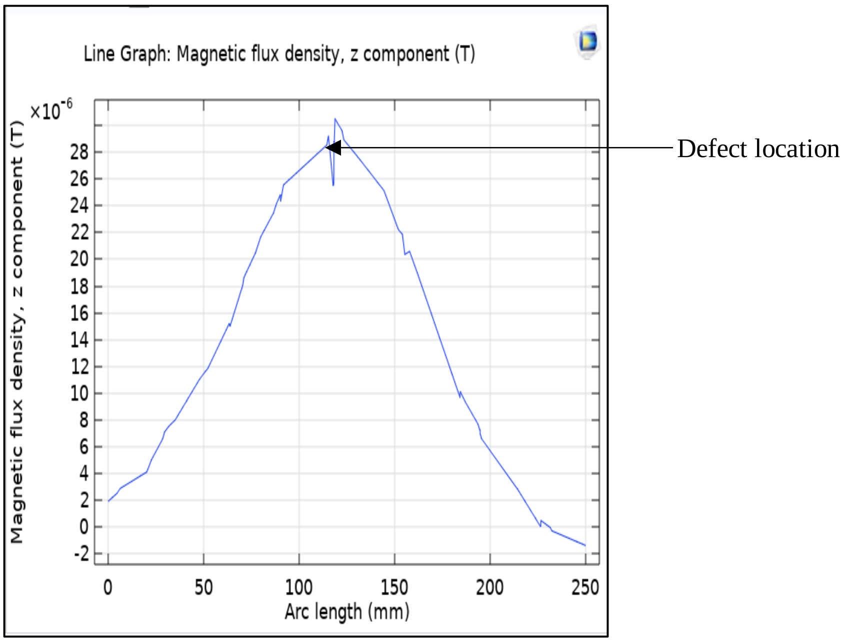

Figure 4.4. *Line graph showing the B_z component for magnetic flux density with defect*

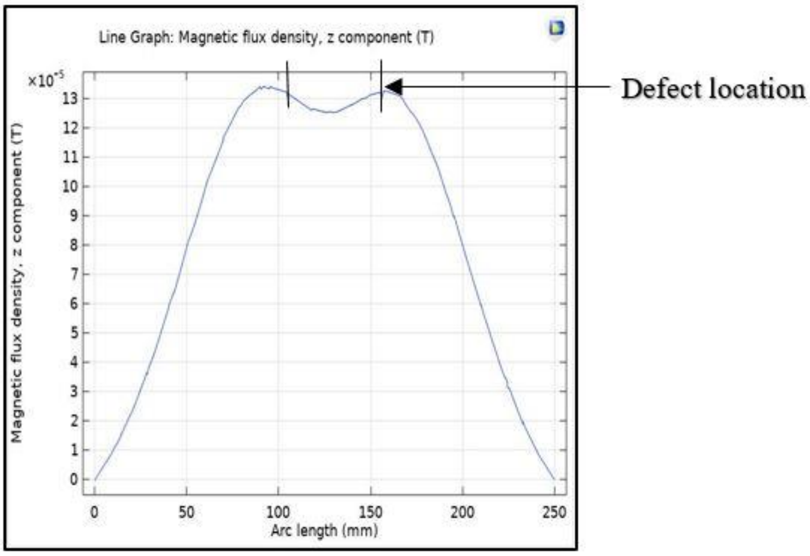

Figure 4.5(a). *Line graph showing the B_z component for magnetic flux density with defect*

Bz component which decreases at the defect location. With increase in depth of the defect, the Bz component decreases [78,125].

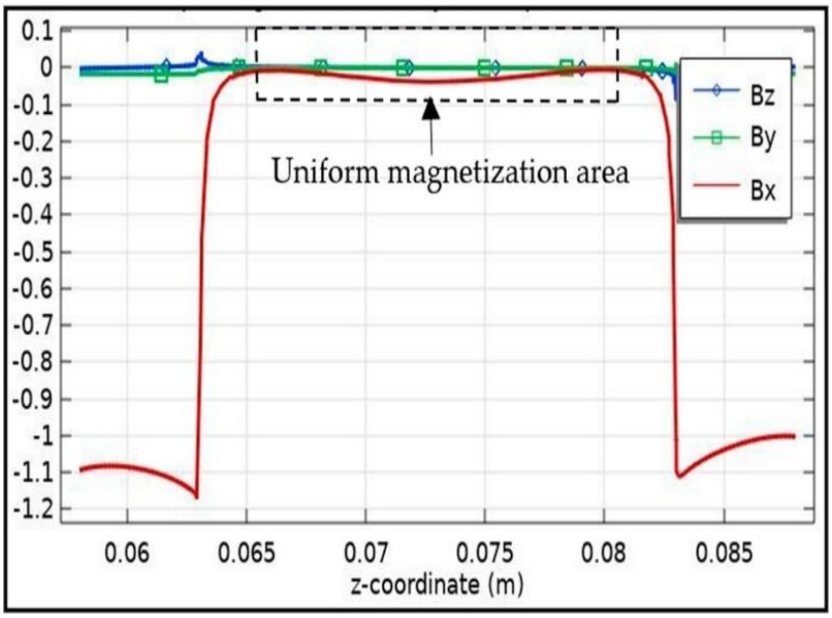

Figure 4.5(b). *Line graph showing the B_x, B_y, B_z component, magnetic flux density without defect. z co-ordinates represent vertical axis.*

The highlighted area as in **Figure 4.5(b)** shows the uniform magnetization area in the pipe wall. The 3D FE model is for any ferromagnetic mixed structures, as an example, the sensor response and the measured parameters can be predicted further. For each increase in pipe sample thickness, magnetic flux density values (B_z component) were obtained, from which realistic values could be predicted [78,80].

4.4.1 Magnetic circuit with multiple probes

As in the previous section, the magnetic circuit was designed and developed with a single probe, further development includes the magnetic circuit with an array of probes placed around the pipe sample as in **Figure 4.6**. Simulations were carried out for pipe sample with and without defect. An artificial defect was created in the pipe sample for determining the wall thickness loss. Defect depth was increased from inside into the pipe thickness, and the simulations were carried out accordingly. Each probe placed on the pipe sample signifies the magnetic field at that particular point which is shown in the plot presented in **Figure 4.7**.

The advantage of placing an array of probes compared to a single probe is that the defect anywhere can be detected within the pipe sample. Time saving is a major advantage and also magnetic field is identical at all specified points. The pipe sample thickness was limited to 8 mm.

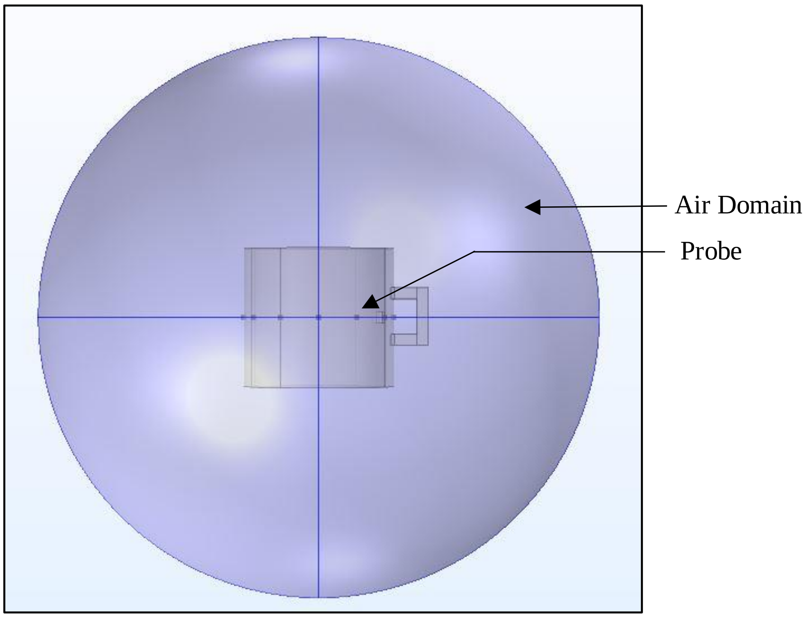

***Figure 4.6**. Magnetic circuit with an array of probes placed around the pipe sample*

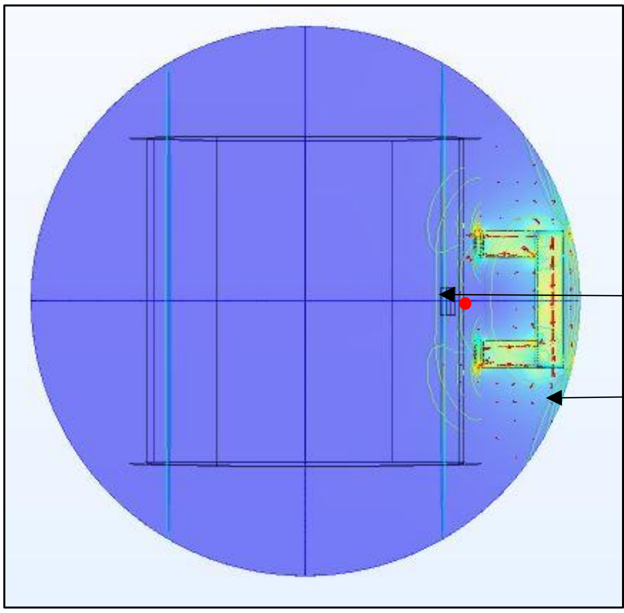

Figure 4.7. *Contour plot showing the B_z component for the pipe sample with defect*

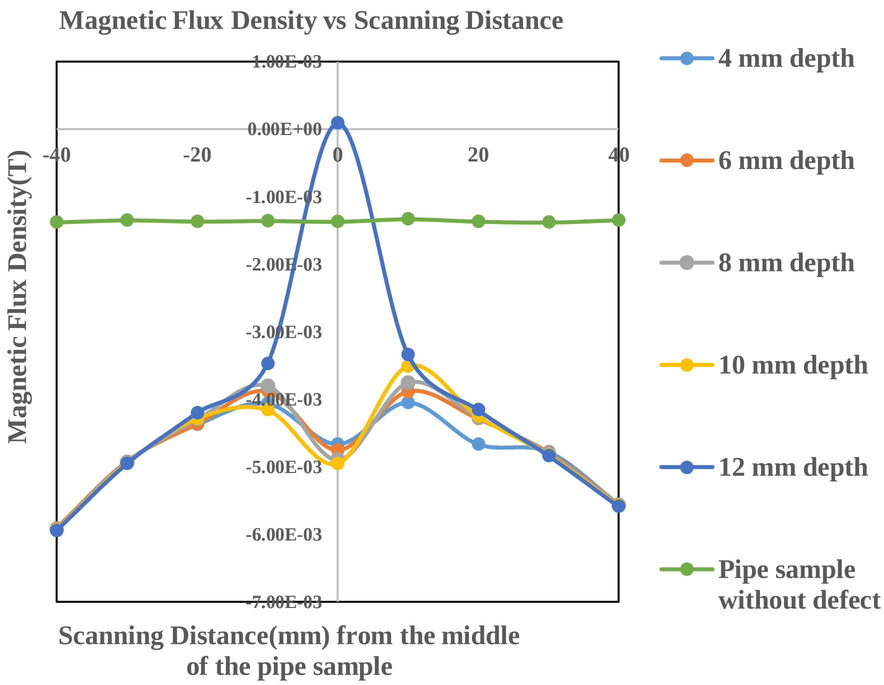

Figure 4.8. *Magnetic Flux Density Vs Scanning distance for the pipe sample with defect*

The defect was gradually increased from 4 mm to 12 mm in depth and the magnetic flux density measurements were carried out and the plots obtained were compared with pipe sample without defect, as presented in **Figure 4.8**. 12 mm depth is of through hole which is depicted as a peak in the plot. Scanning distance is the distance measured from the middle of the surface of the pipe sample. Lift-off is an important factor to be considered in all the three conditions investigated; room temperature, underwater and high temperature. The usage of the holder for positioning of the sensor also created an additional lift-off between the pipe sample and the sensor. Under high temperature conditions, heat will affect the sensors and during the underwater tests, sensors are affected by water ingress. Henceforth lift off is unavoidable under both of these conditions.

The graph presented in **Figure 4.8** clearly indicates the location of the defect. In conclusion, the above findings show that the defect location is specified with the magnetic flux density taken into consideration and this shows the efficiency of the simulation to predict faults in pipeline smoothly, instead of physical inspection which requires preparation and arrangement in the vicinity of the defect.

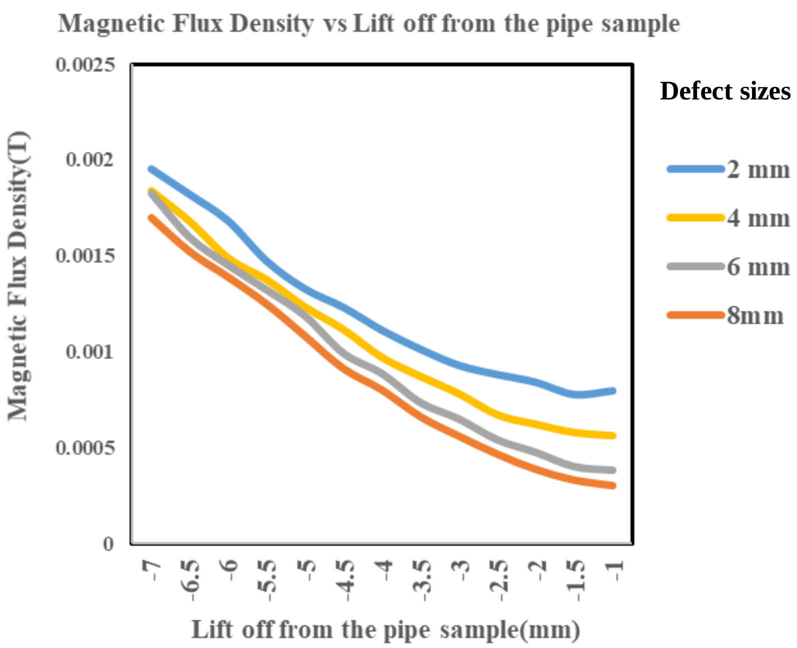

Figure 4.9. *Lift off vs Magnetic Flux Density*

The above simulation was carried out with lift-off playing an important role. The plots in **Figure 4.9** show that as lift-off increases, the magnetic flux density is seen to decrease.

4.5 Design of an EM sensor

Steel structural material qualities, particularly magnetic and electric properties, alter as temperature rises. Steel structures' magnetic permeability increases with increasing temperature until it falls below the curie temperature. To estimate the zero crossing frequency of an EM sensor, a 2D model (U and H-shaped) is constructed (in an alternating current, the zero-crossing [86] is the instantaneous point at which there is no voltage present). This is done by measuring the true inductance of both (sensing and excitation) coils with frequency and comparing the data acquired from both sensors for a steel sample of varied thicknesses. This study also looks at how real inductance varies for steel samples with different relative permeability [86,87].

Varying frequency EM sensors are sensitive to both changes in relative permeability and resistivity of the steel, with the low frequency inductance values being directly related to the permeability. The EM sensor measurements are non-destructive, have a fast response, can operate in a non-contact manner, are unaffected by dust, water and are relatively inexpensive [6]. In recent years, the use of magnetic techniques based on EM sensors, for NDT have increased [6-9].

To achieve axial magnetisation of the pipe sample, a U shaped EM sensor was developed for non-destructive mild steel characterisation, in particular phase balance, grain size and strength in dual phase (DP) steels which is a high-strength steel that has a combination of two different (ferritic–martensitic) microstructure [20,85,86]. It is known that the low frequency inductance measured using an EM sensor depends on the relative permeability of the sample and that the permeability is affected by microstructural features (i.e. phase fraction / distribution and, to a lesser extent, grain size are the important features in DP steel) [2]. Phase fraction refers to the metal composition [86]. The phase in an AC circuit, with inductors involved, the current and voltage do not peak at the same time. For the U-shaped EM sensor, when an input current is passed onto the excitation coil, the magnetic flux generated passes on to both coils equally and the real inductance becomes zero as both inductance from the coil cancels out passing through the steel sample [85,86]. Mutual inductance needs to be calculated which is given by the formula [85-87]:

$$\boldsymbol{M = N\emptyset/I} \qquad (4.5)$$

where M is the magnetization of the excitation coil and N is in the number of coil turns, A is in the cross-sectional area in m^2, I_p is the driving current [2,86], Φ is the magnetic flux in tesla. For a particular steel sample of different thicknesses, real inductance values are obtained for various frequencies.

Previously from the idea of U shaped EM sensor, H shaped sensor was developed with the dummy coil moving onto the opposite side of the active coil exactly as shown in the **Figure 4.10**.

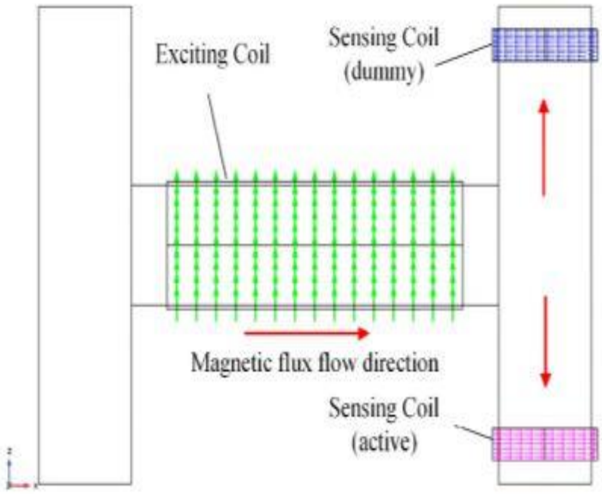

***Figure 4.10**. Coil current directions and induced magnetic flux flow direction inside the ferrite core for the H-shaped sensor arrangement [86]*

When an alternating current of 1 Ampere is passed into the excitation coil, magnetic flux is generated which moves upwards and downwards towards the active and dummy coils. The active coil faces the target sample which is the steel plate and so the magnetic flux generated penetrates into the metal sample as shown in **Figure 4.11[86,87]**. There is more flux generated by the dummy coil than the active coil as it leaks into the air domain.

The magnetic flux gets concentrated more on the area between the two edges of the core on the steel sample than the other surface. On the other side, when there is no sample present, the dummy coil zeros in the signal combining with active coil [86]. The active sensing coil detects the voltage induced in the steel by the excitation coil.

At higher frequencies, the eddy currents decrease analogues to the depth of penetration which also decreases. The excitation coil runs at a frequency range of 100 kHz to 1600 kHz. The value of 50 turns were given for both active and dummy coils. At lower frequencies, eddy currents increase with a corresponding increase in depth of penetration. At a specific frequency, no voltage is observed and the real inductance changes from positive to negative which is said to be the zero-crossing frequency [85-87]. Once the zero-crossing frequency is obtained, magnetic permeability can be calculated for the steel sample of particular thickness. The table 4.2 shows the parameters and specifications of the active and dummy coil in the comsol model.

Table 4.2 Specifications of the active and dummy coil

Required input	Excitation coil	Active and dummy coil
Conductor model	Homogenized multi-turn	Homogenized multi-turn
Input current	1Ampere	-
Number of Turns	50	50

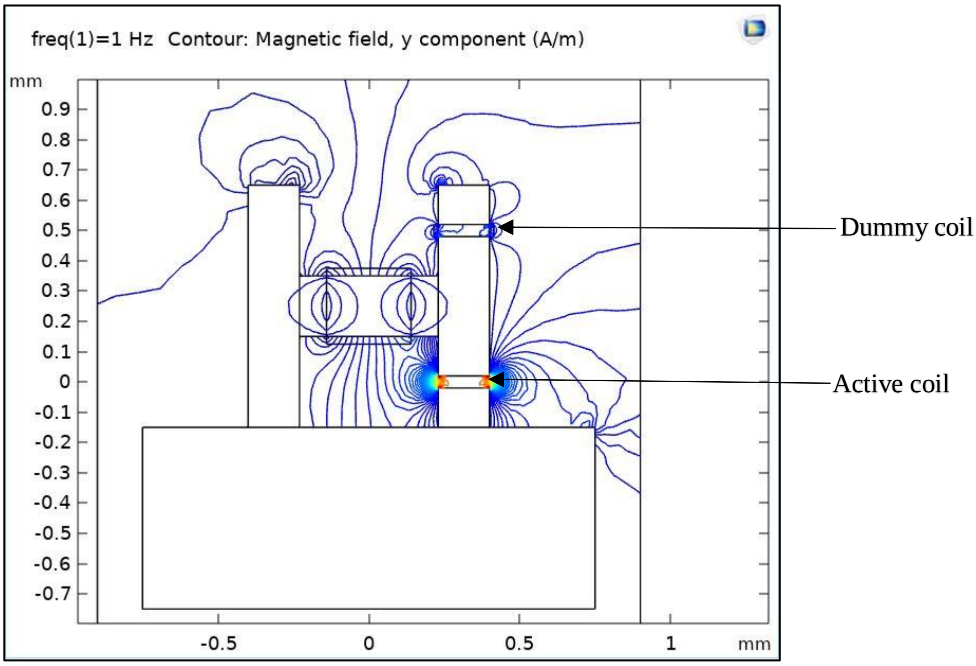

Figure 4.11*. The contour plot (the magnetic field y component) for a frequency of 1 Hz for the H-shaped sensor arrangement*

For an H- shaped ferrite core, the active and dummy coil are on the same leg and the contour plot obtained is shown as in **Figure 4.11**. For each increase in frequency, the real inductance keeps on decreasing and it is with respect to each increase in sample thickness.

The frequency increases slowly, the current flowing through the inductor also reduces in value as in **Figure 4.12**.

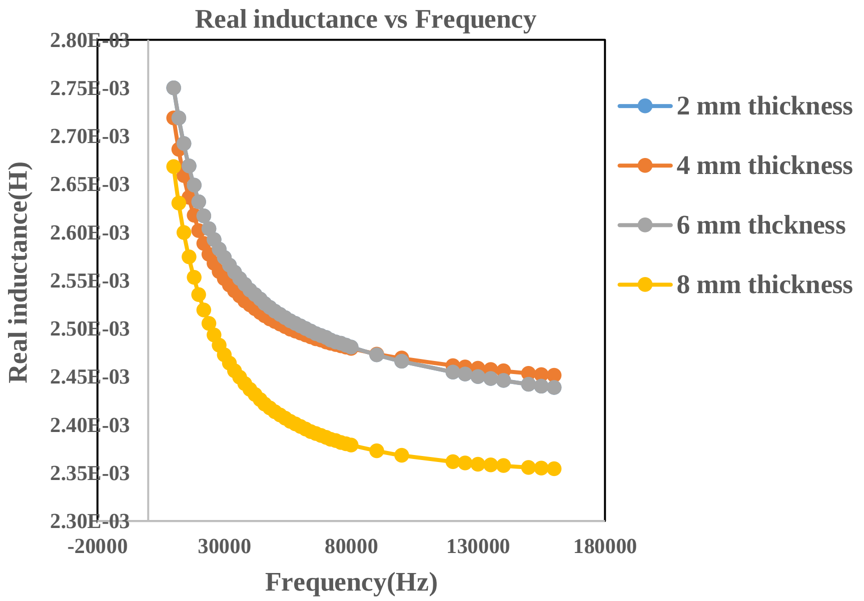

Figure 4.12. *Frequency vs Real inductance*

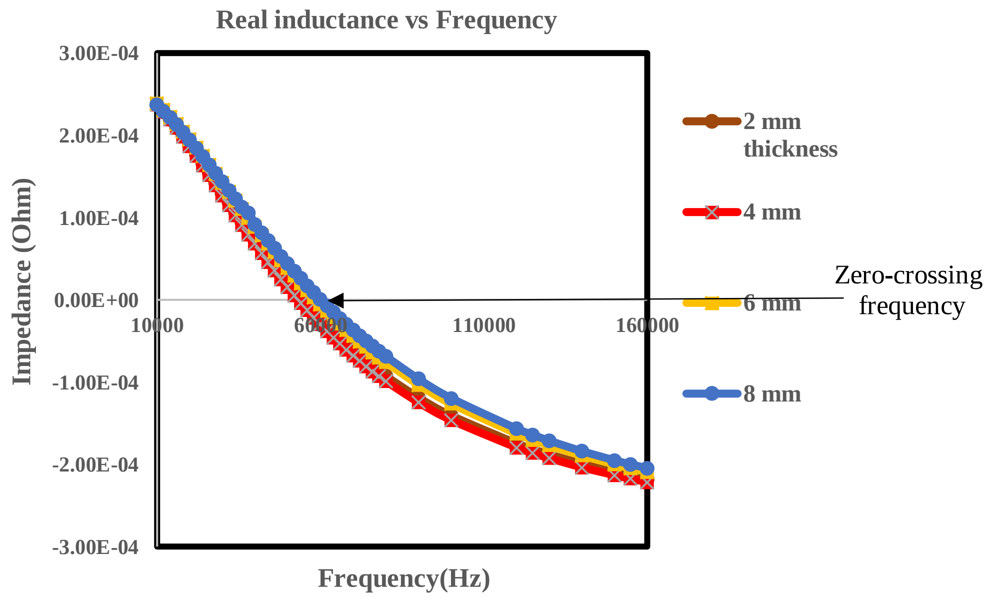

Figure 4.13. *Zero crossing frequency vs Real inductance*

Figure 4.13 shows the real inductance vs zero crossing frequency plot for a steel sample of varying thicknesses. The plot for the H -shaped EM sensor shows that with increase in frequency the coil inductance of the sensing coils decreases.

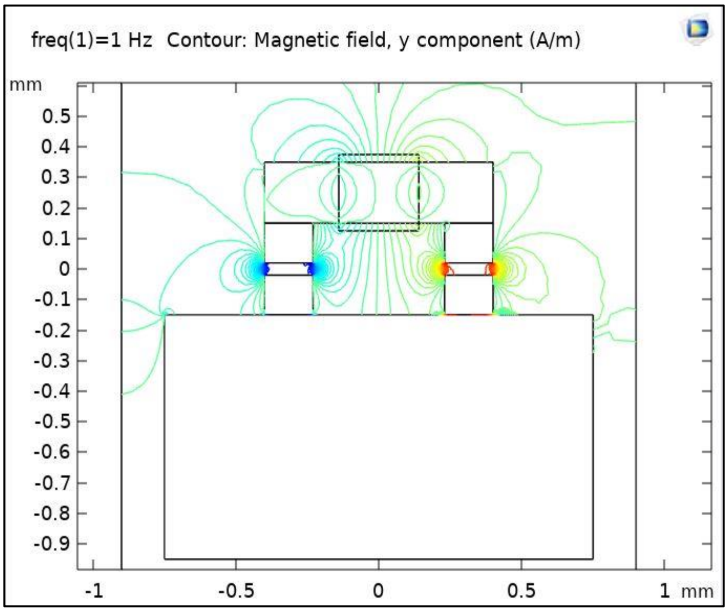

***Figure 4.14**. showing the contour plot (the magnetic field y component) for a frequency of 1 Hz*

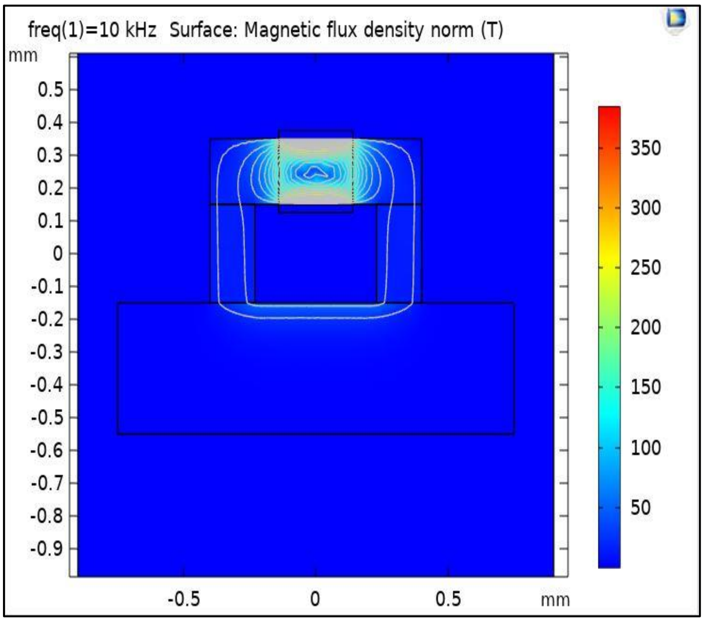

***Figure 4.15**.Also showing the magnetic field lines flowing through the ferrite core*

The magnetic field is flowing through the coil through the middle of the yoke as in **Figure 4.15**. The field lines penetrate through the metal sample.

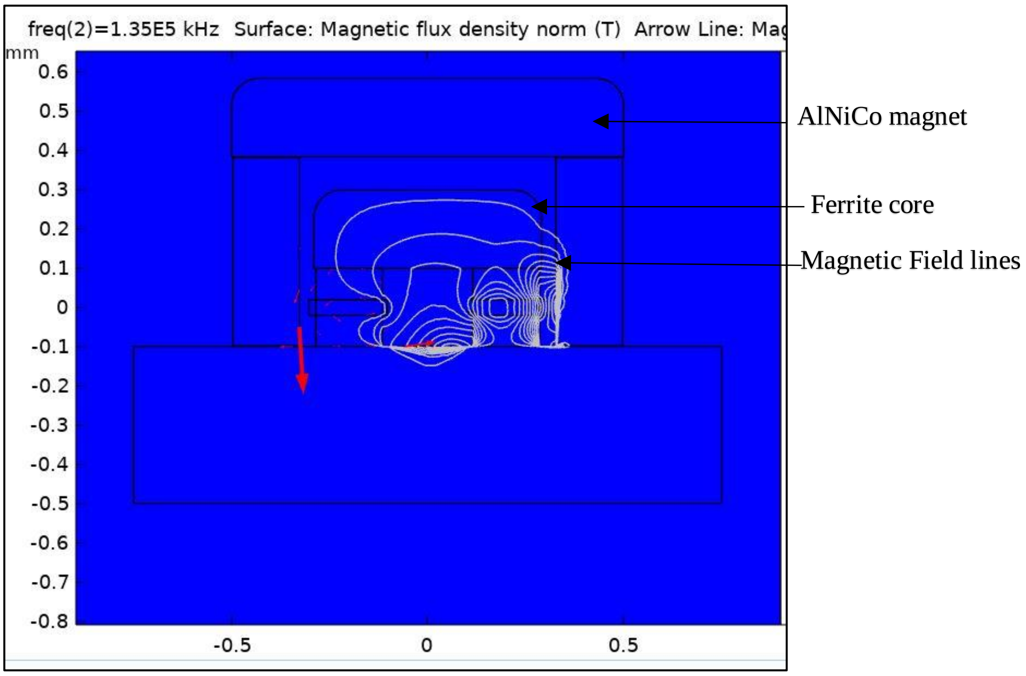

Figure 4.16*. showing the magnetic field lines flowing through the ferrite core along with the permanent magnet*

The magnet and the ferrite core are placed symmetrical.The surface plot clearly shows the magnetic field lines penetrating through the right leg of the core as in **Figure 4.16**.

Further magnetic circuit simulation with the coil sensor was carried out.The developed coil sensor is placed between the two poles of the magnet.Two physics are used in this AC/DC module.For magnetizing the pipe sample with the permanent magnet,magnetic flux conservation step is used.For the coil sensor,magnetic field with no current module is used. Fine tetrahedral mesh provides a clear solution for all the components together.Finally stationary solver was used to compute the model.The direction in which the magnetic field flows through the magnet is specified accordingly as in the **Figure 4.16**.

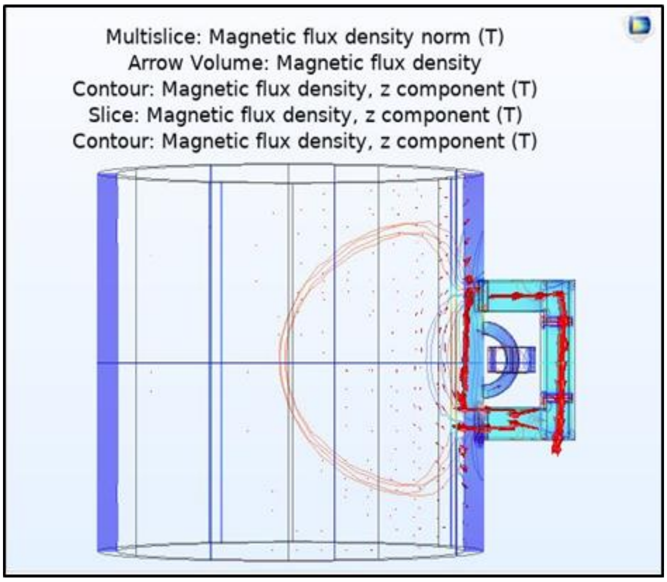

Figure 4.17. *Magnetic circuit for room temperature conditions*

A model probe is placed at the middle of the ferrite core so as to calculate the magnetic flux leaking out of that area as in **Figure 4.17**.All the components are placed in symmetrical position over the pipe sample.The ferrite core with the coil is placed in close contact with the magnet.The magnetic flux that comes through the magnet crosses path with the flux passing through the ferrite core.Bx,By,Bz component can be calculated through the simulation carried out.Bz component specifies the direction of the magnetic flux. **Figure 4.18** shows the comsol results for various pipe sample thicknesses.

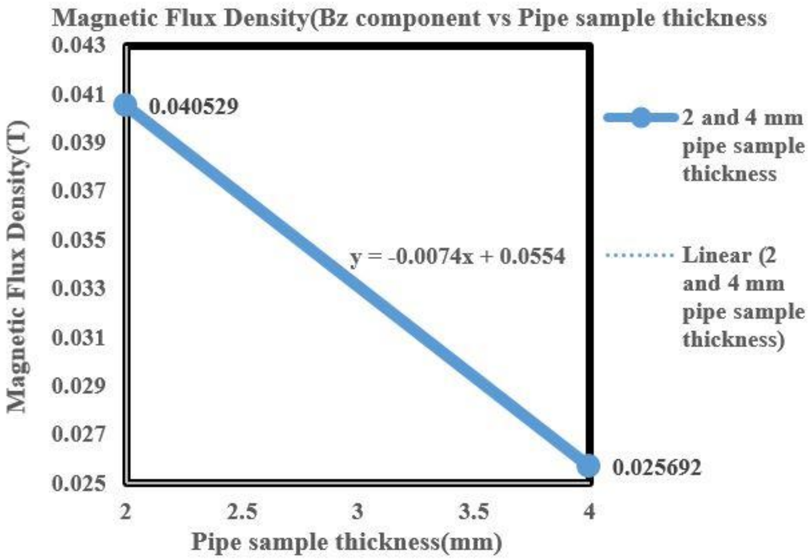

Figure 4.18. *Magnetic Flux Density vs Pipe sample thickness*

Magnetic flux density Bz component is measured accordingly. With each increase in wall thickness, the magnetic flux density is decreasing. The values obtained are plotted accordingly which signifies the fact that magnetic flux density decreases with increase in thickness of the pipe sample.

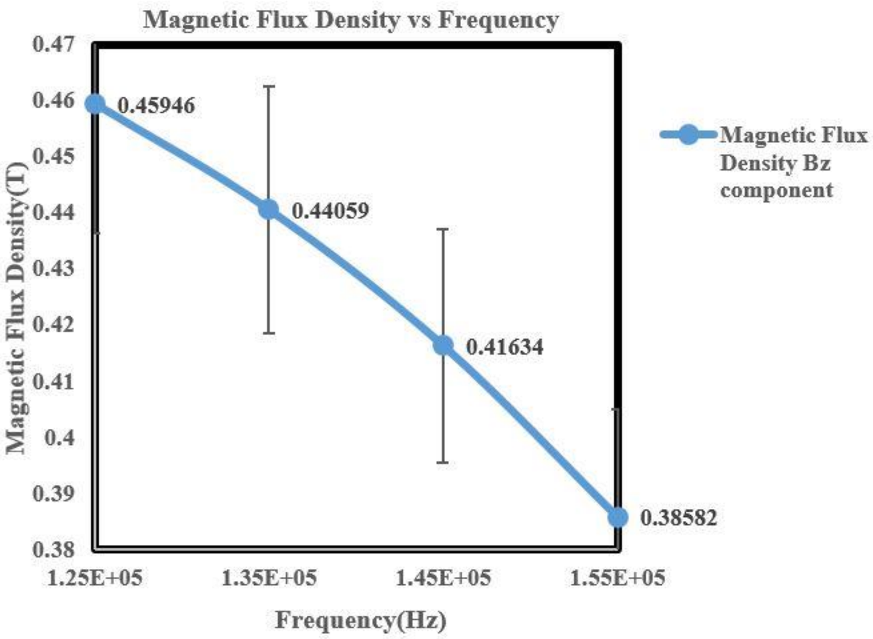

Figure 4.19. *Magnetic Flux Density vs Frequency*

The magnetic flux density decreases with increasing frequency as in **Figure 4.19**.

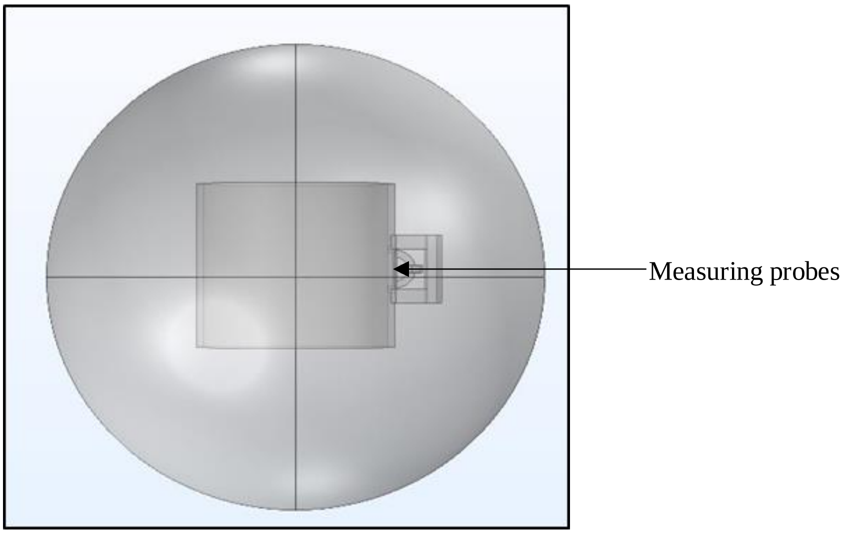

Figure 4.20. *COMSOL model with measuring probes placed*

Each probe placed measures the magnetic field with respect to that area as in **Figure 4.20**. Magnetic and electric properties (such as low field relative permeability and resistivity) are sensitive to changes in both steel microstructure and temperature.

The model is based on solving maxwell's equations using certain boundary conditions, which can be written as [14,86,89]

$$(\boldsymbol{j\omega\sigma} - \boldsymbol{\omega}^2\mathcal{E}_0\mathcal{E}\mathbf{r})\mathbf{A} + \nabla \times \mathbf{H} = \mathbf{j}_\mathrm{e} \tag{4.6}$$

$$(\boldsymbol{\mu}^{\mathbf{0}^-}\mathbf{1} \times \boldsymbol{\mu r}^-\mathbf{1} \times \boldsymbol{B}) = \boldsymbol{H} \tag{4.7}$$

$$\boldsymbol{\nabla} \times \boldsymbol{A} = \boldsymbol{B} \tag{4.8}$$

Where **A** is the magnetic vector potential, **H** is magnetic field, $\mathbf{J_e}$ is external current density, $\boldsymbol{\omega}$ is angular frequency, $\boldsymbol{\sigma}$ is the electrical conductivity, **B** is magnetic flux density, $\boldsymbol{\varepsilon_0}$, $\boldsymbol{\varepsilon_r}$ are vacuum and relative permittivity respectively and $\boldsymbol{\mu_0}$, $\boldsymbol{\mu_r}$ are vacuum and relative permeability respectively [86,89].

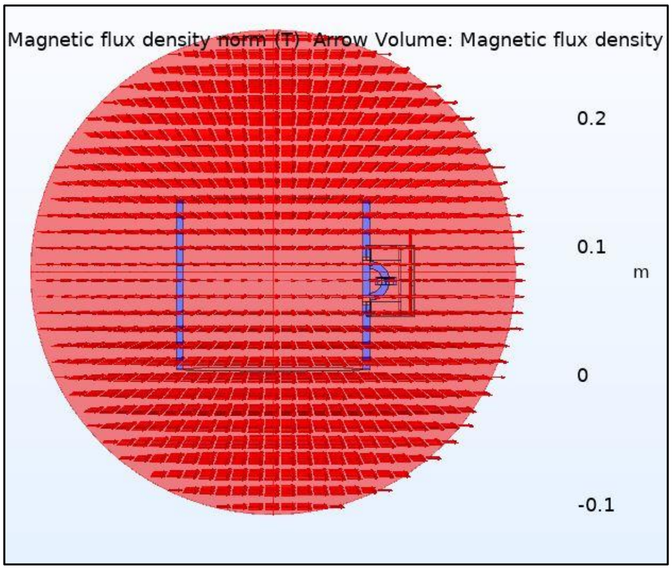

Figure 4.21. *Arrow volume showing the heat over the magnetic circuit above room temperature*

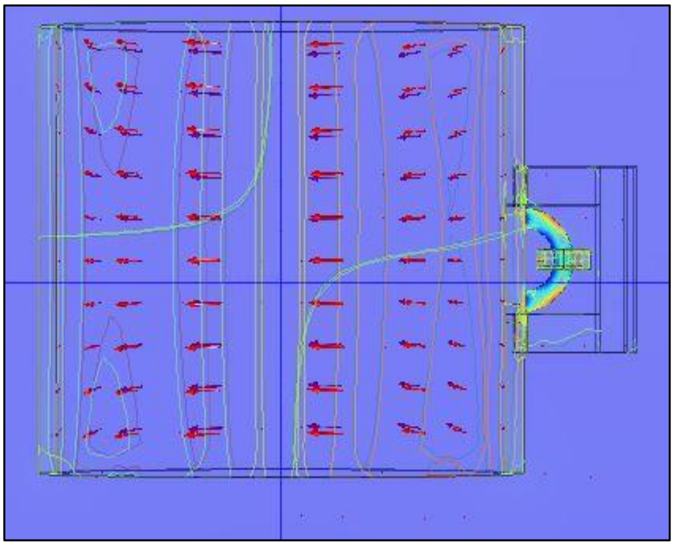

__Figure 4.22__. Contour plot showing the flow of magnetic field lines above temperature

Heat flow over the magnetic circuit is shown in the **Figure 4.21** before applying temperature parameters on the magnetic circuit.Contour plot as in **Figure 4.22** displays the flow of magnetic field with increasing temperature.

4.6 FEA Results and discussion

In this work, it is shown that the permeability can be determined from the low frequency mutual inductance measured using a U-shaped EM sensor for any sheet thickness. In general, magnetic permeability follows an increasing trend with temperature and after a particular stage it stabilises and then decreases as it reaches the curie temperature [86,87]. In addition, the success of the simulation must be verified experimentally as illustrated in the following chapter.

- A cutline measurement is carried out which clearly signifies the magnetic flux path. A cut line is created that cuts through the magnetic circuit starting from one pole of the ferrite core till the other end. The magnetic flux density is plotted accordingly with respect to the measuring points as in **Figure 4.23**.

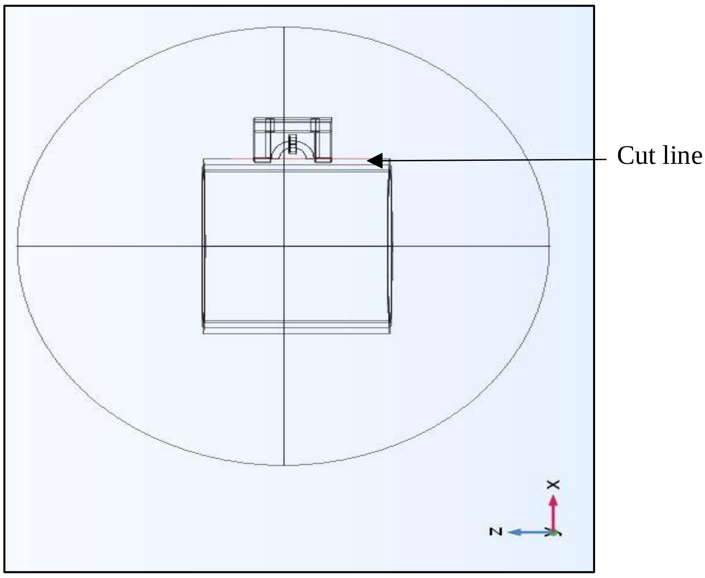

***Figure 4.23**. Cutline placed horizontally on the pipe sample*

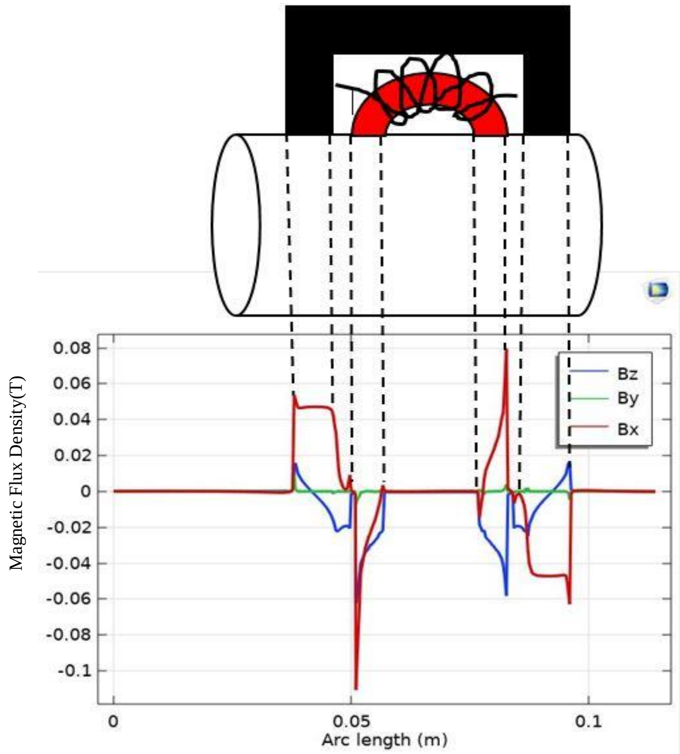

***Figure 4.24**. B_x, B_y, B_z field components measured for the magnetic circuit*

Figure 4.24 shows the comsol results for various pipe sample thicknesses. The simulation was carried out for one measuring probe first ,then it was further modelled for calculation of magnetic flux density at all points starting from the north pole of the permanent magnet till the south pole.All through the coil sensor, totally thirty four measuring probes are placed and magnetic flux density is calculated accordingly.In the above model,the points are replaced with a cutline which provides the plot for all the three components i.e B_x,B_y,B_z.

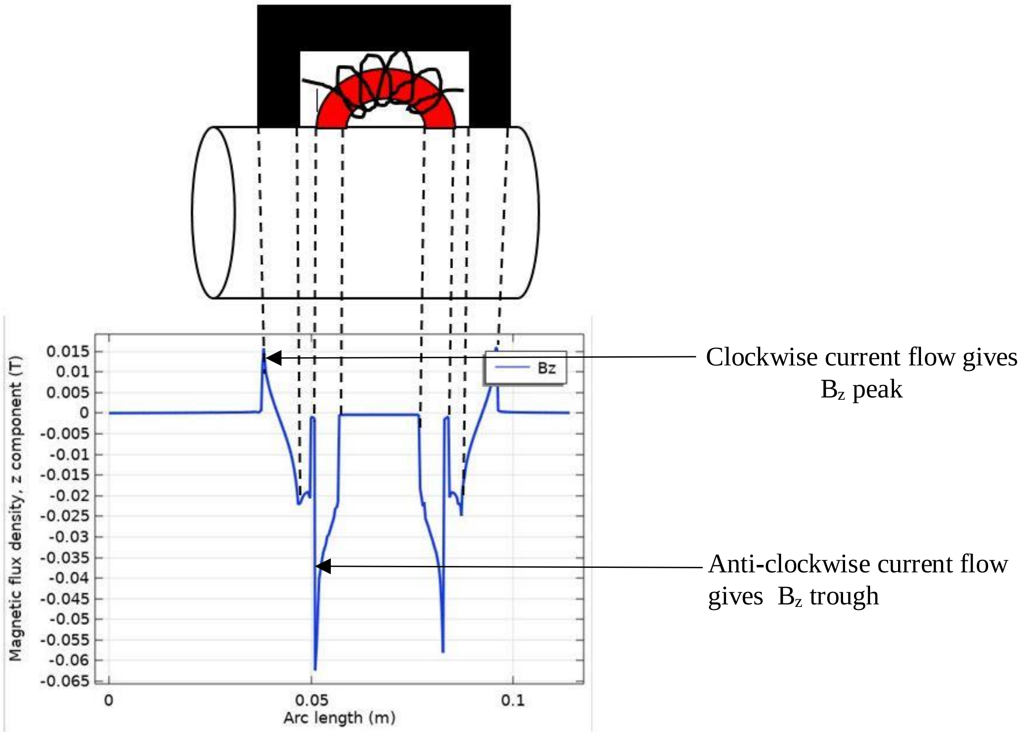

Figure 4.25. *B_z field component measured for the magnetic circuit*

The B_z component plot as in **Figure 4.25** clearly shows the magnetic flux path where clockwise current flow gives B_z peak and anti-clockwise current flow gives B_z trough.

Later the cut line was placed at various distances starting from the pipe surface and slowly penetrating into the pipe. The plot obtained for B_x and B_z component as in **Figure 4.26** and **4.27** shows the magnetic flux density of the cut line measurement at various distances starting from 57 mm till 80.5 mm on the surface.

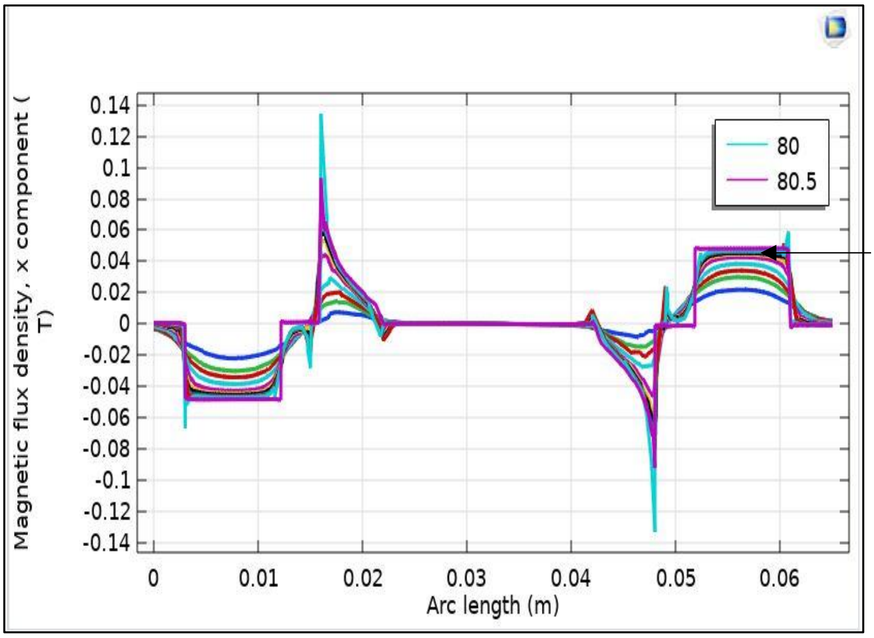

Each line signifies the distance from the surface of the pipe

Figure 4.26. *Magnetic Flux Density B_x component for cutlines 80 and 80.5 mm*

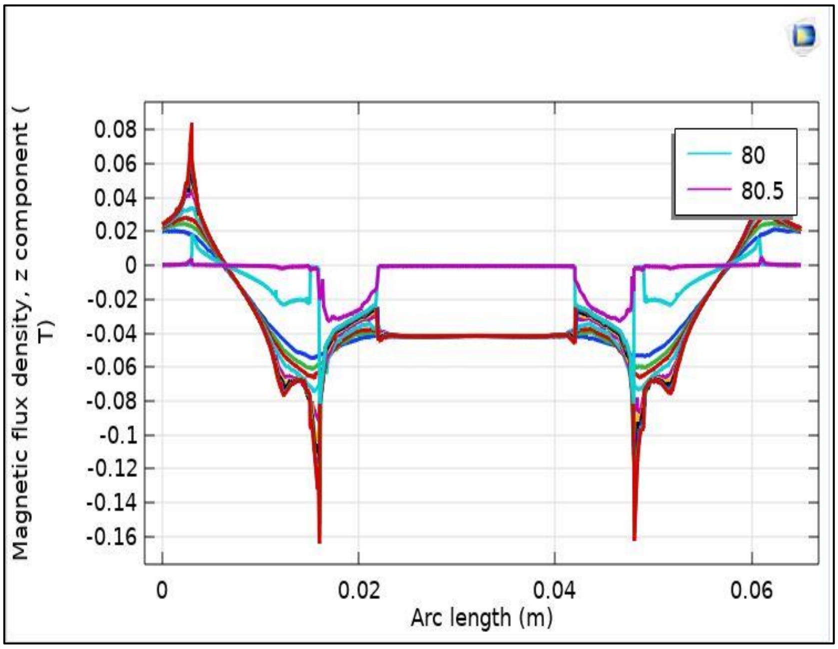

Figure 4.27. *Magnetic flux density B_z component for cutlines 80 and 80.5 mm*

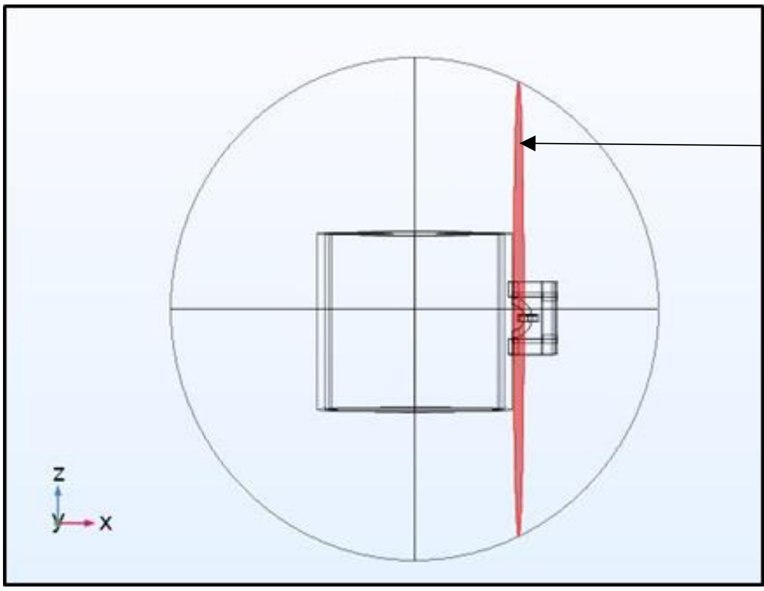

Figure 4.28* .*(a) *Cut plane passing horizontally through the magnet and the ferrite core in the xz direction*

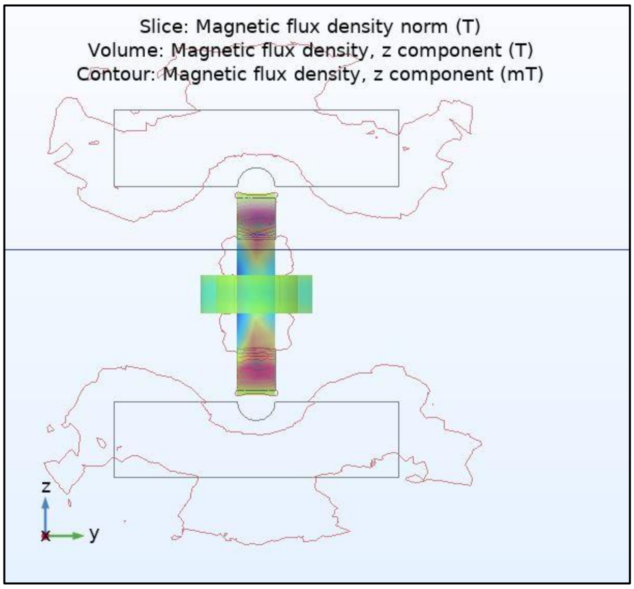

(b) *Contour plot showing the* B_z *component*

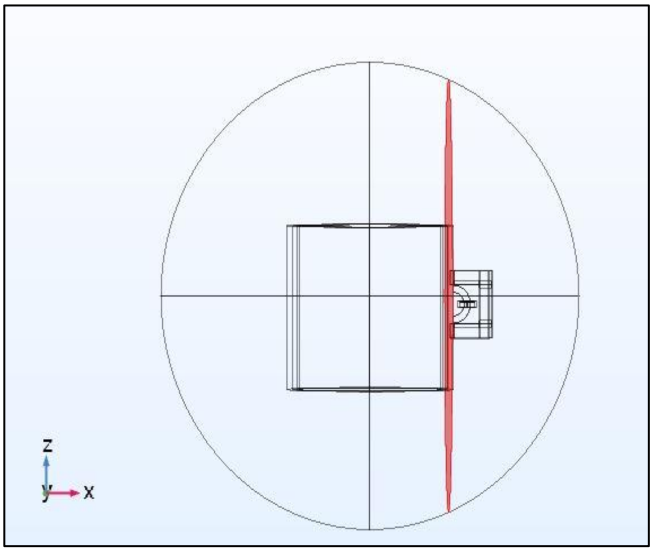

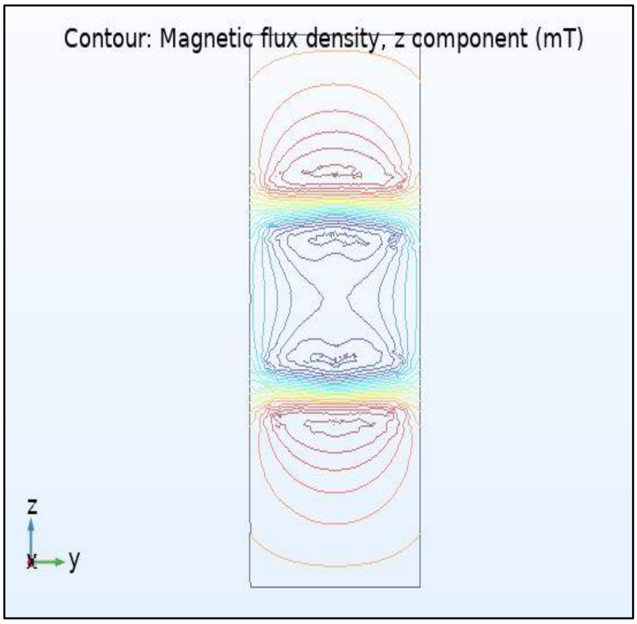

Figure 4.29. (a)*Cut plane passing horizontally through the magnet, ferrite core and pipe sample in the yz direction* ***(b)*** *Contour plot showing the B_z component*

The lines that are closer in the contour plot show the area where magnetic flux density is higher and the farther lines show the area where magnetic flux lines are the least as in **Figure 4.29(b)**. Coil impedance needs to be calculated for the ferrite core with the coil as it plays an important role where with each increase in frequency,the impedance is decreasing.

- From the coil impedance,the real part shows the resistance and the imaginary part shows the reactance.Coil impedance was obtained for frequency upto 50 kHz.

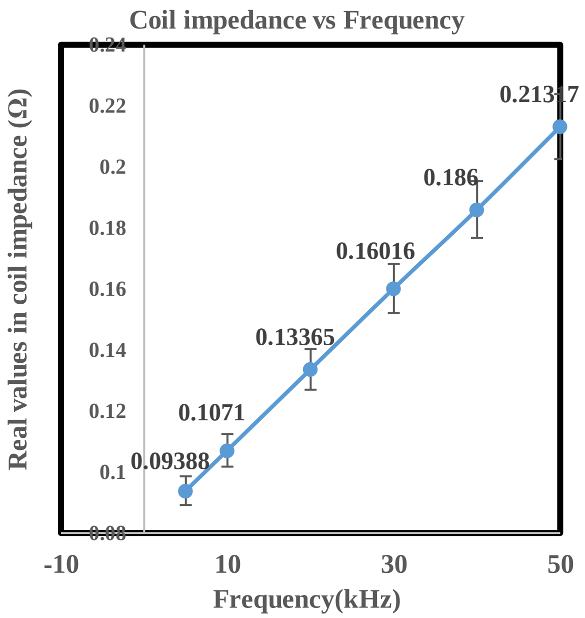

Figure 4.30. *Frequency vs Real values in coil impedance*

Figure 4.30 displays the frequency vs real inductance values where the real values in impedance increases with increase in frequency.

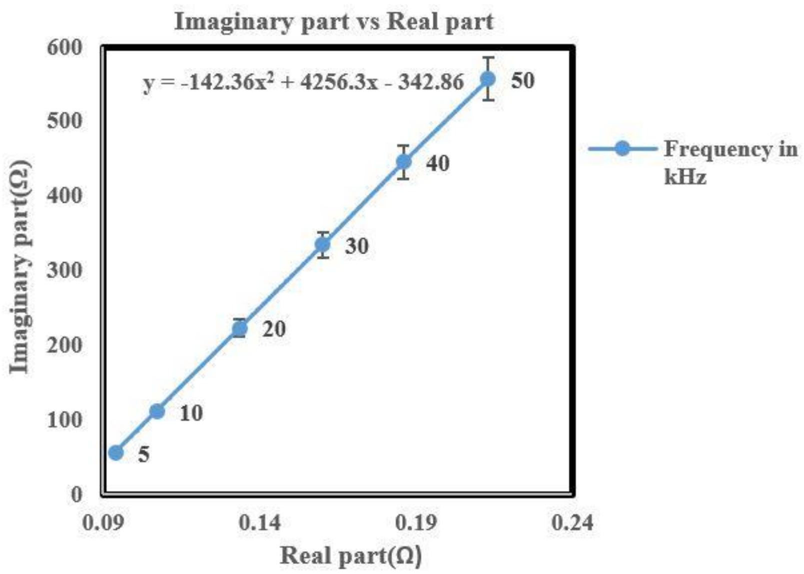

Figure 4.31 *Real vs imaginary part in coil impedance*

Real vs imaginary plot as in **Figure 4.31** was obtained using matlab coding which signifies the values increasing with frequency.

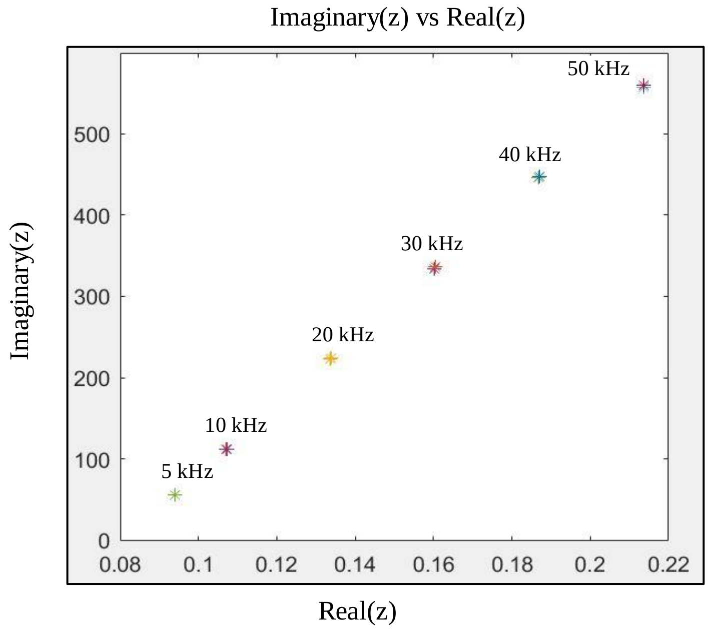

Figure 4.32*. Real vs imaginary plot upto 50 kHz*

Through the MFL coil sensor simulation, magnetic flux density was calculated for the measuring points placed across the pipe sample. For two varying pipe sample thicknesses (2 and 8 mm), the magnetic flux density was obtained. Only at the poles of the ferrite core, the magnetic flux density varies. B_z and B_x component shows a variation in magnetic flux density.

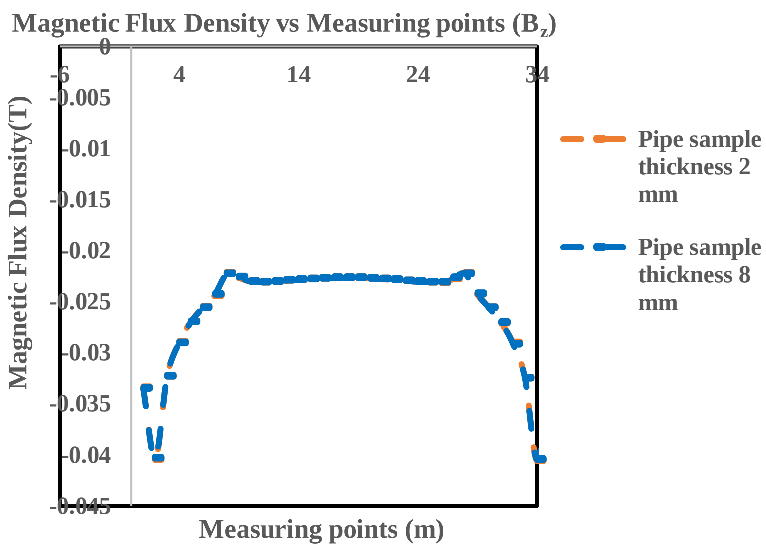

Figure 4.33. *Distance vs magnetic flux density for B_z component*

The middle portion in the plot in **Figure 4.33** shows the uniform magnetization area. At one end of the pole of the ferrite core,there is negative flux which is the trough and on the other side there is increase in magnetic flux which is the peak as in **Figure 4.34**.

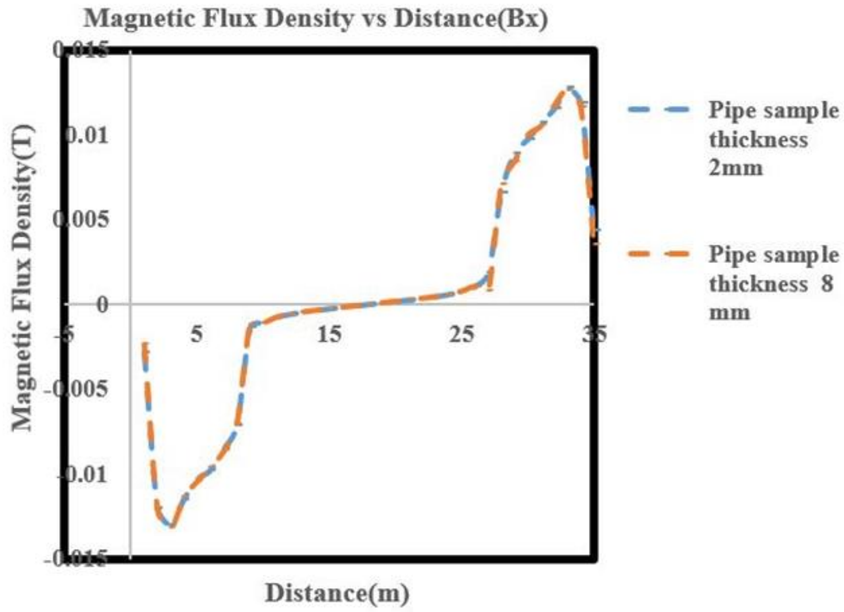

Figure 4.34. *Measuring points vs magnetic flux density for B_x component*

Figure 4.34 shows the magnetic flux density for all the measuring points on the surface for the B_x component.

4.7 Summary

This chapter focuses on the theoretical investigation of the magnetic circuit at room temperature conditions which involves determining the magnetic flux density components (B_x, B_y, B_z). FEA models were implemented for the calculation of the electromagnetic response of a MFL coil sensor at room temperature. Bx and Bz measurements which gives clarity of interpretation of the defect behaviour.

- The future development of this system will include quantitative characterization and fault calibration based on the combined results of Bx and Bz. The results obtained from this study show that this MFL coil sensor can propagate the signals in the right direction according to the literature. The same configuration was studied regarding its EM performance at high temperatures.

- However, the signal received is significantly weak and the effect of temperature rise on essential components and properties of ferrite core and pipe sample were taken into consideration.
- Consequently, the model provides a qualitative idea of the performance of the already existing technology at high temperatures. A detailed study of the coil structure and the thickness of each material was conducted in terms of MFL theory.
- FEA modelling provides a future scope of using array of sensors to detect defects especially corrosion in steel pipes which can be used for experimental testing. Also a sensor– sample system microstructure-permeability model was used to predict the magnetic flux density at room temperature. Therefore, an FE model to determine the magnetic flux density is essential.
- Also, based on the literature review, investigation on ferrite core (U and H-shaped) with active and dummy coil is done. The results obtained for a set of frequency determines the effect on the sample used.

Chapter 5
Underwater Experiments

5.1 Introduction

This chapter describes the specifications, experimental apparatus and procedures used for this work. First, the features and specification of apparatus that are common to both underwater and high temperature experiments performed are described, and then the details of each experiment are presented. The first experiment was a study of propagation of magnetic flux signals along healthy steel pipes of varying thicknesses at normal room temperature conditions and in air. The second series of experiments were the study of data transmission using RF technique underwater in corroded and non-corroded pipe samples of varying thicknesses and finally evaluation of the detection and source location capabilities for such sources. The third set of experiments involves the application of RFID on pipe samples and obtaining data underwater. All experiments were carried out at room temperatures using four pipe samples (2,4,6,8) of varying thicknesses. For underwater experiment, RFID technique is used for water to air data transmission.

5.2 Design of underwater system

Marine and industrial environments are highly corrosive and hence it is necessary to understand the stability of magnets in such environments. Condition monitoring has become essential in industries for the life expectancy of pipelines and equipment [70,73]. On an average, ocean water salinity equals approximately 3.5 percentage. Salinity is evaluated by determination of Cl^- ion concentrations in water. Corrosion rate increases, when water conductivity increases. According to EUROCODE3, corrosion rate of 0.08 mm/year corresponds to seawater in the zone of high attack. Corrosion of steel in water will increase from 2 to 4 % per 1.5 F(1ºC) increase [73]. Mild steels are not resistant against corrosion in a marine environment. Stainless steels have a high general corrosion in seawater due to their protective chromium oxide layer [73]. Copper and its alloys are resistant against general corrosion in seawater and also depends on the alloying elements and surface finish.

Underwater wireless communication links have up until recently almost exclusively been implemented using acoustic systems. Optical links have proved impractical for many applications for a variety of reasons. Although underwater radio links were experimentally evaluated in the pioneering days of radio, they were unable to meet the requirements within the stipulated time. Considering modern operational requirements and ready availability of digital communications technology it is now time to re-evaluate the role of EM signals in the underwater environment [73,74]. Two important factors to be considered with regard to this environment are temperature and pressure. Water to air transmission is quite a difficult task.

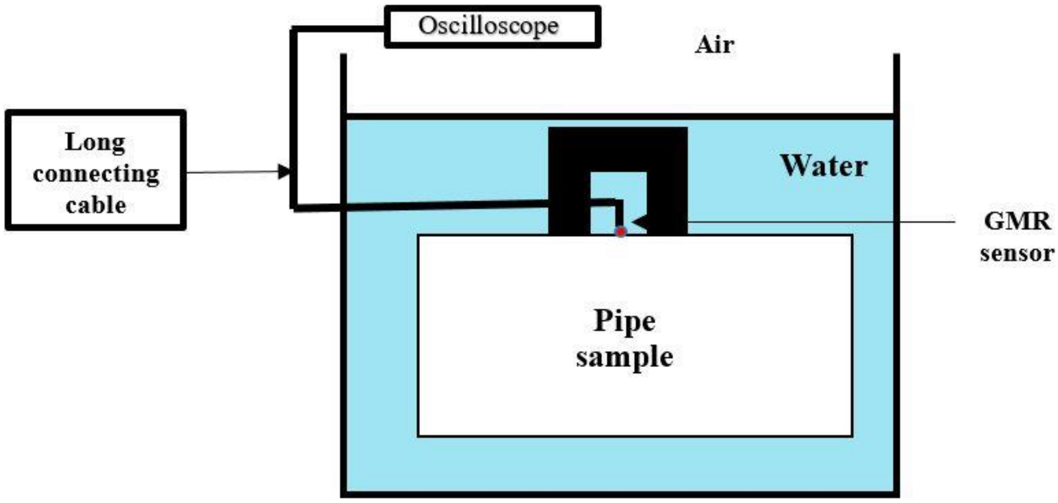

***Figure 5.1**. Schematic diagram of the experimental setup for data transmission underwater with wired sensor network solutions*

In that case, data transmission can be done using wired and wireless networks. The properties to be considered for transmission medium includes communication range, loss of transmission medium which includes the maximal transmission distance that it can propagate underwater.

5.3 Experimental set up and procedure with wired sensor network

The proposed experimental setup involves a magnetic circuit, an oscilloscope to obtain the varying signal voltages and the DC power source placed at room temperature conditions.

5.3.1 Room temperature MFL testing with GMR sensor

The magnetic circuit developed needs to be tested at room temperature first. The magnetic circuit that involves the permanent magnet, magnetic sensor is placed at a symmetrical position on the pipe sample. At normal conditions, the variations in signal output is to be obtained for varying thicknesses of pipe sample.

The magnetic sensor considered in this case is the GMR sensor. The 2007 Nobel prize in physics can be understood as a global recognition to the rapid development of the GMR, from both the physics and engineering points of view. Low cost, compatibility with standard CMOS technologies and high sensitivity are common advantages of these sensors. At room temperature, MR sensors are, generally, more sensitive than hall effect based ones, so avoiding the need of major amplification.

The existing GMR sensor circuit was developed using NI simulation 4.2 software and the results obtained are shown in the **Figure 5.2**.

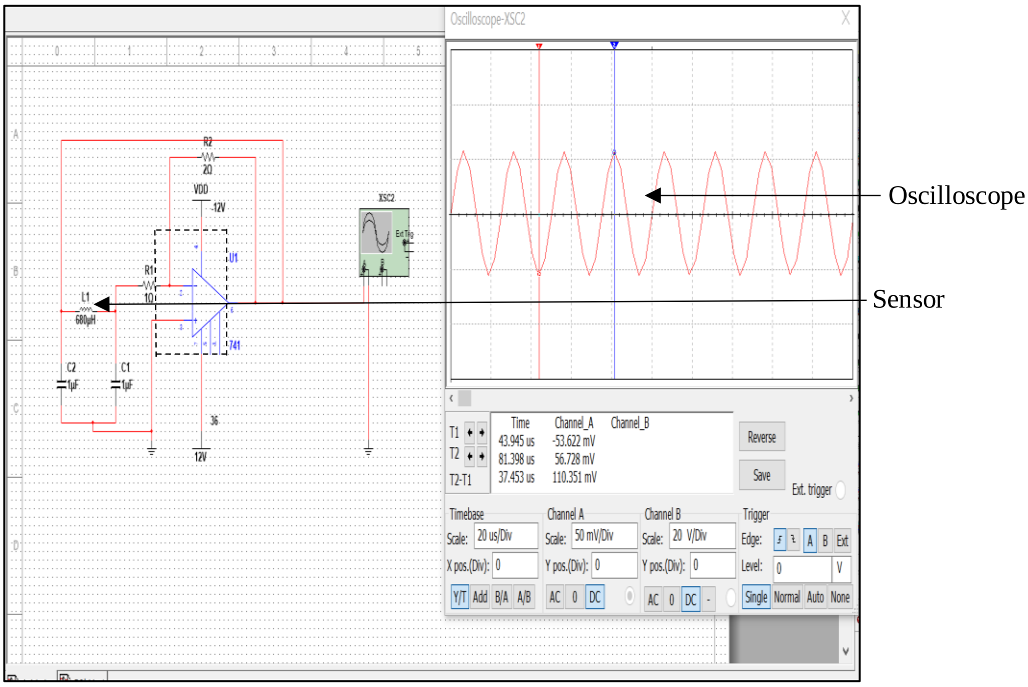

Figure 5.2*.GMR sensor circuit using NI multisim*

Two resistors are connected in parallel to the operational amplifier along with two capacitors. The oscilloscope is used to show the output signal.

5.3.1.1 Experiments conducted in air

Firstly, AlNiCo magnet as (Table 5.1) is placed at a centered position in the pipe sample of specified thickness and the GMR sensor as in (Table 5.2) is positioned in the middle according to the orientation of the magnet. The three connections start from the sensor with one connected to ground and the other two connected to input and output respectively. In the oscilloscope, the frequency changes occur as the sensor starts giving signals from the pipe sample. The data is obtained for various pipe sample thicknesses.

Table 5.1 displaying the specification of GMR sensor: AA002-02

Supply voltage (Volts)	Max-24
Maximum operating temperature(°C)	150
Maximum sensitivity(mV/VO$_e$)	4.2
Output at maximum field	60mV/V
Maximum hysteresis	4%

Table 5.2 displays the AlNiCo magnet characteristics [72]

Material	Red Alnico horseshoe magnet
Dimension	54x83x70 mm
Pull force	47 kg
Maximum operating temperature	500°C

DC Power supply: +/- 5V

PicoScope 2000 series oscilloscope: displays varying signal voltages, usually as a two-dimensional plot of one or more signals as a function of time. Four pipe samples (low carbon steel) of varying thickness (2,4,6,8 mm) were used for experiment. Permanent magnets used are

- Samarium Cobalt=24mm x 12mm x 6mmA - $SmCo_2$ - 4.56 Kg pull force
- Neodymium-Iron-Boron=24mmx12mmx7mm-Grade N42
- AlNiCo=48mmx20mmx25mm

Procedure

First the magnetic field of the pipe samples was measured with GMR Sensor in air with the (Neodymium-Iron-Boron (Nd-Fe-B), AlNiCo, Samarium Cobalt (Sm Co)) permanent magnets using gauss meter which has a hall probe in it. While AlNiCo and Nd-Fe-B magnets were strong enough, Sm Co was brittle and got broken while the experiment was conducted.

Although there is a strong evidence of literature review that samarium cobalt magnet works efficiently upto a temperature of 300ºC without coatings, its brittleness is a disadvantage. AlNiCo magnet has the highest corrosion resistance and it is considered for underwater testings.

The magnetic sensor is placed at a specified distance between the two poles of the magnet. Pipe samples before testing and after corrosion are shown in the **Figure 5.3 and 5.4**:

Figure 5.3*. showing the non-corroded samples*

Figure 5.4*. showing the corroded pipe pipe samples*

Figure 5.5*. showing the rusted Nd-Fe-B*

Figure 5.6*. showing the damaged magnet*

Saltwater conducts electricity more efficiently than freshwater. With the increase in salt concentration the impact of magnetic field is also increasing which results in an appreciable decrease in the electrical conductivity. The decrease in electrical conductivity causes the metal to get rusted.

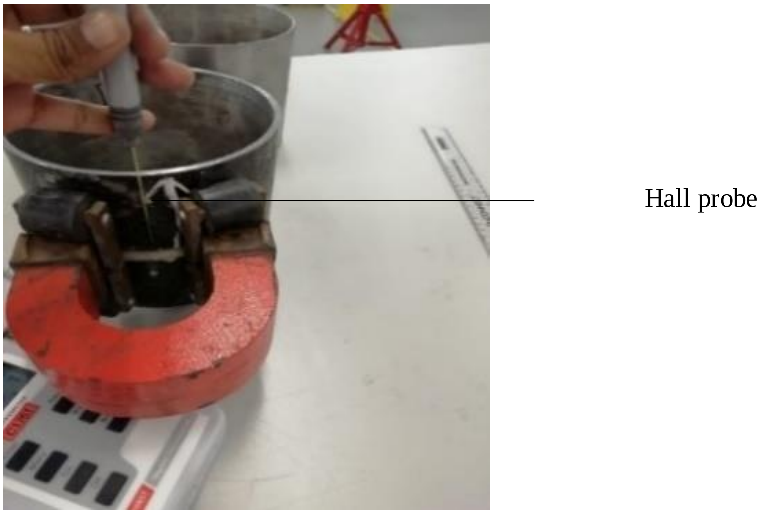

Figure 5.7. *Pipe sample tested with Nd-Fe-B magnet using gauss meter*

Figure 5.8. *Pipe sample tested with AlNiCo magnet using gauss meter*

Figure 5.9. *Pipe sample tested with Nd-Fe-B, AlNiCo and Sm Co magnets using gauss meter*

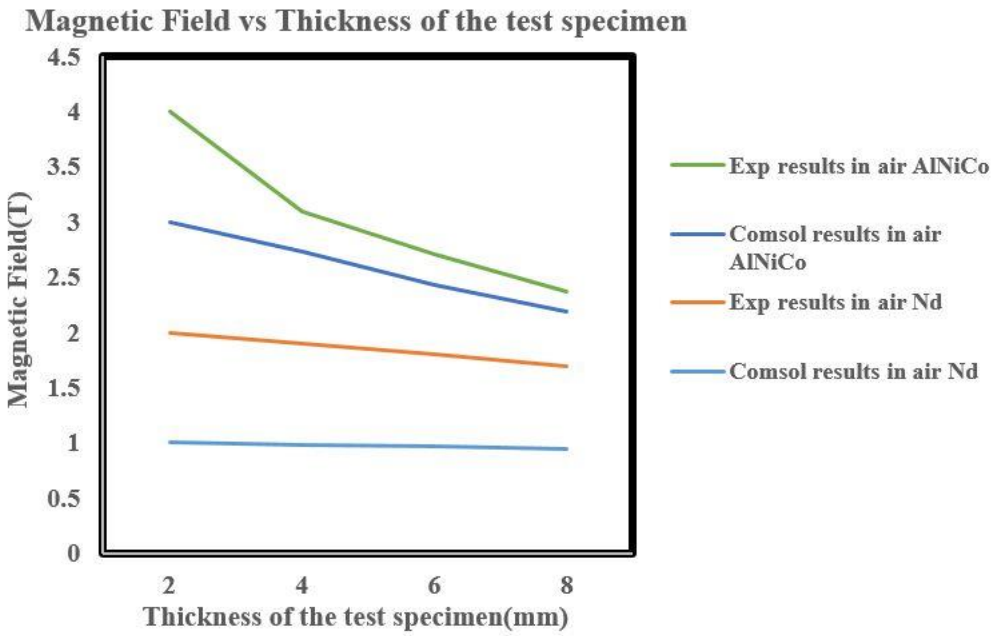

Figure 5.10. *Plot showing the comparison of COMSOL and experimental results of Nd-Fe-B and AlNiCo magnets in air*

Nd-Fe-B magnets show higher magnetic field when compared to AlNiCo in both simulation and in testings. With results compared at room temperature conditions, Nd-Fe-B magnets show greater effect in terms of magnetic field.

From the results obtained, it can be concluded from the above plots that compared to AlNiCo magnets, NdFeB show better results.

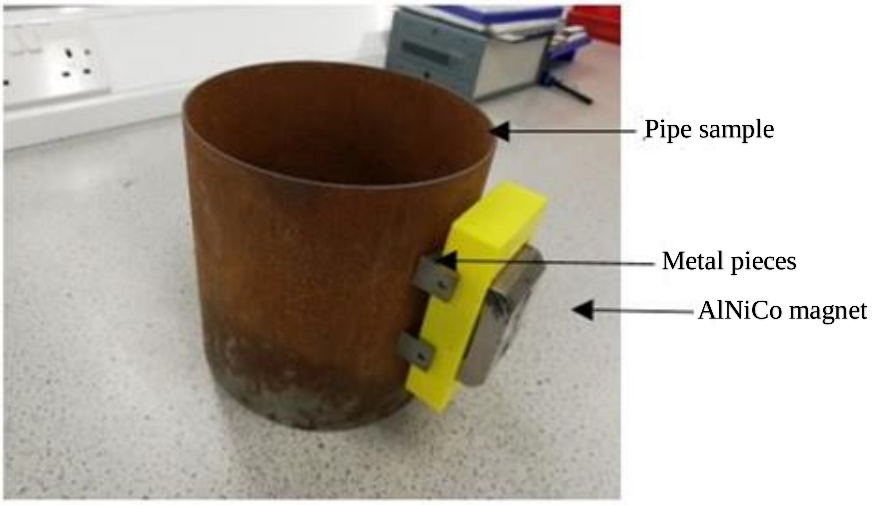

Figure 5.11. *The schematic diagram of the magnetic circuit*

The holder was designed using Autocad software with 3D Dremel Digilab software as in **Figure 5.11**. The design of the holder involves a small slot for positioning of the sensor and two larger slots for seating of the magnet poles with four holes, each drilled on the corners for the wires to pass through. The sensor placed inside the slot is fixed in a position based on the magnet orientation and the readings are obtained accordingly.

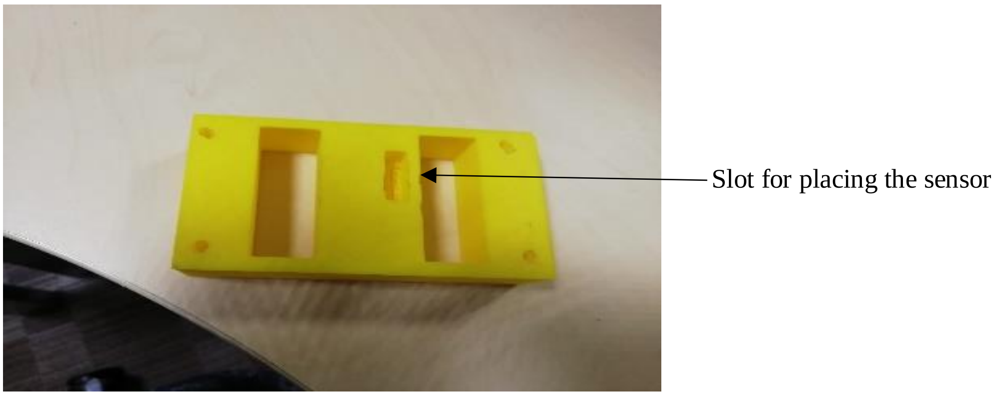

Figure 5.12*. Holder designed using for holding the magnet and positioning the GMR sensor*

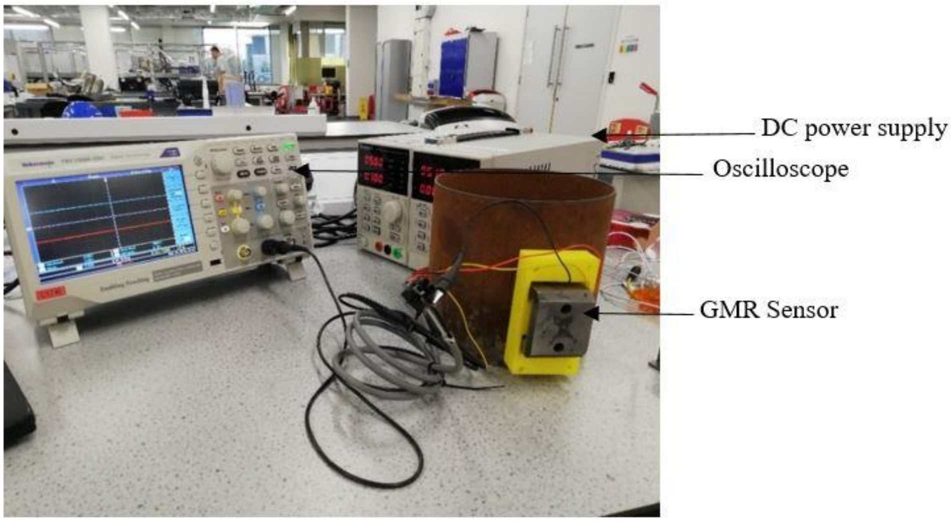

Figure 5.13*. The real setup involving magnetic circuit modelled with pipe sample of thickness 8 mm*

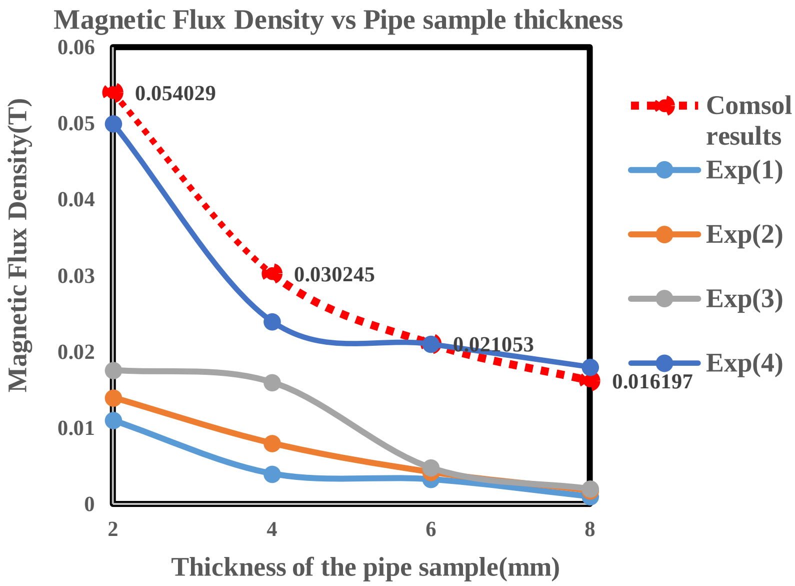

Figure 5.14. *Plots showing the comparison between COMSOL and experimental results*

The experimental results obtained were compared with the COMSOL Multiphysics simulation results. There is a slight variation between the experimental and simulation results obtained due to lift off that is shown in the above plot as in **Figure 5.13**.

5.3.2 Underwater MFL testing

Constantly used under water, the pipe samples and the Nd-Fe-B magnets got rusted as shown above as in **Figure 5.5** and **5.6**. The magnetic properties affect significantly when the magnets are corroded. Based upon the literature review conducted, Nd-Fe-B magnets have less corrosion resistance compared to AlNiCo magnets.

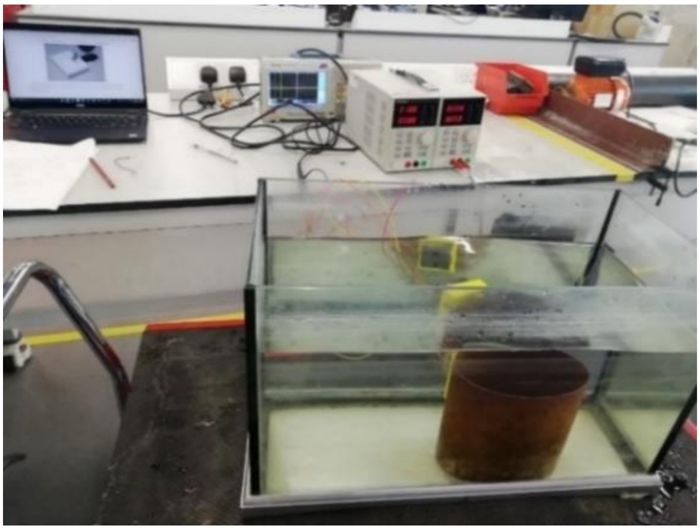

Figure 5.15. showing the experimental setup for underwater testing

5.3.2.1 Experiments conducted in air and freshwater with AlNiCo magnet

Testing was conducted with freshwater first and then the magnetic circuit deployed under seawater again as in **Figure 5.14**. The experimental and comsol results were obtained accordingly. The variations in the plot indicates the change in electrical conductivity between the fresh and seawater. The electrical conductivity of seawater is four times higher than that of fresh water.

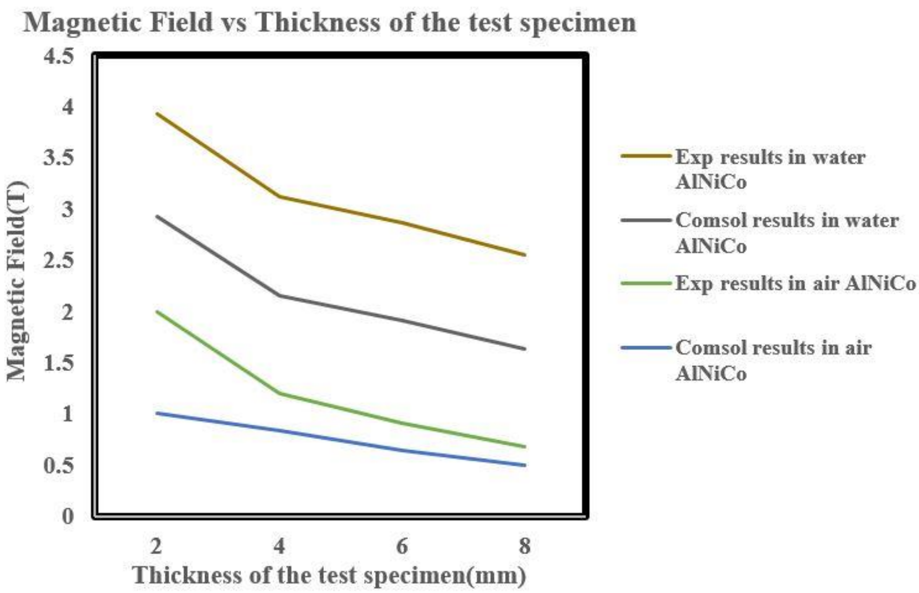

***Figure 5.16**. Plot showing the comparison of COMSOL and experimental results of AlNiCo magnet in air and underwater*

Testing was also conducted by varying the depth of the magnetic circuit underwater with two varying pipe sample thicknesses 2 and 8 mm respectively as in Figure **5.15**.

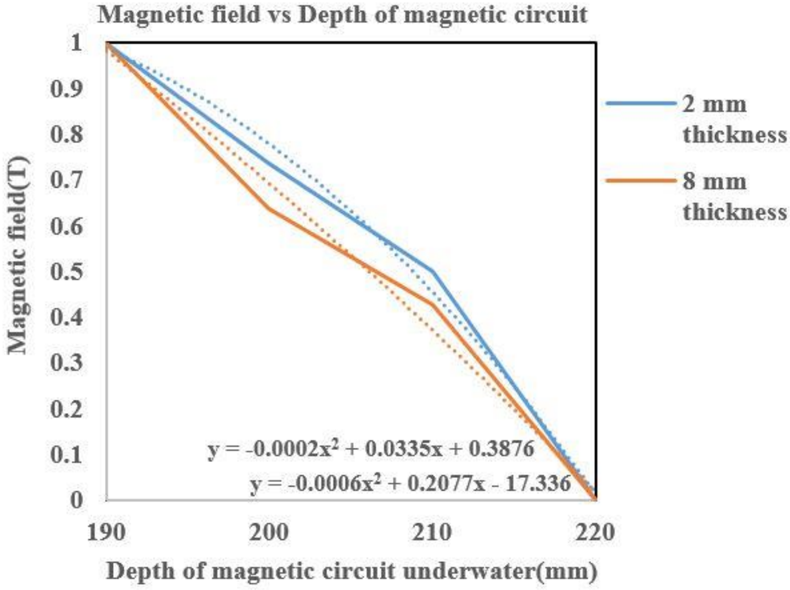

Figure 5.17. *Magnetic Field vs Depth of magnetic circuit*

The comparison of the 2 and 8 mm thickness pipe sample for under water testing is shown in **Figure 5.16**.The above plot concludes that as the depth of the circuit increases,the magnetic field decreases.

5.4 Data transmission using RF technique in air for various thicknesses of specimen

Anguito etal.,2009[70] presented an overall review of the different types of data telemetry in the aquatic environment. This research mainly focusses on the effects of EM propagation in the aquatic environment, the impact of wavelength on increasing frequency and highlights the degree to which wavelength is shortened under free space, fresh and seawater [68-70]. They conducted experiments and have also concluded that there is variation in key parameters against frequency for representative fresh and sea water conductivities. The research work that can be carried out is with propagation distance of EM radiation underwater. This article by [69,70], is concerned mainly with the transmission characteristics of radio waves underwater. The extent to which the radio amateur might make use of these characteristics and also includes the examination of the transmission options for what was lowest amateur RF (1.8MHz) when the article was first published. In detail, he has concluded that radio communication under the sea is not an attractive option for experiment by the radio amateur as it requires the use of very low frequencies [122], large antenna systems and very high powers. An option would be to conduct experiments with lower frequency band with larger distances. The experimental set up for data transmission with wireless sensor network includes the magnetic circuit, GMR sensor/hall effect sensor, an arduino micro-controller and a RF transceiver [78-80].

Primarily testing were conducted with GMR sensor by moving the magnet and the sensor along an axial line over the non-corroded pipe samples of varying thicknesses. With an interval step of 10 mm distance, the readings were obtained accordingly through the arduino software. Later on, the same testing was carried out for corroded pipe samples. The experimental set up was repeated for testing with hall effect sensor as in **Figure 5.17**. The results obtained clearly indicates that hall effect sensor has a better accuracy than GMR sensor.

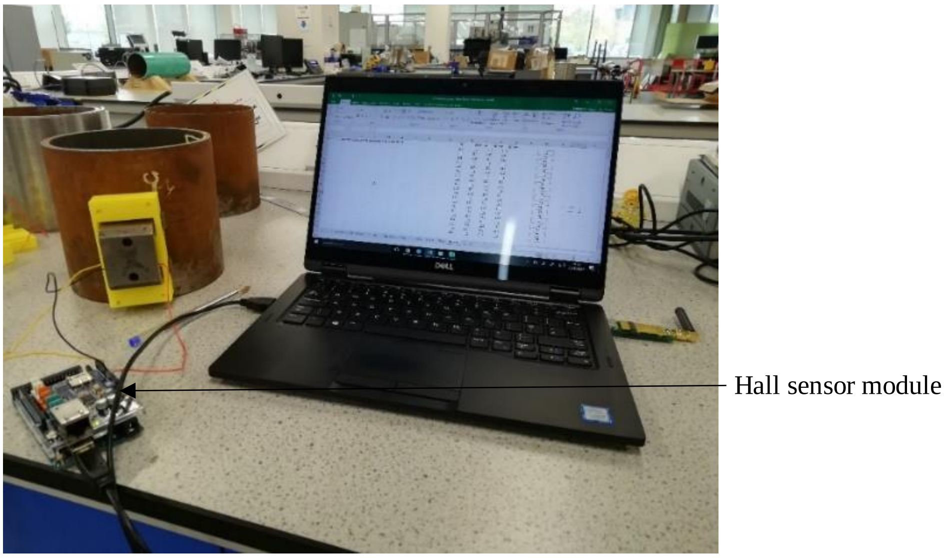

Figure 5.18*. The real set up for data transmission involving the magnetic circuit*

5.4.1 RF transceiver with hall effect sensor module

Figure 5.18 shows the signal comparison of the four pipe samples of various thicknesses. Of the four pipe samples, 2,6,8mm samples are corroded and 4 mm pipe sample is non-corroded.

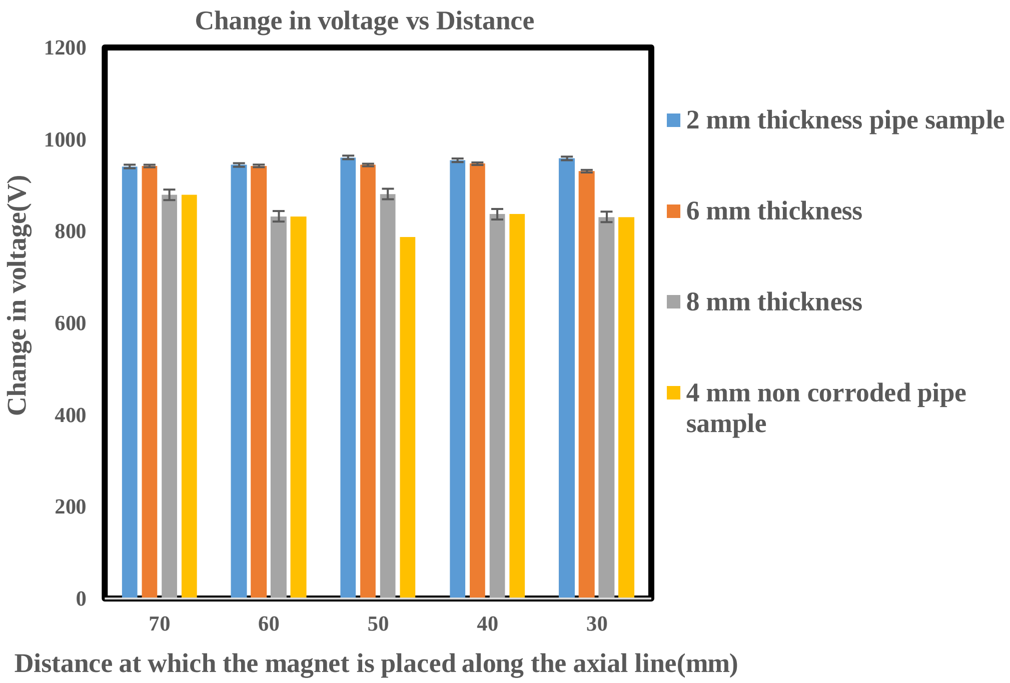

Figure 5.19. *Change in voltage vs Distance*

From the above plot, it can be concluded that with increasing distance, 2 mm pipe sample thickness is showing greater significance in terms of data transmission.

5.4.2 Data transmission using RFID technique underwater

Although radio communication under the water is not an attractive option for experiment, it requires the use of very low frequencies, large antenna systems and very high powers as it has certain gap in research that is described as follows:

A detailed description of the relationship between several propagation parameters of EM waves for underwater communication are studied. This includes skin depth, propagation velocity, total path loss, wavelength and frequency for different values of distance and conductivity of the water medium [71,78,119]. They confirmed that EM wave propagation is characterized mainly by four parameters: permeability, permittivity, conductivity and volume charge density.

In RF communications, researchers work with very low frequency (VLF), decreasing the frequency in order to have a more effective range of communication. Concretely, some researchers of the Swansea Metropolitan University, U.K., performed their simulations at 3 kHz and distances between nodes of about 40 meters [68,70,121]. In Frater et al.,2006 [69,74] compared RF and acoustic communications and measured the maximum distances for RF. The paper shows the maximum distances for several frequencies (approximately 6 m at 100 kHz, 16 m at 10 kHz, and 22 m at 1 kHz). They concluded that RF communication offers higher performance than acoustic communication in certain ranges.

5.4.2.1 RFID tag and RFID reader

RFID can be used for pipeline condition monitoring. RFID tags that works on radio waves needs to be attached to the pipe sample to be monitored, it is within the range of the reader.

RFID systems are widely used for quality control where inspections are required to test the quality of products located at number of stations. Apart from that RFID is used for system and data security as well. RFID system is suitable for harsh environmental conditions as they are insensitive to dust, moisture, oils, coolants, cuttings, gases, high temperatures and similar problems that can occur in a manufacturing environment. Glass and plastic transponders usually comply with protection type IP67; that is, they are totally dust and waterproof.

Passive transponders, i.e. transponders that do not have their own power supply, are supplied with energy via the RF field of the reader. To achieve this, the RF interface draws current from the transponder antenna, which is rectified and supplied to the chip as a regulated supply voltage.

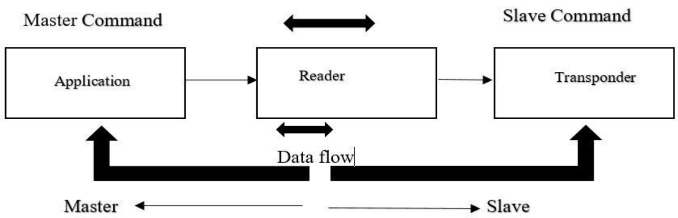

Figure 5.20.*Working principle between application software,reader and transponder*

RFID works on the concept of EM induction. Backscatter is a phenomenon that occurs in passive RFID tags in which a shift in the EM or RF wave is detected by the reader (via the antenna), which then interprets the data [6].

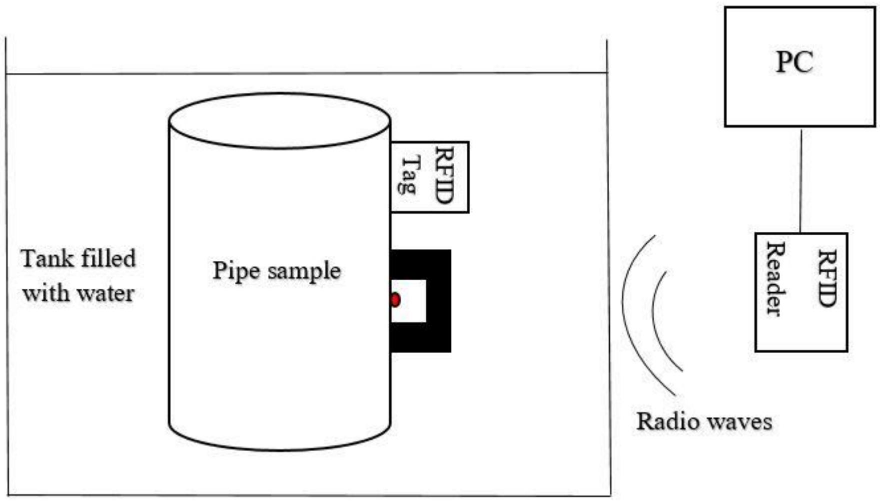

Figure 5.21. *Schematic diagram of data transmission with RFID underwater*

RFID transponder follows back scattering mechanism where the signal send by the reader is received by the transponder which in turn sends back the signal to the reader as in **Figure 5.20**.

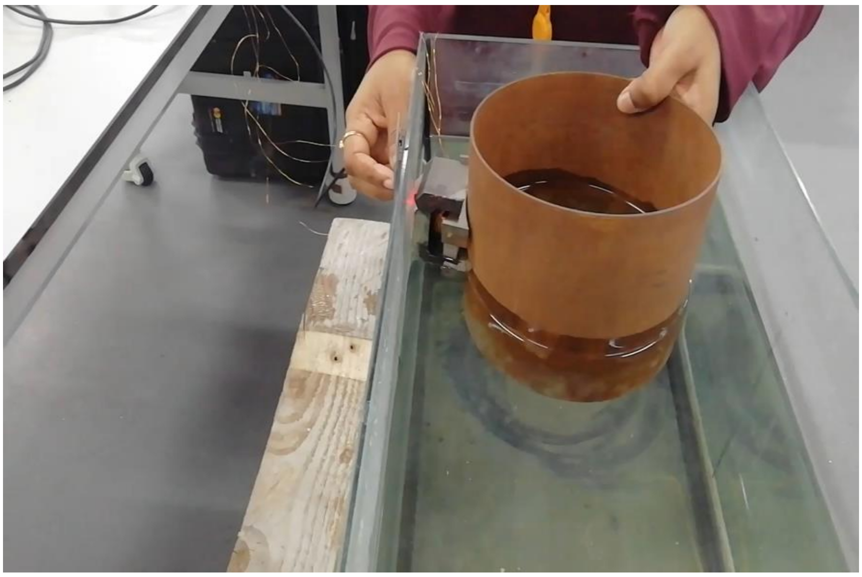

Figure 5.22. *Data transmission with RFID underwater*

5.4.2.2 Experiments conducted at various ranges

Premilinary testings were conducted with RFID reader with readable only RFID tags as in **Figure 5.21**.Measurements were taken for different environmental conditions which includes the following as in Table 5.3.

Table 5.3 Specification of the components and measurement ranges

Tag-type	Frequency kHz	Air cm	Fresh water cm	Salt water cm
PPS + Epoxy	125	10	5.0	3.0
ABS	125	5.5	5.3	5.1
Nylon	125	4.6	4.2	4.1
PVC disc	125	4.9	3.6	3.3
Plastic	13.56 MHZ	1.2	5.0	4.0

5.5 RFID communication

Communication is a key issue where existing terrestrial wireless sensor network implementations have relied on EM waves so far. Underwater sensor data could be collected in certain ways using wireless sensor networks: (1) with an autonomous robot acting as a communication link using short-range optical communication, and (2) with a node-to-node acoustic communication network [111]. Some issues, such as power availability, deployment, and repair, are typical in land-based wireless sensor network deployments, but they are more difficult to address in the underwater environment [111].

RFID technology is used in a variety of sectors, including manufacturing, agriculture, transportation, and industry [111]. As a result, the majority of research into the possibility of interacting underwater using EM fields is concentrated in the marine environment. Compared to other communication techniques, RFID is omnidirectional which is its major advantage. Due to the fact that EM fields are greatly affected by water, particularly saline water in an underwater environment, RFID, as a radio-frequency technology, has only one drawback i.e. the range of data transmission. RFID readers can read several tags simultaneously, store more data on the tag and it can be manipulated [4, 5]. The cost of implementing RFID technology is also decreasing, making commercial implementation with a higher Return on Investment (ROI) more feasible. RFID tags are mainly used for identification of physical objects and store an ID called an Electronic Product Code (EPC) in the tag [109]. In this case, a specific technological solution was investigated in order to enable the device to function properly even when submerged in water.

5.5.1 RFID Technology

When a longer read range, quick scanning, and versatile data carrying capability are needed, RFID technology is more efficient. RFID is also one of the most widely used automated object identification systems, with applications such as access control, object tracking, and detection of humans and animals. In any case, there are only a few applications where RFID is used underwater. RFID has a fast reading speed and can operate in the presence of a barrier [107,109].

5.5.2 RFID systems

A transponder and a reader make up an RFID system. Transponders are divided into three categories: active, semi-passive and passive tags. Active RFID tags can communicate over longer distances than passive tags as it uses its own power supply. An active RFID system works on two main frequencies-433 MHz and 2.45 GHz. Semi passive tags are a combination of the characteristics of active and passive tags [109]. Unlike active tags, a RFID reader sends a signal to passive tags. The reader sends energy to the transponder's antenna, which transforms it into an RF wave that is sent into the reader's range. When the RFID tag is read within the reader's range, the energy from the RF waves is used by the tag's internal antenna as described in **Figure 5.23**. In terms of power supply, a passive transponder has an advantage over other transponders. It gets its power from the reader, while active and semi-passive tags need to be charged by a battery [107,109]. Active and passive tags are more prone to industrial applications.

A passive tag is one that lacks a battery and is regulated by the reader. The coiled antenna inside a passive RFID tag generates a magnetic field as it comes into contact with radio waves from the reader [7]. The tag draws strength from the reader, which powers the tag's circuit.

RFID implementations use a variety of frequencies, including 125 kHz, 13.56 MHz, and 860-930 MHz for passive RFID; 433MHz and 2.45GHz for active RFID. The following is a list of RFID standards: ISO 10374, ISO 10536, ISO 11784, ISO 14443, ISO 15693, IS0 18000, EPC global [9,10]. The correspondence between an RFID reader and a tag is controlled by these requirements. These standards operate on specific frequency bands (e.g., UHF 860–915 MHz or HF 13.56 MHz) [107,111].

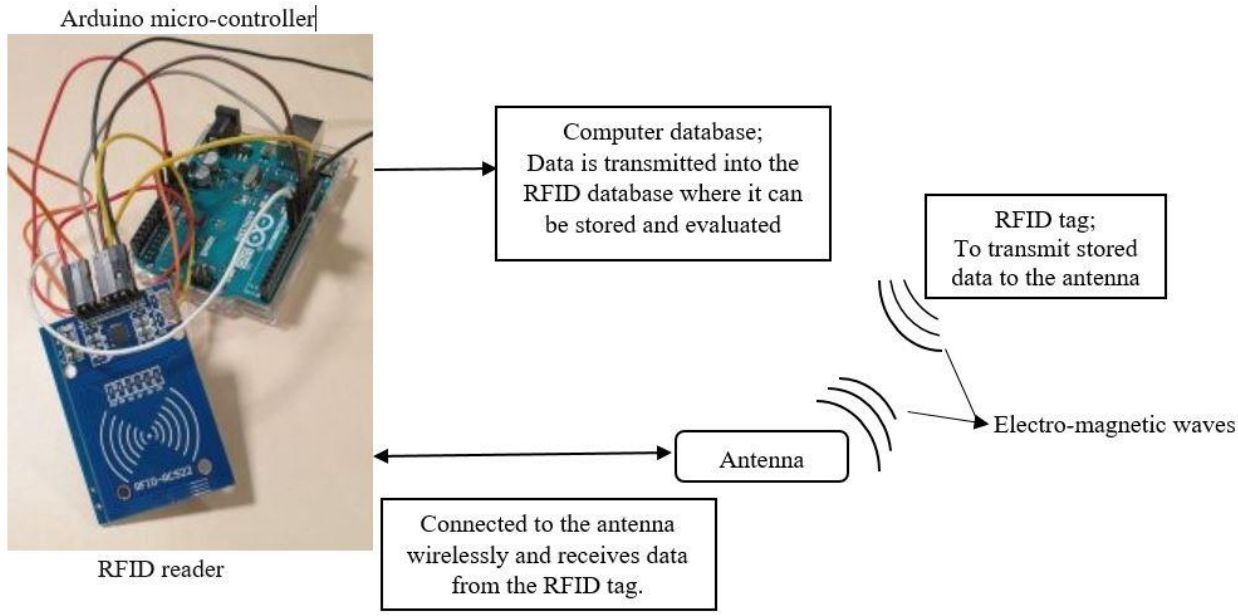

***Figure 5.23**. RFID system*

Two magnetic fields have a lot of significance, and their frequency varies. They are as follows: near field and far field. Near field uses a method similar to transformer, and employs inductive coupling of the tag to the magnetic field circulating around the reader antenna [12].

Far field, on the other hand, uses a method similar to radar backscatter reflection by coupling with the electric field [13]. The distinction between the RFID systems with far fields to the near fields is that the near fields use low-frequency (LF) and high-frequency (HF) bands [12, 14]. While RFID systems with far fields usually use longer read range ultra-high-frequency (UHF) and microwave [7, 12].

5.5.3 Underwater communication using RFID

For underwater applications, only two RFID technologies are available: high frequency systems operating at 13.56 MHz and low frequency systems operating in the 125-134 kHz range [4]. Since EM waves cannot pass through electrical conductors, RF waves can only be used to communicate underwater for close ranges. While the conductivity of water cannot be changed to increase the probability of using radio waves underwater, the only variable that can be changed is the RF [15]. Investigations have shown that the ability to transmit radio signals underwater is primarily determined by two factors: water conductivity and radio wave frequency. When RFID-based sensing is tested with a metal in a marine setting, the reading distance between the tag and reader is significantly reduced [15, 16]. Furthermore, the sensing region of RFID-based sensing is determined by the size of the tag's coil.

5.5.4 Underwater radio waves

Pure water is an insulator, but the presence of dissolved salts or other materials in natural water turns it into a partial conductor. Attenuation depends on the conductivity of water and from the frequency of the radio wave. In particular, it grows with the increase of both conductivity and frequency, and can be calculated as [4]:

$$\alpha = 0.0173\sqrt{f\sigma} \tag{5.1}$$

$$\alpha = 0.0173\sqrt{(13.56 \times 10^6 \times 4)} = 127.41 \text{ dB/m}$$

The value obtained shows the attenuation for a frequency of 13.56 MHz and an electrical conductivity of 4 S/m. Where, $\boldsymbol{\alpha}$ denotes attenuation , **f** denotes frequency in MegaHertz, **σ** denotes electrical conductivity in S per meter.

In general, a tag may be put anywhere as near as possible to the reader's antenna range. Since the RFID method is used in salt or fresh water, there are several variations. Starting with saltwater, the calculations show that for systems requiring a long reading distance, only low frequency RFID can be used (over 50 cm). At a frequency of 125 kHz, the average penetration depth (using a salinity of 4 S/m) [4] is

$$\Delta_{13.56\text{MHz}} = \frac{1}{\sqrt{\pi f \mu \sigma}} = \frac{1}{\sqrt{(\pi \times 13.56 \times 10^6 \times 4\pi \times 10^{-7} \times 4)}} = 0.0683 \text{ m} \tag{5.2}$$

Where, Δ denotes average penetration depth, μ denotes relative permeability. This value is just below a low frequency device's maximum reading range, which is usually less than 1m. Once the water conductivity value has been determined, the penetration depth and attenuation values can be calculated. This means that low-frequency RFID could be used to distinguish underwater objects. While at lower conductivity values the realization of an efficient long range RFID system could still be possible, when the water conductivity grows the penetration depth drops down to values [4] that make this solution difficult to be implemented or even totally impossible. The chance to use high frequency(HF) RFID in particular environments like rivers or lakes has to be carefully evaluated case-by-case [4]. As the frequencies increase, these instruments become almost impossible to use for long-range detection. The calculation of penetration depth yields an extremely low value as in equation 5.2.

5.5.5 Underwater RFID

RFID technology has been used to monitor pebbles underwater, with displacement playing a key role. Parks et al. [14] used three types of transponders to read the range of the pebbles in the device. To determine the reading range, tests were performed under a variety of conditions, and passive transponders were inserted into pebbles, with a core 125 kHz reader selected to transmit EM waves to the transponder [10]. An acoustic signal was toned when a pebble was detected, and the pebble's unambiguous identification code was displayed on the screen of a portable laptop connected to the reader [14, 15]. The position of the pebbles was recorded using a complete station. Since the latter was given attenuation, the best results were obtained with a 125 kHz system rather than a 13.56 MHz system. Because of the reduced reading range, high-frequency systems operating at 13.56 MHz have certain drawbacks. For common desktop antennas, the reduction in range can be up to 80%, requiring the transponder to be attached to the reader antenna. For low-frequency systems operating in the 125-134 kHz band, the reduction is lower (around 30%), and a 50 cm reading range can still be achieved with longer range antennas [4]. Some attempts have been made to use HF systems (13.56MHz), which are the most common and present the widest choice of devices available in the market. In particular, the authors have conducted experiments using a common Universal Serial Bus(USB) HF reader in order to evaluate the reduction of the read range with both the devices (the reader and a transponder) located under water [5].

5.5.6 Advantage of RFID technique underwater

Passive transponders are found more suitable for underwater application due to their larger range of detection. The technique is particularly valuable because it allows to research movement of single elements [115,117] in natural environments within fixed period of time compared to normal RF systems. RFID provides reliable data and takes less time to process than other RF techniques. Furthermore, the RFID technique has been found to be more appropriate for data transmission over short distances. Other advantages of RFID include its cost-effectiveness and ease of use of off-the-shelf hardware, and its increased efficiency [117].

5.6 Sensor data storage using RFID underwater

The concept of data-on-tag has been used in production control and maintenance documentation in manufacturing, tracking patients and medical equipment in healthcare [115]. In one example, additional information for garments was stored in the tag [111-113]. RFID transponders offer a more comprehensive data storage capacity [113-115]. There is a necessity for a system to collect and store the data send by the GMR sensor. For monitoring corrosion in pipes underwater, the data needs to be retrieved later and a backup is required. For monitoring corrosion in pipes at normal environmental conditions, MFL coil sensors were effectively used. For extreme temperature conditions, (ferrite core) MFL coil sensor proved to be highly efficient up till 200°C. RFID system provides data accuracy and also involves shorter processes. The data sent by the GMR sensor must be stored in order to detect corrosion. The RFID system ensures data integrity while also reducing the time it takes to complete tasks. The tag functions like a USB where the data gets stored [113]. The amount of information to be stored inside the tag depends on the type of tag to be used, and the storage capacity of each RFID tag varies.

5.6.2 Design of the system

Two different types of underwater environments were considered for the study. The first was freshwater, which involved immersing the RFID tag in a small tank filled to a certain level with water and the RFID reader placed outside, as described in **Figure 5.24**. Transponder waterproofing is important for many applications, and many devices have been developed that provide a high level of protection against water contact. While wristbands have been customised to be worn in the bath, plastic tags are waterproof by nature [109,114]. However, none of these devices are intended to be read underwater and are only designed to survive water immersion. Moreover, no reader has ever been planned for use underwater. The specifications of the equipment used are as follows: RFID Reader, Tag – 28340, range of the tag = 125-134 kHz, maximum supply voltage 5.5 V. The RFID tag can be mounted anywhere within the tank that is within the reader's range. Table 5.3 displays the specifications of the components used for testing at underwater conditions.

Table 5.4 Specification of the components

Component	Operating frequency	(app)Range
RFID Tag-28340	125-134 kHz	2-8 mm

RFID tag mifare1 S50	13.56MHz	8-10 mm
RFID reader/writer-MFRC 522	13.56MHz	

5.6.1.1 The readable transponder

With a frequency of 125 kHz, the RFID reader used in this experiment reads passive RFID transponder tags. When the RFID reader starts monitoring, it turns red, and when it is idle, it turns orange. With a maximum supply voltage of 5 volts and a data rate of 2400 bits per second, the RFID reader is a powerful device. Using the experimental setup, the effective reading distance between the tag and the corresponding reader is measured directly. At a distance of 2 millimetres between RFID tag and reader antenna, signals (ID number) were obtained, with a maximum distance of 8 millimetres measured.

Following initialization, the reader sends an EM (radio-frequency) signal to the tag to energise it every 500 milliseconds during a reading time, obtaining the tag's ID number [118,119]. Regardless of any position the RFID tag can be scanned as long as it is within the range of the reader as in **Figure 5.24** and **5.25**.

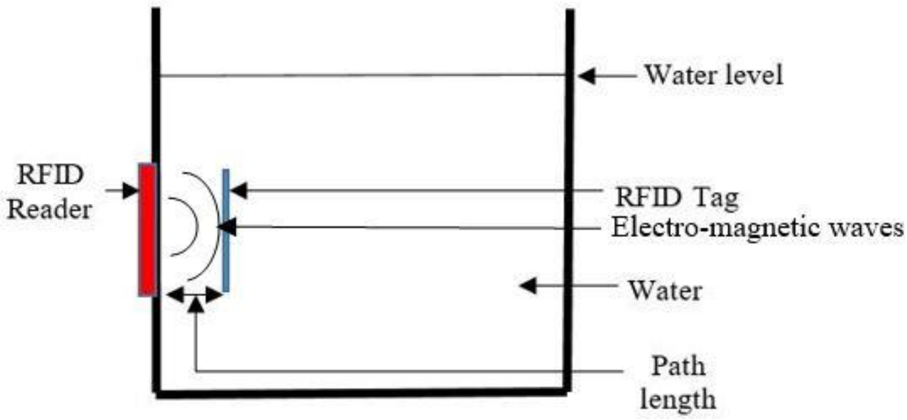

Figure 5.24. *Horizontal path length measurement*

The RFID transponder was scanned by moving the reader horizontally and vertically to determine the path length, demonstrating that RFID tags positioned in any location can be detected within the RFID reader's range.

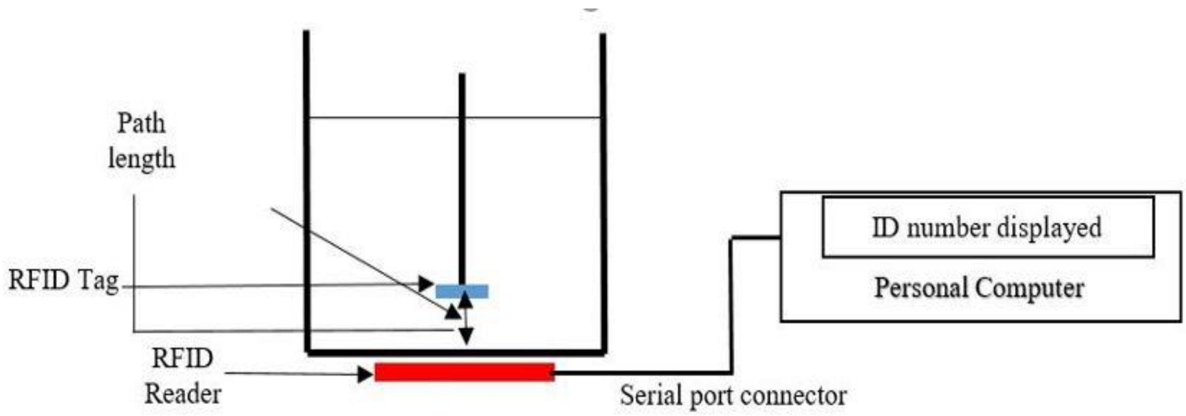

Figure 5.25. *Vertical path length measurement*

5.6.1.2 Testing with varied salinity level

The corrosion rate tends to increase when water conductivity increases. As salt water contains a lot of dissociated ions, it tends to cause corrosion. There is a necessity to carry tests with varying salinity level as RFID tags can possibly be used under sea water for monitoring operations with the pipe. Certain tests were conducted to analyse the effect of salinity on RF waves and how far the range varies which could provide a solution to the application of RFID in salt water. The salinity of the water was altered by adding salt to it. A different salinity value corresponds to a different conductivity value. Sea water conductivity varies from 300 to 600 S/cm whereas fresh water conductivity, for example, ranges from 30 to 2000 S/cm [118-122].

The electrical conductivity metre was used to calculate the variation in the salinity level of water in micro siemens per centimetre. The salinity of 150,180,210,240,270 grams immersed in water was determined. A measurement was taken for each salinity level using electrical conductivity meter, and the result plotted with best linear fit as shown in **Figure 5.26**. As noted the range, i.e. the distance between the RFID tag and reader, decreased with increase in electrical conductivity.

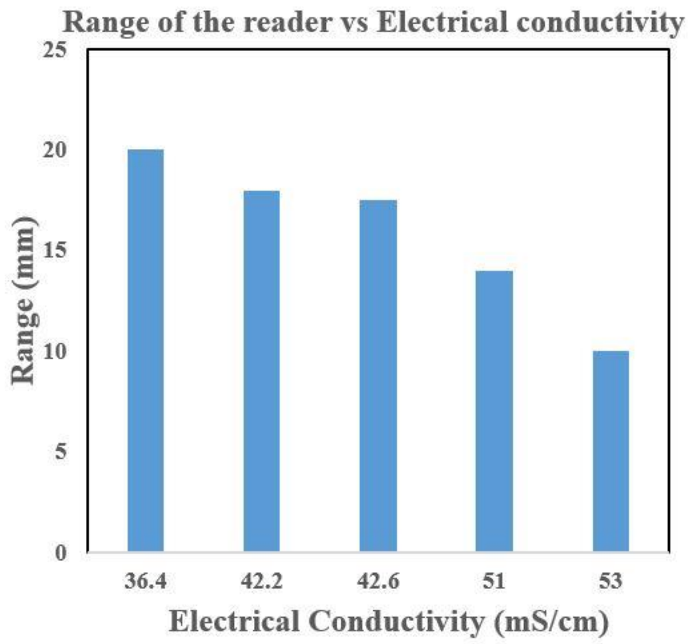

Figure 5.26*. Electrical conductivity vs Range of the reader*

Table 5.5. Solutions used for the experiment, temperature at which they were mixed, their salinity and calculated conductivity for each solution

Solution	Salinity kg	Temperature ºC	Measured Conductivity(mS/cm)	Measured Range(mm)
Freshwater	39	19		
	150		36.4	20
	180		42.2	17
Salinewater	210	19	42.6	15
	240		51	12
	270		53	10

5.6.1.3 The rewritable transponder

The magnetic circuit placed inside the casing was immersed in the tank filled with water along with the RFID system, which comprises of an arduino microcontroller connected to the reader as shown in **Figure 5.27 and 5.28**. The arduino microcontroller was connected to the laptop through a serial port connector. By running the code, the data from the GMR sensor was collected through the RFID system. Thus, the sensor data goes via the arduino micro-controller to a writable RFID tag, and the reader reads this and sends it to the PC. The output pin of the

GMR sensor is connected to the A_0 pin in the microcontroller through which the output is obtained. Ground and input pin are connected accordingly.

As noted, with the sensor placed within the magnetic circuit, the sensor output varied over distance. The sensor resistance causes a drop in voltage, and due to the power utilization in the long run, the voltage should decrease since the RFID tag is placed outside the casing and not in direct contact with water.

The RFID tag was in close contact with the casing, and with the RFID tag submerged in water, the casing acts as a buffer between the reader and the tag, resulting in signal variation.

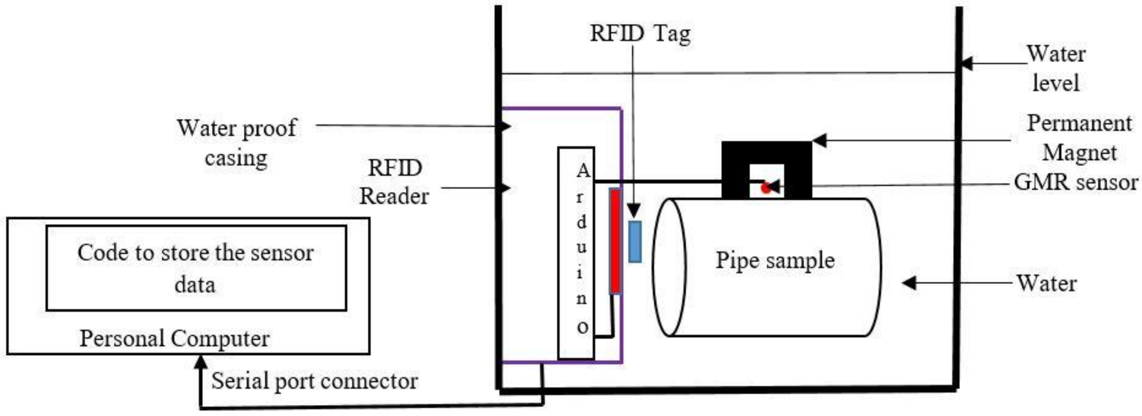

Figure 5.27. *Experimental setup with the RFID tag placed outside the casing*

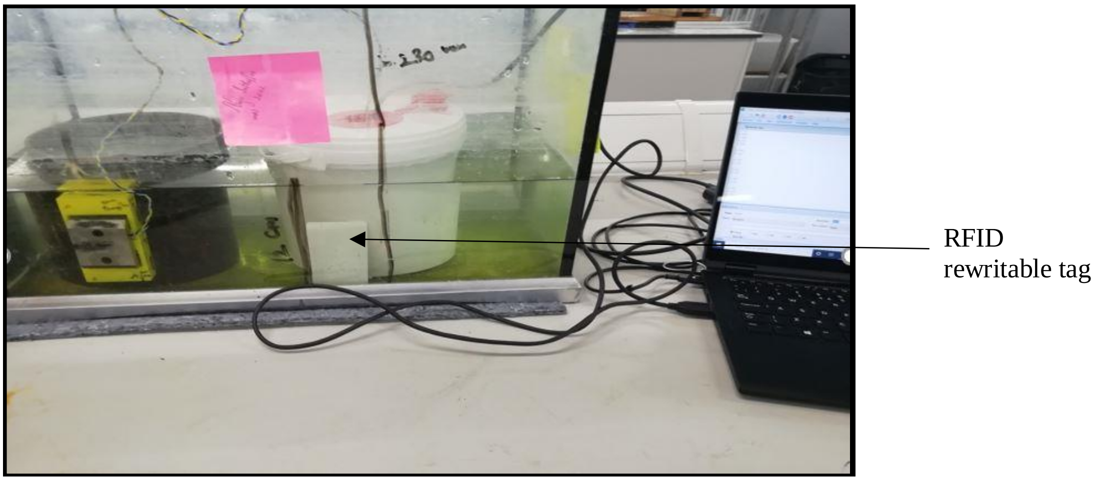

Figure 5.28. *RFID tag placed outside the casing*

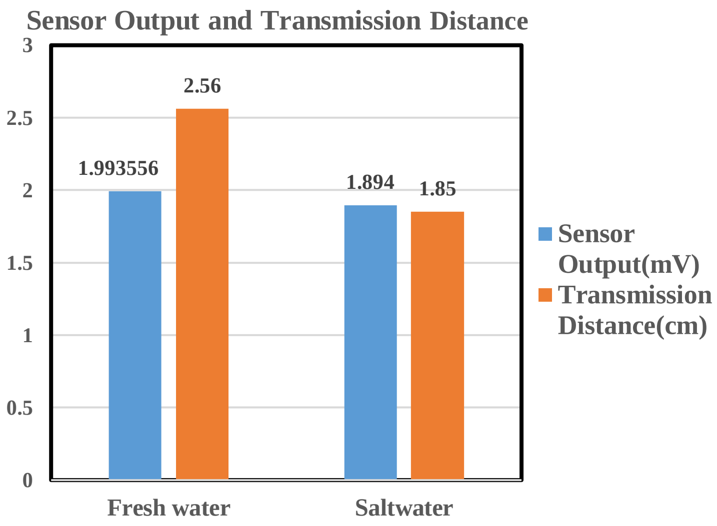

Figure 5.29. *Distance vs Sensor output*

5.7 Power requirements

Pipeline systems are usually installed to be used for years. Therefore, the associated communication systems should also be long lived. RFID type of sensor network is better suited for underwater real-time monitoring system. Type of power transmission used, whether AC or DC, could be decided by the power transmission distance based on the reactive power drawn from the source. Especially in offshore applications, each type of transmission system (AC and DC) has its own advantages and limitations.

Few studies have looked into the possibility of using RFID systems for underwater monitoring operations in fluvial environments [114]. While the technical limitations of these circumstances can be insurmountable in certain cases, ad hoc studies have shown that RFID technology can work even under water [113,114].

This research work focuses on the development of a device to collect and store data from a magnetic circuit with GMR sensor for underwater corrosion monitoring using RFID. The findings show that RFID systems can be used to store data at near ranges regardless of frequency. This research also provides an investigation into RFID, transponders, and reader classification, as well as existing applications underwater and their benefits.

Until recently, the offshore industry preferred placing the converters and power system equipment for supplying the subsea loads on shore or on the subsea vessel at the topside of the ocean. This was mainly because it is challenging for humans to install equipment at the bottom of the ocean due to harsh environments. With advancements in robotics and different technologies such as Autonomous Underwater Vehicles (AUVs), it has become possible to install more and more equipment on the seabed [1]. Power consumption is critical to the life span of pipeline communication systems. In that case saltwater batteries, like every other form of energy storage, store electricity for later use.

5.7.1 Prototype of saltwater battery

A liquid solution of salt water is used to capture, store, and eventually discharge energy in saltwater batteries. A saltwater battery, unlike a standard lithium-ion battery, uses sodium, the same element found in table salt, as its major constituent for conducting electricity. Whereas lithium ion battery uses lithium as its main ingredient. The building blocks of a battery are the cathode and anode, as well as an electrolyte. This allows the cathode and anode to exchange ions in one direction as they deliver electricity or in the other direction as it is being recharged. A prototype for the saltwater battery was developed and it's showing an output of 1.4 V. Increasing the salt content in the water would generate more voltages. Aluminum and copper sheets of thin thickness were soldered and immersed in salt water as shown in **Figure 5.30** and the two leads are connected to the voltmeter accordingly.

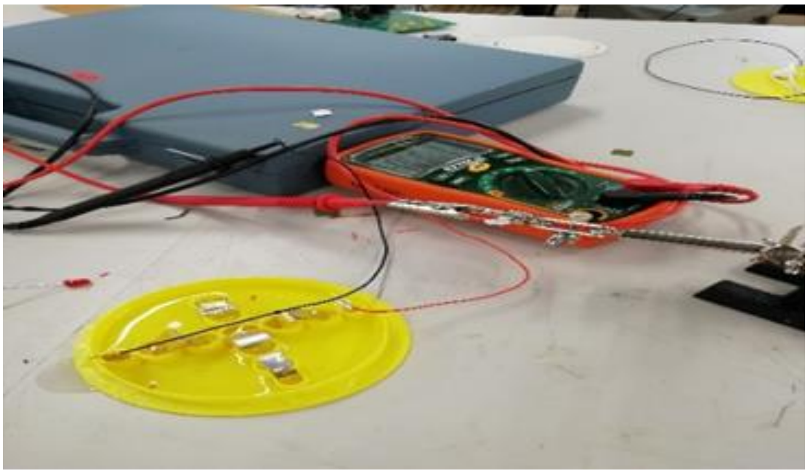

Figure 5.30. *Prototype of a saltwater battery*

5.8 Summary

In this chapter, underwater testing has been conducted with the magnetic circuit and measurements taken accordingly. Theoretical investigation behind RFID technique is carried out and experiments were conducted for 125 kHz and 13.56 MHZ frequency respectively. The results obtained concludes the measurement ranges that can be obtained using RFID under various environmental conditions. It signifies the importance of RFID where data from the magnetic circuit can be collected using RFID. The following chapter follows the high temperature experiments.

Chapter 6
High Temperature Experiments

6.1 Introduction

Pipelines, tanks, pressure vessels and absorbent tubes carrying flammable liquids will suffer from defects like creep, thermomechanical fatigue and hot corrosion due to high temperatures [1]. This could lead to the collapse of the interior or external structure of the parts and components, which might result in the closing of the plant, economic harm and in some cases to severe hazard for human life as furthermore [1]. The structural assessment of those parts and components is of high importance and since defects will be detected, localised associated sized in an early stage before an irreversible failure of the structure occurs by using NDT techniques, the probabilities of the structures being damaged becomes less [1].

In that case, NDT techniques will be used for structural observance or monitoring of structures operating at extreme temperature. The factors that limits the amount of NDT techniques which will be used includes the operational conditions with relevancy to the environment, access, size of the structure and structural complexity of the component under monitoring. Previously certain NDT techniques such as Acoustic Emission (AE), Eddy Current (EC), Laser Ultrasonic, Interferometry, thermography and Guided Wave Testing (GWT) are used at high temperatures. The high-temperature performance of the sensors or transducers used will limit the potency of the technique getting used [1].

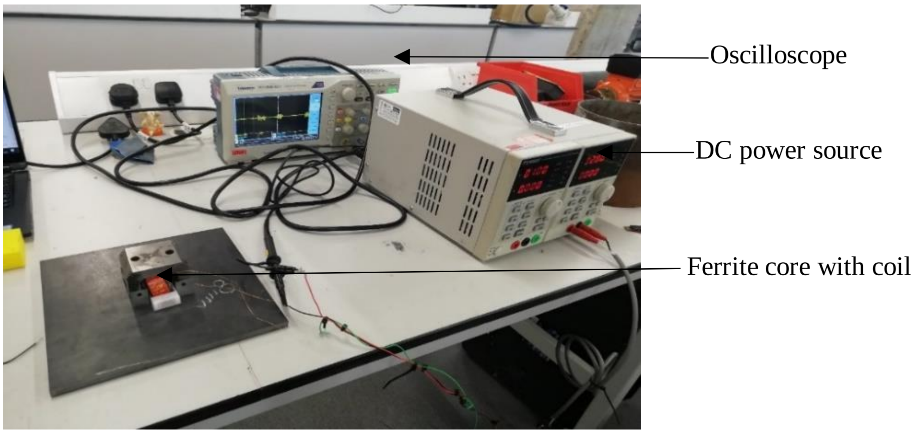

Figure 6.1. *Testing with MFL coil sensor on a plate sample*

6.2 Design of high temperature system

The system operates as follows: The permanent magnet generates a magnetic field of force within the direction that is sensitive to the axis of the GMR sensor (this moves the GMR sensor response to a linear operation). Relating to the configuration of the permanent magnet, the magnetic field of force lines are nearly parallel, so resulting in a lot of homogeneous magnetic field at the placement of the GMR sensor. This can be done as a result of the used magnet produces a way stronger magnetic field of force than is critical and necessary for linearizing the sensor output, and can easily saturate the GMR sensor response for the sort of operation custom-made [37]. The permanent magnet is exactly placed such that the polarization field for every sensor is sort of a similar. In order to extend the magnetic field of force, this magnet can be rotated/turned or shifted up/down slightly when at the same time monitoring the sensors output to ensure similar polarizing fields [37,38]. The results done for every increase in temperature.

Ranging from room temperature with a progressive step of 10°Celsius, the temperature was increased and therefore the variation in voltage that was displayed within the electronic equipment was noted. The readings were taken till 80°Celsius because the holder designed using 3D printer, for putting the sensor features a most operational temperature of 90°Celsius. Higher than a selected level, the thermal stability of the setup is negatively impacted as heating happens and there is a drastic drop in voltage. Thus, it will be noted that the temperature drift of the offset is affected principally by the temperature dependence of the GMR impact [8]. Also, we are able to note that any temperature drifts within the operating range of the magnet placed in a very explicit direction [8,98] with relation to the component leads to no significant amendment to the magnetic field of force as we have a tendency to estimate that the temperature of the component is no larger than 80°C throughout our tests.

Thus, it can be noted that the influence of the external currents will be decreased by a proper design of the measurement system using the subsequent observations: The external current lines (if they exist in the sensor's regime) should be directed parallel with the axis of sensitivity (i.e., the magnetic field of force they produce is perpendicular to the axis of sensitivity) [5].

Table 6.1 shows the specification of the GMR sensor

Analog Series	NVE AA002-02
Maximum operating temperature	150^0 C
Magnetic field range	>400 mT

Figure 6.2 shows the measurement system which includes the corroded pipe sample of 2 mm thickness, DC power supply, an oscilloscope to display the change in voltage. A holder is used for placing the GMR sensor intact as positioning is important in order to obtain signals [124].

Figure 6.2. *Measurement system using GMR sensor*

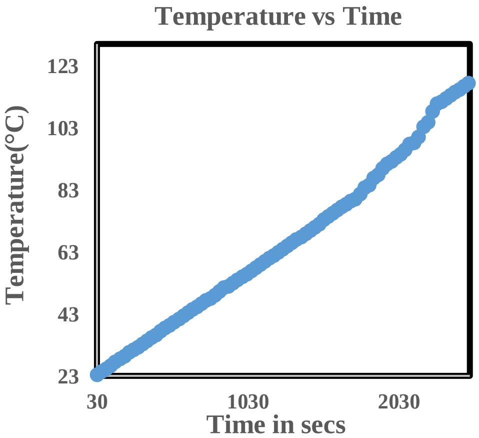

Figure 6.3. *The readings obtained from the thermocouple for temperature vs time*

The readings obtained through thermocouple are plotted accordingly, with respect to time. With a time, interval of 30 seconds the temperature increase is shown in the y-axis. The plot shows a linear curve with temperature increasing with time [124].

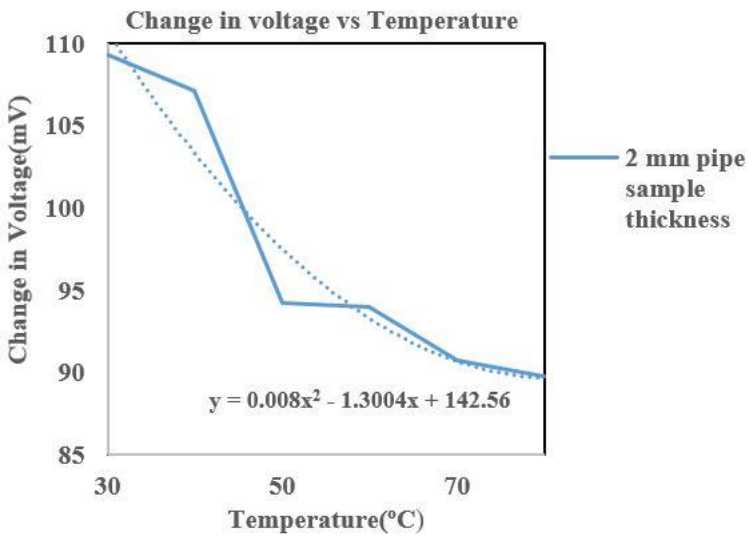

Figure 6.4. *The response obtained from the measurement system for change in voltage vs temperature*

From the above plot, it can be concluded that for each increase in temperature, the voltage decreases. Furthermore, resulting from the operation of the measurement system at varying temperatures, the following general equation can be derived for an input parameter *x* and a temperature variation ΔT [5]:

$$\mathbf{y} = (\mathbf{K_s}x + S\Delta T) \tag{6.1}$$

y represents the output; $\mathbf{K_s}$ is the sensitivity of the sensor for the input signal. Considering that the sensor is thermally balanced, one can assume that $S_1\Delta T \rightarrow 0$. As the current through the trace creates a magnetic field H=C·I (where C is a constant) [5] we can express the output voltage of the system as:

$$\Delta U = (K_s.H + S\,\Delta T + K_s.\ Hext) \tag{6.2}$$

The sensor output created by external magnetic field is negligible.

$$\Delta U = (K_{s1}.\ C.I + S_1\,\Delta T + K_{s1}) = K_s\,(C.I + 1) + \mathbf{S}\,\Delta T \tag{6.3}$$

Where **S(V/A)** is the sensitivity of the measurement system.

Recent analysis reveals that Honeywell has introduced a brand new warmth magnetic sensor, the HTMC 1021D [33]. This new magnetic sensor is tiny in size and could be a low value alternative to flux gate sensors and it would even be accustomed to replace hall effect sensors where reliability in high temperature environments is required [33]. The HTMC1021D sensor reliably over the complete temperature range of -55°C to +225°C and offers a magnetic field range of +/- 6 Gauss. The sensor is ceramic coated and is rugged and secured to handle high vibration under complex and advanced environments [33]. It also offers vital performance benefits for sensor signal conditioning and data acquisition in hostile environment over historically used silicon circuits [33].

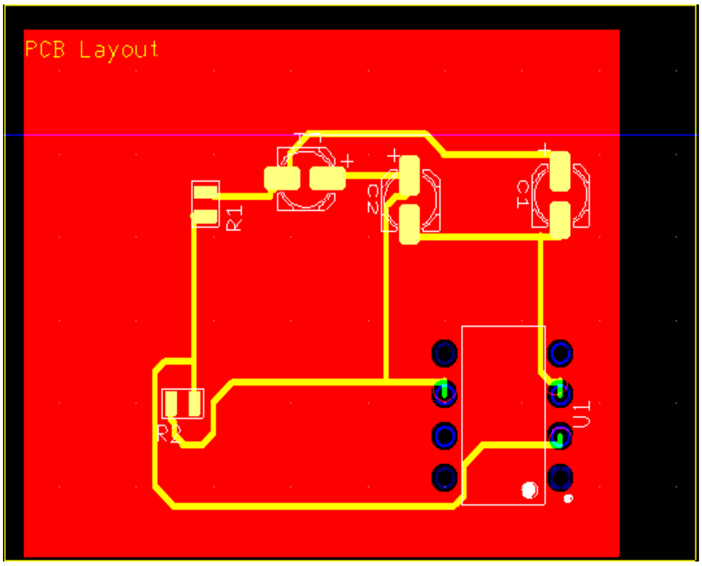

Figure 6.5*. The response obtained from the measurement system for change in voltage vs temperature*

6.3 High-temperature experiments-short term exposure

6.3.1 Experimental set up and procedure

The coil impedance, as well as the number of wire loops wound around the ferrite core, are important parameters to consider in an MFL coil sensor. A basic test as shown in **Figure 6.5** was carried out with an impedance analyzer, in which plate samples of thicknesses 2, 4, 6 and 8 mm were used with varying frequency while the positions of the magnet and coil sensor were kept fixed. Later pipe samples were considered for the experimental testing at room and high temperature conditions. Tests were carried out for up to a frequency of 50 kHz, and the electrical impedance at each frequency was determined for the 2 - 8 mm thick plate samples accordingly as in **Figure 6.6**. The electrical impedance increases with frequency, and that at each frequency the impedance decreases with increasing the sample thickness as in **Figure 6.7**. Since the measurements were conducted at low frequencies, the thickness of each plate sample was determined with less variation. As noted, electrical impedance values indicate that the MFL coil sensor can penetrate through plate sample thickness of 8 mm sample.

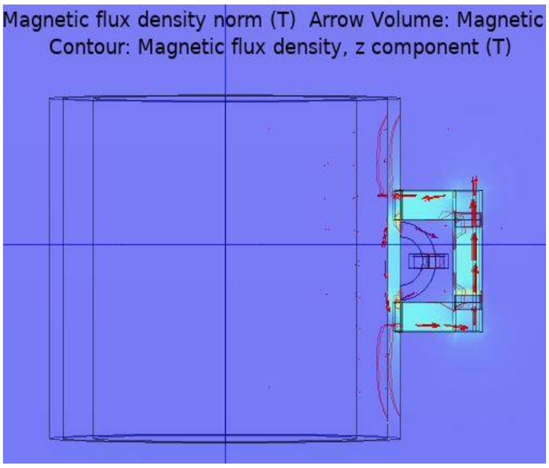

(a) Magnetic flux lines from the magnet and coil sensor

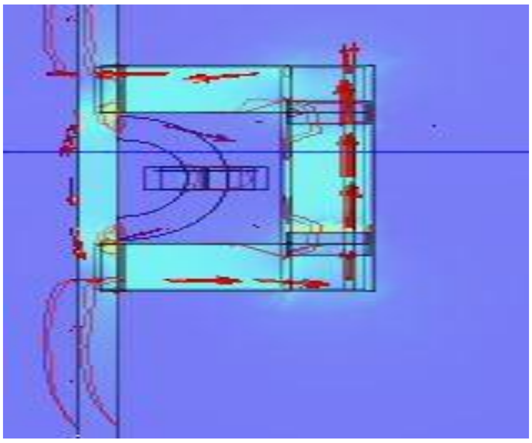

(b) Zoom out picture of flux lines from the ferrite core with the coil

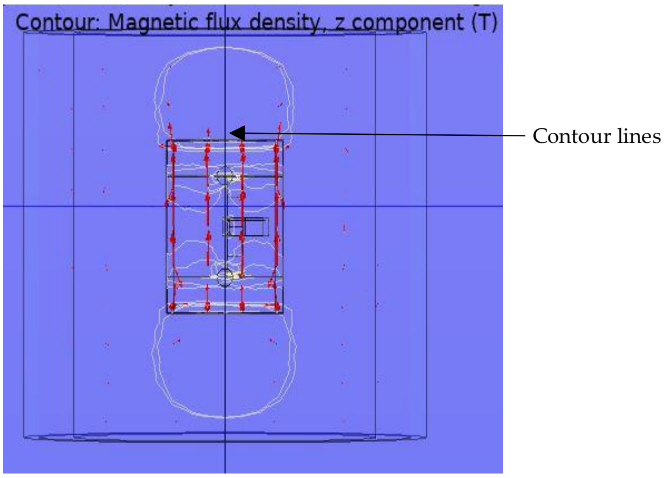

(c) Top view of the contour plot showing the magnetic flux flow
Figure 6.6. *The magnetic flux pattern along the pipe in the z direction.*

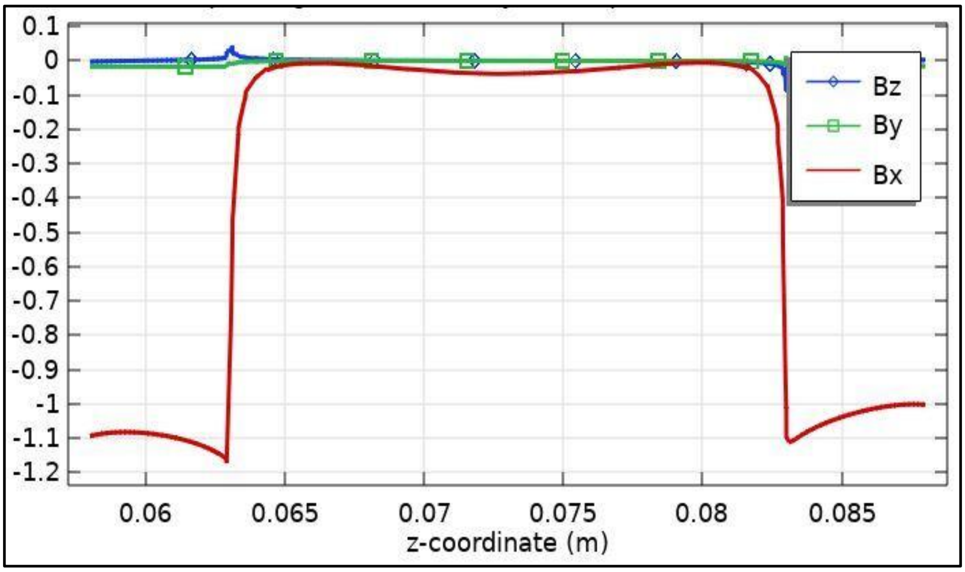

Figure 6.7. *Line graph: The magnetic flux density (B_x, B_y, B_z component) distribution in the pipe wall.*

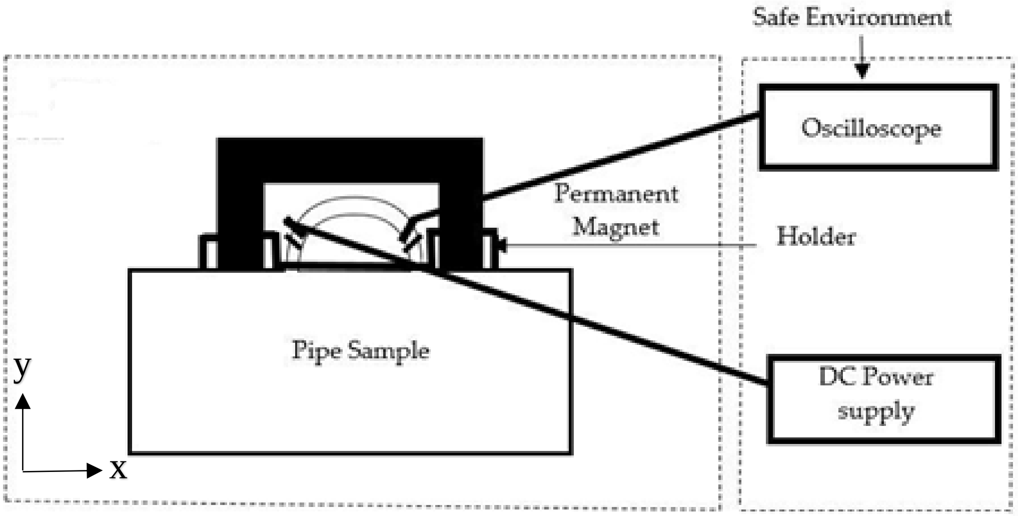

Figure 6.8. *Experimental setup for high temperature*

6.3.2 MFL coil sensor performance against various thicknesses of specimen

A sensing coil with less turns wound results in a much more compact coil with less occupied space, as well as reduced thermal heat. Furthermore, since copper wires have lower number of turns, printing them on a small circuit board is much easier. As a result, a coil sensor with 200 turns of wire cannot only be easily printed and fitted onto a small circuit board, but it can also detect small cross-sectional losses with ease, and therefore a coil sensor with 200 turns of wire was considered [38,124]. The change of coil impedance (phase and magnitude) reflects the properties of the conducting object under test and it is important to be calculated with a measurement setup as in **Figure 6.9**.

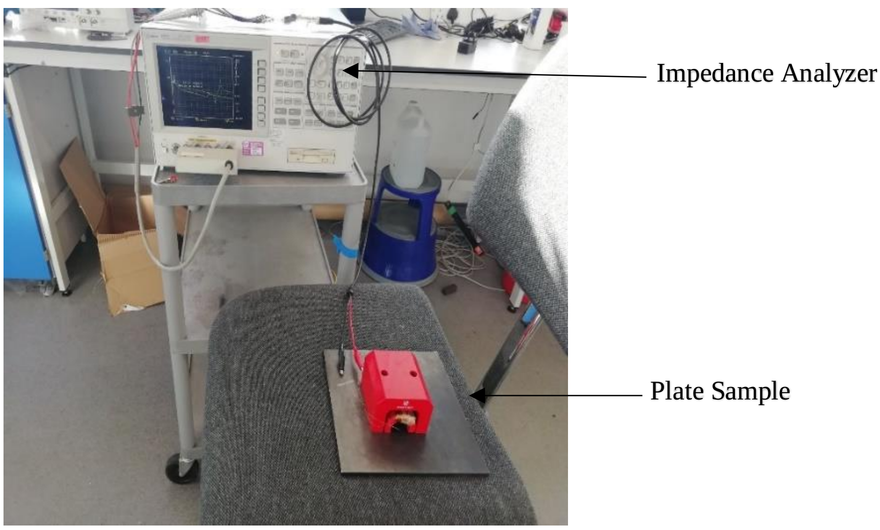

Figure 6.9. *Magnetic circuit with impedance analyser*

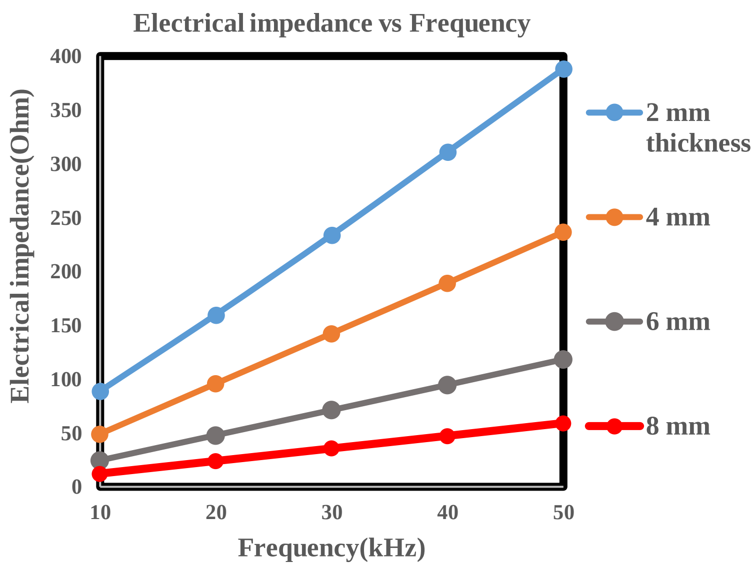

Figure 6.10. *Frequency vs Electrical impedance*

The relationship between changes in voltage and varying pipe sample thickness is found to be linear. Magnetic sensors transform magnetic induction signals obtained into voltage signals, which are observed using an oscilloscope [12].

As noted in **Figure 6.10**, the output voltage varies for each thickness of pipe sample at both temperature conditions. The difference in output voltage of the coil sensor, between 2 and 4 mm thick pipe samples was found to be 0.003563 V at room temperature, and between 4 and 6 mm thick samples was found to be 0.006627 V. The change in voltage observed between 6 and 8 mm thick pipe samples was 0.083568 V. As compared to other pipe sample thicknesses, the voltage difference between room temperature and 200°C for 8 mm thick sample was vastly different. Since the ferrite core's highest operating temperature is 180°C, there is a greater difference in output voltage at high temperatures for 8 mm pipe sample thickness compared to room temperature [124].

Preliminary measurements for the MFL coil sensor were taken with the experimental setup as in Figure 6.11 and results obtained as in Figure 6.12.

Figure 6.11. *Experimental setup of MFL coil sensor at room temperature condition*

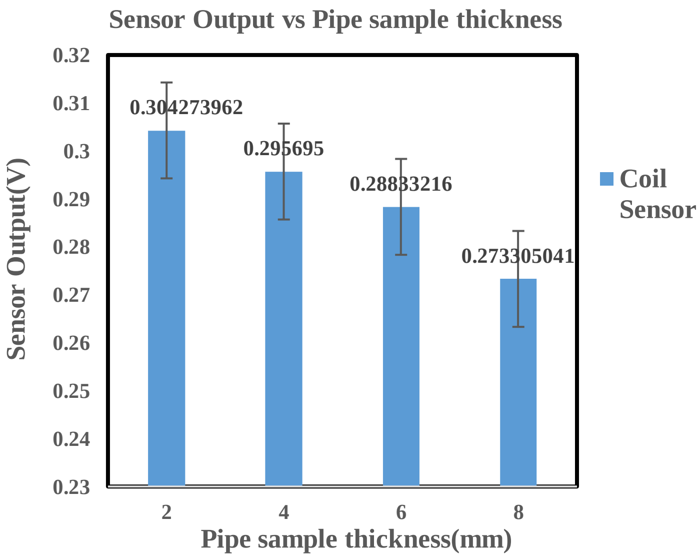

Figure 6.12. *Sensor Output Vs Pipe sample thickness at room temperature*

Figure 6.13*. Experimental setup for high temperature testing with coil sensor*

All of the components inside the oven, except for the ferrite core, have a maximum operating temperature of over 200°C as in **Figure 6.13**. The efficient functioning of the magnetic circuit at the stated condition is allowed by two separate environment measurement setups.

An initial test was carried out with the magnetic circuit by increasing the temperature from 32˚C with a progressive phase of 10˚C. The difference in voltage displayed inside the electronic equipment was noted. The measurements were taken at temperatures up to 220°C, with the ferrite core's maximum operating temperature being 180°C. It was noted that the output voltage obtained with the coil sensor for each varying thickness of the pipe sample decreased continuously with room temperature as in **Figure 6.14**. Furthermore, the output voltage decreased with increasing temperature until 220°C.

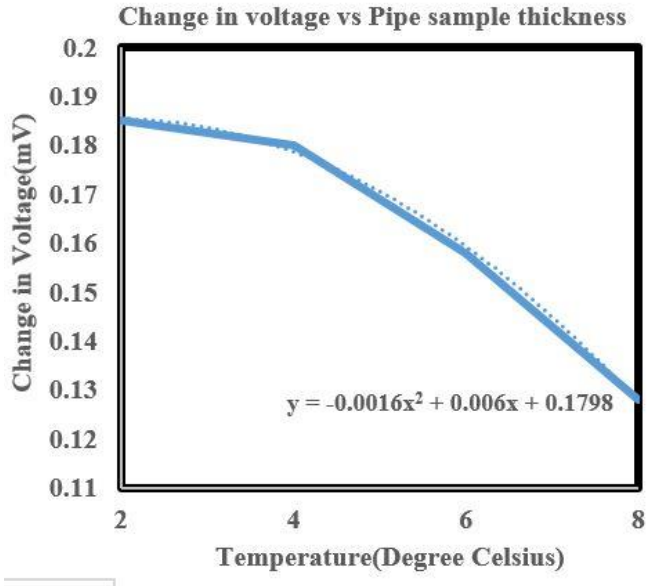

Figure 6.14. *Sensor output vs pipe sample thickness using coil sensor at room temperature*

An experimental test as in **Figure 6.15** was conducted for comparison between GMR analog sensor and the coil sensor to show that the coil sensor functions better than GMR sensor uptill 80^{o}C.

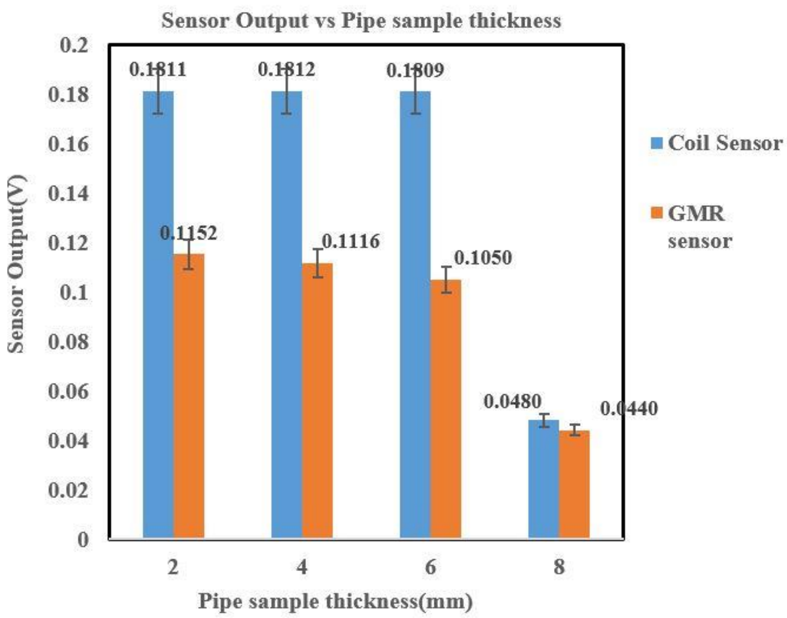

Figure 6.15. *Sensor Output Vs Pipe sample thickness of GMR and Coil sensor (up to 130°C)*

Sensor output of the coil sensor was compared with the GMR sensor in that coil sensor showed great progress than GMR sensor as in **Figure 6.16**.

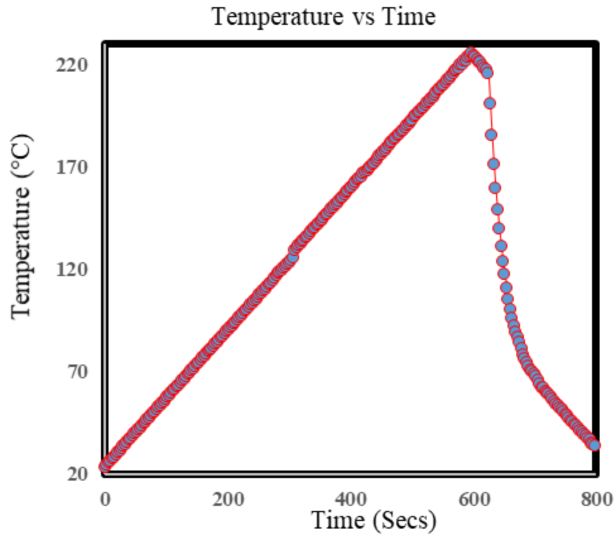

Figure 6.16*. Temperature vs Time data recorded with thermocouple (up to 220°C)*

Temperature was recorded along with time using thermocouple as in **Figure 6.17**. With an incremental step of 3 seconds, the temperature was recorded. Using Picologger software, the temperature of the thermocouple connected to the pipe sample inside the oven was recorded at each second over time. The temperature increased in lockstep with the passage of time. The results obtained are shown in **Figure 6.18** for various pipe sample thickness upto 200°C. Further tests were carried out on the pipe samples at room temperature and at 200°C, in order to compare the difference in sensor output at room temperature and the maximum temperature it can sustain as in **Figure 6.19**.

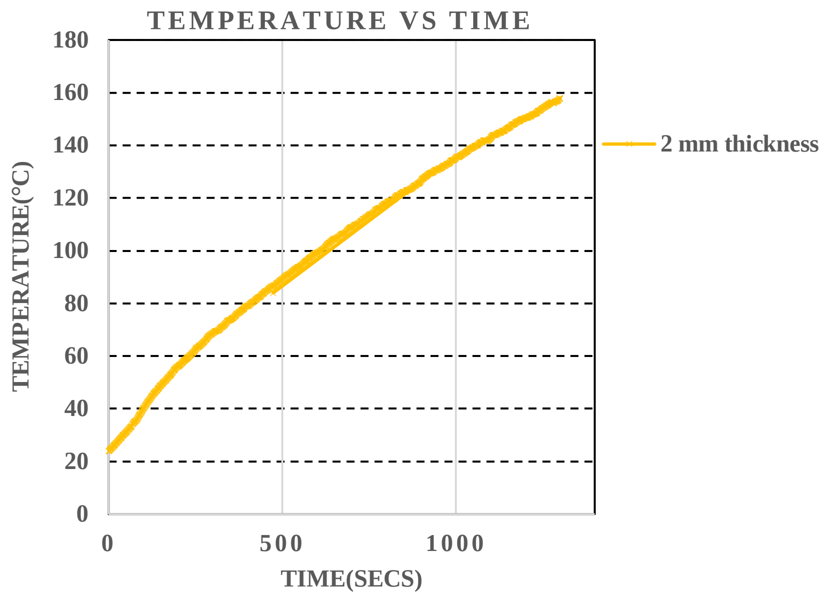

Figure 6.17. *Temperature vibration over time for pipe sample thickness 2 mm*

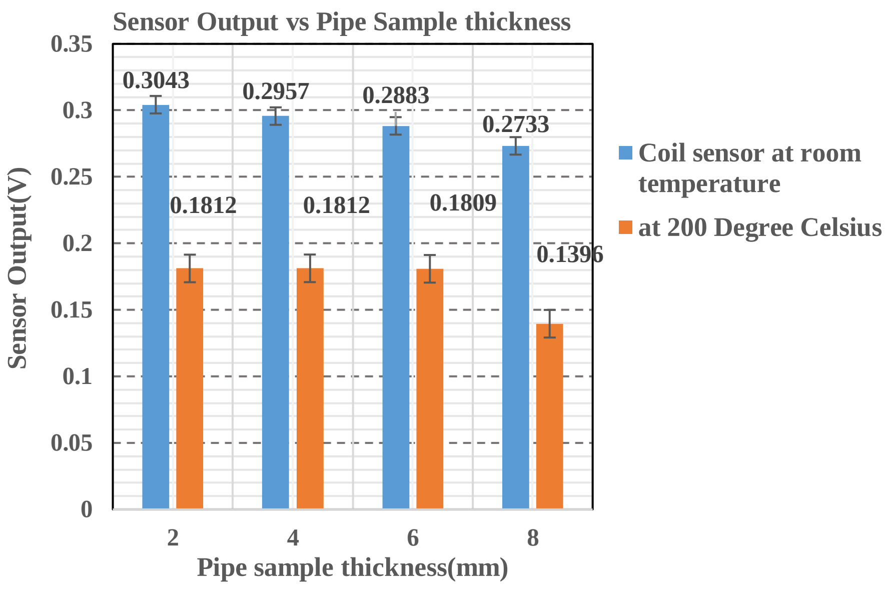

Figure 6.18. *Comparison of the output voltage of the MFL coil sensor at room temperature and at 220°C.*

Comparison of the output voltage of the MFL coil sensor at room temperature and at 220°C gives an idea of the difference in output obtained and provide the scope of improvement in further performance.

6.4 Summary

- MFL coil sensor tested up to temperature conditions 200ºC. Data collected accordingly for four varying pipe sample thickness (2,4,6 and 8mm) respectively. Time vs Temperature data recorded for the above temperature condition and cooling off accordingly which showed that with an incremental step of 10 seconds, temperature was increasing slowly and there was a rapid decrease while cooling off.
- FEA analysis was performed regarding the material selection, MFL coil sensor design and operating conditions against room temperature. FE model developed for the MFL coil sensor magnetic circuit simulation at room temperature condition which can be further processed for higher temperature conditions.

Chapter 7
Results and Discussions

7.1 RFID technique for data communication under sea water

To detect a pipeline defect, such as corrosion, it's critical to choose the right technique, the right atmosphere, and the right product flowing through the pipe. Evaluating the environment in which a pipeline is or will be located is very important to corrosion control, no matter which method or combination of methods is used. Additionally, sensitivity, precision, and reliability, as well as factors involving technique selection, such as size, distance, environmental conditions, and pipeline condition, must be taken into account. Sensor networks for underwater pipeline monitoring are usually linear, and the data sensed by the sensors can be forwarded in one of three directions: left, right, or both [73,74]. Furthermore, when considering the aquatic environment, the salinity level of seawater is a significant factor, which is around 3.5 percent on average and decreases to 0.05 percent in freshwater, meaning that a different value of salinity often means a different value of electrical conductivity, and in particular, the electrical conductivity of freshwater is around zero percent [73].

Regardless of the frequency range, RFID technique can be adapted with the reader and the transponder placed in close contact in order to obtain the data from the sensor [74]. The values obtained through above tests refer to a short range communication while long range communication requires even lower frequencies. For low-frequency, the depth of penetration is few metres. Due to limited bandwidth with lower range frequencies, this communication channel can be used to transmit data and not audio signals.

7.2 Effect of RFID technique for short range data communication

- The data obtained from the sensor reveals that the developed RFID system can collect data from the GMR sensor. Data were obtained using the developed RFID system with a unique transponder and reader.
- Regardless of the frequency range, the reader and the transponder should be placed in close contact within the range of the reader in order to obtain the data from the sensor. The path length of the signal depends upon the position of the magnetic circuit over the sample.

- The values obtained through above tests refer to a short range communication while long range communication requires even lower frequencies. For low-frequency, the depth of penetration is few metres.
- Due to limited bandwidth with lower range frequencies, this communication channel can be used to transmit data and not audio signals. Data has been obtained for a pipe sample thickness of 2mm with the magnetic circuit using GMR sensor and stored in the RFID system which can be retrieved later for further analysis.
- At higher frequencies, the chances of setting up efficient solutions for fresh water remain high than salt water based on the data obtained. Based on the above results, especially for short-range applications, RFID becomes practically usable for fresh and salt water.
- However, the ability to use lower frequency bands has led to the advancement of certain RFID applications for particular purposes in both marine and freshwater environments. The development of RFID sensor measurement has been presented and evaluated for underwater data collection.
- The experimental investigations show satisfactory results. The findings show that only at low frequencies can solutions for long reading ranges be created, both for salt and fresh water. The system has been developed for data storage with a single RFID tag whereas testing can be carried out with multiple tags as well.
- Multiple RFID systems can be used for collection of data at various ranges within the reader, and this will be a subject of future research.

Chapter 8
Conclusions

8.1 Thesis Findings

A new high-temperature MFL coil sensor for monitoring of pipe samples has been designed, developed and experimentally evaluated. Based on the literature review presented in Chapter 2, various NDT techniques, including AE, eddy current, thermography, laser and conventional ultrasonic testing, have been successfully applied at least up to 220°C with shortcomings, though, like qualitative results, sensitivity to noise and laboratory use. Guided wave testing is an emerging NDT method that has been widely employed for the structural assessment of large structures in oil/gas, nuclear and solar thermal industry. Although the dominant technology of transducers for GWT is piezoelectric, EMAT is an attractive candidate for applications where non-contact measurements are needed.

The work described in this thesis demonstrated the systematic approach taken to develop and test a MFL coil sensor for monitoring of pipe samples up to 220°C. The theoretical basis that was required for the implementation of the FEA models and analysis of both theoretical and experimental results were described in Chapter 3. MFL coil sensor was tested at room temperature regarding their defect detection capabilities, and high-temperature performance. They were exposed for three hours at 250°C and they both managed to operate efficiently for the entire duration of the experimental procedure.

8.1.1 MFL coil sensor model for room temperature conditions

Main findings from Chapter 4 related to the theoretical study of MFL technique at room and high temperatures in terms of its magnetic properties are given below.

8.1.2 Requirements and limitations of MFL coil sensor under extreme conditions

A 3D FEA model for the prediction of the MFL performance at room temperature was implemented in commercial software COMSOL Multiphysics 5.4. Simplifications were performed regarding the current variation on the developed magnetic circuit with respect to varying pipe sample thicknesses.

As no coil sensor for MFL at high temperatures has been designed before, the limitations of the existing technology for MFL had to be explored firstly. The work in this thesis detailed the design of EM based sensor for MFL testing and studies a relationship between magnetic and mechanical properties of a ferromagnetic pipe sample. The study reviewed the current major systems and EM techniques, which are employed in the NDT field. One of the areas focussed is the development of a permanently installed corrosion monitoring system that would work efficiently under extreme conditions. The NDE of flaws in ferromagnetic materials through MFL technique, with the flux leak arising around defects, the significance of which is the possibility to avoid the use of multiple and complex system for ferromagnetic materials.

An experiment was carried out to measure magnetic field distribution at the top surface of a ferromagnetic pipe sample. It was possible to detect changes in the sensor output for differences in pipe sample thicknesses. This change in magnetic field was enough to be detected by the experiment using the newly developed MFL coil sensor. The major contribution of this PhD study is described in chapters four and six concerned with DC and B-field variations with mechanical properties, respectively.

In summary, the major contribution of the study is revealing the direct relationship between the measured magnetic field, relative permeability and determining the magnitude of magnetic flux density. This has made it possible to predict through simulation that how far the MFL coil sensor has succeeded in penetrating through the ferromagnetic pipe sample.

8.2 Recommendations for future work

A holder made of a heat resistant material or a metal such as Aluminium is needed to hold the sensor in position. The sensor has a maximum operating temperature of 180°C. Based upon the testing results, it can survive up to 220°C.

Recent research involving extreme conditions, to protect the sensor head from high temperature environments, a system with the sensor head set in a ferritic stainless-steel canister was used in a recent study [91]. It included a housing with a water jacket to keep the sensor head cool while measuring a hot steel sample [91]. Similarly, a jigs and fixtures kind of mechanism would be designed as a future work that would protect the magnet and sensor from getting affected by heat. The mechanism made of heat resistant material could be able to protect the magnetic field from the magnetic sensor and the magnet.

Given the existing challenges in wireless underwater communications, it is worth exploring alternatives, such as RFID. In this technology, the water salinity is a problem, as it increases the conductivity of the medium and, therefore, its attenuation of RFID signals.

Promising results have been obtained with the newly developed MFL coil sensor. Variation in pipe sample thicknesses of upto 6 mm thickness is carried out by the MFL coil sensor and data is transmitted through a lossless wire or wirelessly and data processing and result visualization is carried out on a separate PC. The MFL coil sensor was able to survive successfully up to 220ºC. The goal of future work is to make the MFL coil sensor work above 220ºC.

With data obtained through room and high temperature experiments, a COMSOL model can be created in order to analyse the defect depths. In reference to the fourth chapter COMSOL models, analyses can be developed further and that is one of the scope for future work.

References

[1] R. K. Miller, and P. Mclntire, "Non-destructive Testing Handbook. Vol. 5: Acoustic Emission Testing”, *American Society for Non-Destructive Testing*, New York, 1987.

[2] U.S Department of Transportation, Pipe Defects and Anomalies (pipeline &safety administration) [Online]. Available at: http:// primis.phmsa.dot.gov/ comm/ FactSheets/ FSPipeDefects.htm? no cache=9047. [Accessed] [06/07/2020]

[3] M.A. Adegboye, W.K. Fung, and A. Karnik, “Recent Advances in Pipeline Monitoring and Oil Leakage Detection Technologies: Principles and Approaches”, *Sensors(Basel)*, doi: 10.3390/s19112548, 2019.

[4] https://www.phmsa.dot.gov/data-and-statistics/pipeline/pipeline-incident-20-year-trends/ (accessed on 11 January 2021).

[5] Z. Liu and Y. Kleiner., “State-of-the-Art review of Technologies for Pipe Structural Health Monitoring”, *IEEE Sensors Journal,* 12(6):19871992,DOI:10.1109/JSEN.2011.2181161, 2012.

[6] M. Coramik, Y. Ege, “Discontinuity inspection in pipelines: A comparison review”, *Measurement*,Volume 111, Pages 359-373, 2017.

[7] D. L. Atherton, "Magnetic Inspection is Key to Ensuring Safe Pipelines", *Oil and Gas Journal*, vol. 87, 52-61, 1989.

[8] Y. Kang, J. Wu and Y. Sun, “The Use of Magnetic Flux Leakage Testing Method and Apparatus for Steel Pipe”. *Mater. Eval*. 70, Issue 7, 821–827,2012.

[9] D. Brondel, R. Edwards, A. Hayman, D. Hill, S. Mehta and T. Semerad, “Corrosion in the Oil Industry”. Oilfield Rev 6, 4–18, 1994.

[10] B. Rao, “Magnetic Flux Leakage Technique: Basics”, *Journal of Non- destructive Testing & Evaluation*,11(3), 7-17,2012. [Accessed]07/08/2020.

[11] D. L. Atherton, “Developments in magnetic inspection techniques for pipelines”, CSNDT Journal, vol. 2, 28-35, 1990.

[12] T. A. Bubenik, J. B. Nestleroth, R. J. Eiber and B. F. Saffell, “Magnetic Flux Leakage (MFL) Technology for Natural Gas Pipeline Inspection”, Topical Report; Battelle Memorial Inst.: Columbus, OH, USA, 1992.

[13] W. Singh, S. Thirunavukkarasu, S. Mahadevan, B.P.C. Rao, C. K. Mukhopadhyay and T. Jayakumar, “Three-Dimensional Finite Element Modelling of Magnetic Flux Leakage Technique for Detection of Defects in Carbon Steel Plates”, In Proceedings of the COMSOL Conference India,2010.

[14] W. Sharatchandra Singh, B.P.C. Rao, S. Vaidyanathan, T. Jayakumar and Baldev Raj, "Detection of leakage magnetic flux from near-side and far-side defects in carbon steel plates using giant magneto resistive sensor", *Measurement Science & Technology*, 19 (1), pp. 015702,2008.

[15] H. V. Sharma and N. Manglani, "Underwater Communication Systems: A Review", Volume 5 Issue 3 ISSN (Online): 2348-4098 ISSN (Print): 2395-4752, *International Journal of Science, Engineering and Technology*, 2017.

[16] J. Blitz, Electrical and Magnetic Methods of Non-Destructive Testing, Adam Hilger publication,1997.

[17] K. Sakai, K. Morita, Y. Haga, T. Kiwa, K. Inoue, and K. Tsukada, "Automatic Scanning System for Back-Side Defect of Steel Structure Using Magnetic Flux Leakage Method". *IEEE transactions on magnetics*, vol. 51, no. 11, 2015.

[18] B. Rao, "Magnetic Flux Leakage Technique: Basics", *Journal of Non- destructive Testing & Evaluation*,11(3), 7-17,2012. [Accessed]07/08/2020.

[19] M. N. Baibich, J.M. Broto, A. Fert, F. Petroff, P. Eitenne, G. Creuzet, A. Friederichand, and J. Chazelas, "Giant Magnetoresistance of (001) Fe/ (001) CR Magnetic Superlattices", *Phys.Rev*. Lett, vol.61, No.21, pp.2472-2475,1988.

[20] W. Sharatchandra Singh, B.P.C. Rao, T. Jayakumar and BaldevRaj, "Simultaneous Measurement of Tangential and Normal Components of Leakage Magnetic Flux using Giant Magneto-resistive Sensors", *Journal of Non-Destructive Testing & Evaluation*, Issue 8, 2009.

[21] W. Sharatchandra Singh, B.P.C, Rao, C.K. Mukhopadhyay, and T. Jayakumar, "GMR based magnetic flux leakage technique for condition monitoring of steel track rope". *Insight*, vol.53, no.7, pp.377-381, 2011.

[22] G. E. C. Bell, C. G, Moore, and S. Williams, "Development and application of ductile iron pipe electrical resistance probes for monitoring underground external pipeline corrosion". *CORROSION*, 2007.

[23] H. A. Khan and S. Aramco, "Using coupons and er soil corrosion probes in applying pipeline". cp criteria, *Mater. Perform*, vol. 46, no. 4, pp. 26– 30, 2007.

[24] H. Kwun, Back in Style: Magnetorestrictive Sensors [Online]. Available: http://www.swri.org/3pubs/brochure/d17/magneto/magneto.html. (1991).

[25] "Technical background on MsS," Southwest Research Institute, San Antonio, TX, Tech. Rep., 2000.

[26] H. Kwun, S. Kim, and G. M. Light, "The magnetorestrictive sensor technology for long range guided wave testing and monitoring of structures", *Mater. Evaluat*, vol. 61, pp. 80–84, 2003.

[27] R. Munser, M. RoBner, M. Hartrumpf, and H. B. Kuntze, "Microwave back-scattering sensor for the detection of hidden material in homogeneities e.g. Pipe leakages", *In Proc. 9th Int. Trade Fair Conf. Sensors Trans. Syst*, Nuremberg, Germany, pp. 275–280, 1999.

[28] Z. Liu, Y. Kleiner, "State of the art review of inspection technologies for condition assessment of water pipes", Kleiner Institute for Research in Construction, Canada, *Measurement* (46)1-15, https://doi.org/10.1016/j.measurement.2012.05.032, 2013.

[29] L. Jogschies, D. Klaas, R. Kruppe, J. Rittinger, P. Taptimthong, A. Wienecke, L. Rising, and M.C. Wurz, "Recent Developments of Magneto resistive Sensors for Industrial Applications", *Sensors*,15,28665-28689; DOI:10.3390/s151128665, 2015.

[30] C. Reig, S. Cardoso, and S.C. Mukhopadhyay, "Giant Magnetoresistance (GMR) Sensors; Smart Sensors", *Measurement, and Instrumentation*; Volume 6, 2013.

[31] J. Paul, C. Schnieders, J. Traute, R. Lehndorff, A. Conca, B. Leven, B. Hillebrands, F. Casper, G. Jakob, and M. Kläui, "Sensors based on tunnel Magnetoresistance-New Technology, New Opportunities", *In Proceedings SENSOR,* DOI 10.5162/sensor/B3.2, 2015.

[32] M. Kogia.,2017, "High temperature electromagnetic acoustic transducer for guided wave", testinghttp://bura.brunel.ac.uk/handle/2438/14491, Brunel University, London.

[33] CIA CIA., 2017. The world factbook. https://www.cia.gov/library/publications/theworld-factbook/fields/2117.html (accessed 30 April 2018).

[34] S. Mizuochi, U.S. Patent No. 4,029,889. Washington, DC: U.S. Patent and Trademark Office, 1977.

[35] S. Datta, and S. Sarkar, "A review on different pipeline fault detection methods", *Journal of Loss Prevention in the Process Industries*, Volume 41,Pages 97-106, DOI: 10.1016/j.jlp.2016.03.010,2016.

[36] W. Xueling, S.X. Yang, A. Wei, **"**Summarization on inspection technique for leakage in oil and gas pipelines", *Nat Gas Oil*, 25,19-23, 2007.

[37] D.G. Murdock, S.V. Sterans, R.T. Lines, D. Lenz, D.M. Brown, and C.R. Philbrick, "Applications of real-world gas detection: airborne natural gas emission lidar(ANGEL) system", *J. Appl.Remote Sens*. 2,023518, 2008.

[38] J. Blitz, Electrical and Magnetic Methods of Non-Destructive Testing, Adam Hilger publication,1997.

[39] http://www.singulgus.de/uploads/txpspublications/Timaris 211114 01.pdf. (accessed on 20 February 2022).

[40] H. Lua, T. Iseley, S. Behbahani, and L. Fu, "Leakage detection techniques for oil and gas pipelines: State-of-the-art". *Tunnelling and Underground Space Technology*, Volume 98,103249, 2020.

[41] Recommended failure rates for pipelines. Energy report, Det Norske Veritas DNV, Oslo,2010.

[42] C.M. Anderson, M. Mayes and R. LaBelle, Update of occurrence rates for offshore oil spills. OCS Report BOEM-069, 2012.

[43] M. Ho, S. El-Borgi, D. Patil and G. Song, "Inspection and monitoring systems subsea pipelines: A review paper", Vol. 19(2)606-645, 2020.

[44] P. Ostapkowicz, "Leak detection in liquid transmission pipelines using simplified pressure analysis techniques employing a minimum of standard and non-standard measuring devices", *Eng. Struct*, 113, 194–205. [CrossRef], 2016.

[45] R. Sheltami, A. Bala, E.M. Shakshuki, "Wireless sensor networks for leak detection in pipelines: A survey", J. *Ambient Intell. Humaniz. Comput*, 7, 347–356. [CrossRef], 2016.

[46] J.C. Martins and P. Seleghim, "Assessment of the performance of acoustic and mass balance methods for leak detection in pipelines for transporting liquids", *J. Fluids Eng*, 132, 011401–011413. [CrossRef], 2010.

[47] X. Haibo, Z. Laibin and W. Zhaohui, "Development actualities of pipeline leak-detection technologies at home and abroad", *Oil Gas Storage Transport*,20,1-5, 2001.

[48] Y. Shi, C. Zhang, R. Li, M. Cai, and G. Jia, "Theory and Application of Magnetic Flux Leakage Pipeline Detection", *Sensors(Basel)*.15(12):31036-31055, 2015.

[49] O. Hunaidi, "Condition assessment of water pipes", *In: Proceedings of EPA Workshop on Innovation and Research for Water Infrastructure in the 21st Century*, pp. 1–6, 2006.

[50] W.A. Yan-Li, A.N. Shi-Qan, "Research on the Coverage of Wireless Sensor Network", *J. Transcluction Technol*, 2, 25–37, 2005.

[51] I. Al-Taie, Hamad A, Alsaiari, A. Amer, F. Abdellatif, A. Outa, H. Trigui, F.D. Ledezma, S. Patel, A. Abedan, "Survey of Underwater NDT Technologies for Offshore Assets", 7th Middle East Nondestructive Testing Conference & Exhibition, At Kingdom of Bahrain,2015.

[52] D. Brondel, R. Edwards, A. Hayman, D. Hill, S. Mehta, and T. Semerad, "Corrosion in the oil industry", Journal Name: *Oilfield Review*; (Netherlands), Journal Volume: 6:2, 1994.

[53] C. Zuo, X. Feng, Y. Zhang, and L. Lu, "Crack detection in pipelines using multiple electromechanical impedance sensors", Smart Materials and Structures 26(10), 2017.

[54] C. Sandberg, J Holmes, K. McCoy, H. Koppitsch, "The application of a continuous leak detection system to pipelines and associated equipment", *IEEE Trans. Ind. Appl*, 25,906-909, 1989.

[55] J. Shijiu, W. Lining, and L. Jian, "Instantaneous negative pressure wave pattern recognition method in leak detection of crude petroleum transported pipeline", *J. Electr. Measurem. Instrument*,12, 59–64, 1998.

[56] R.A. Silva, C.M. Buiatti, S.L. Cruz, and J.A. Pereira, "Pressure wave behaviour and leak detection in pipelines", *Comput. Chem. Eng*. 20, S491–S496, 1996.

[57] D. Marlow, S. Heart, S. Burn, A. Urquhart, S. Gould, M. Anderson, S. Cook, M. Ambrose, B. Madin, and A. Flitzgerald, "Condition assessment strategies and protocols for water and wastewater utility assets", *Water Environ.Res*. 2007.

[58] J. Zhang, "Designing a cost-effective and reliable pipeline leak-detection system", *Pipes Pipelines Int*, 42, 20–26. 37, 1997.

[59] G. Geiger, D. Vogt, and R. Tetzner, "State-of-the-art in leak detection and localization", *Oil Gas Eur*. Mag., 32, 1–26, 2006.

[60] W.A. Yan-Li, A.N. Shi-Qan, "Research on the Coverage of Wireless Sensor Network", *J. Transcluction Technol*, 2, 25–37, 2005.

[61] M. Henrie, P. Carpenter, and R.E. Nicholas, Pipeline Leak Detection Handbook; Joe Hayton: Chennai, India; pp. 1–317, 2016.

[62] W. Xiadong, H. K. Zhi, X. Hua, L. Yaohua, C. Hongjia, "Present stage of the development of oil-gas pipeline leak-detection technologies". Pipeline Tech. *Equipment* 16,24-26, 2008.

[63] W. Jiayong, L. Haina, W. Likun, X. Bin, W. Hongchao, C. Yongjun, L. Shengnan, T. Zhigang, "Performance evaluation indices of pipeline leak monitoring systems". *Oil Gas Storage Transport*. 36,209-213, DOI: 10.6047/j.issn.1000-8241.2017.02.014,2017.

[64] Pipescan: http://www.silverwingndt.com/magnetic-flux-leakage/pipescan-pipe-corrosion-detection.html/(accessed on 03 October 2020).

[65] H. Zuoying, Q. Peiwen, and C. Liang, "3D FEM analysis in magnetic flux leakage method", *J. Ndt & E International*, 39(1): 61-66, 2006.

[66] J.B. Nestleroth, "Circumferential MFL in-line inspection for cracks in pipelines", *[M]. National Energy Technology Laboratory (US)*,2003.

[67] S. Climent, J.V. Capella, N. Meratnia, and J.J. Serrano, “Underwater Sensor Networks: A New Energy Efficient and Robust Architecture”, *Sensors*, 12, 704–731, 2012.

[68] S. Jiang, and S. Georgakopoulos, “Electromagnetic wave propagation into fresh water”, *J. Electromagn. Anal. Appl*., 3, 261–266, 2011.

[69] X. Che, I. Wells, G. Dickers, P. Kear, and X. Gong, “Re-evaluation of RF electromagnetic communication in underwater sensor networks”, *IEEE Commun. Mag*., 48, Issue 12, 143–151,2010.

[70] http://news.mit.edu/2018/wireless-communication-through-water- air-0822 Wireless communication breaks through water-air barrier/(accessed on 12 September 2020).

[71] L. Butler, Underwater Radio Communication 1987.

[72] I. Wells, A. Davies, X, Che, P. Kear, G. Dickers, X. Gong, and M. Rhodes, “Node pattern simulation of an undersea sensor network using RF electromagnetic communications”. *In Proceedings of Ultra-Modern Telecommunications Workshops*, St. Petersburg, Russia, 12–; pp. 1–4, 2009.

[73] M.R. Frater, M.J. Ryan, and R.M. Dunbar, 2006 “Electromagnetic communications within swarms of autonomous underwater vehicles”, *In Proceedings of ACM WUW Net*, Los Angeles, CA, USA, pp. 64–70, 2006.

[74] D. Anguita, D. Brizzolara and G. Parodi, “Optical communication for underwater wireless sensor networks: A VHDL-implementation of a physical layer 802.15.4 compatible”, *In Proceedings of IEEE OCEANS*, Bremen, Germany, 11–14; pp. 1–2, 2009.

[75] Moore and R. Richard, “Radio Communications in the Sea”, *lEEE Spectrum*, Vol 4, pp 42-51, 1967.

[76] Achuta S. Rao, ALNICO PERMANENT MAGNETS AN OVERVIEW

[77] G. Benelli, and A. Pozzebon, “RFID Under Water: Technical Issues and Applications”, DOI:10.5772/53934, 2013.

[78] K. Finkenzeller, "RFID Handbook, fundamentals and applications in contactless smart cards, Radio Frequency Identification and Near-Field Communication", John Wiley & Sons, Ltd, UK, 2010.

[79] J.H. Kim, G. Sharma, N. Boudriga, S.S. Iyengar ,and N. Prabakar, “Autonomous pipeline monitoring and maintenance system: a RFID-based approach”, *EURASIP Journal on Wireless Communications and Networking*, Article number: 262, 2015.

[80] R. Kumar, A. Louzir, and J.Y.L. Naour, “RFID Tag Coupled with a Magnetic Sensor for Wireless Sensing of Home Electrical Devices”, *In Proceedings of the 48th European Microwave Conference*, France, 2018.

[81] J. Zhang, G.Y. Tian, A.B. Zhao, “Passive RFID sensor systems for crack detection & characterization”, *NDT&E Int*, 86, 89–99,2017.

[82] Significant Pipeline Incidents by Cause. Available online: http://www.phmsa.dot.gov/pipeline/library/ data-stats/flagged-data-files (accessed on 26 May 2018).

[83] S. Mondal, D. Kumar, M.I. Ghazali, P. Chahl, L. Udpa and Y. Deng, “Monitoring and localization of buried plastic natural gas pipes using passive RF tags”, *AIP Conference Proceedings 1949*, 020020 , https://doi.org/10.1063/1.5031517,2018.

[84] Pozzebon and Alessandro, “Bringing Near Field Communication under water: short range data exchange in fresh and salt water”, *International EURASIP Workshop on RFID Technology (EURFID)*, p152-156, 5p,2015.

[85] J. Shena, L. Zhou, W. Jacobs, P. Hunt, and C. Davis, “Real-time in-line steel microstructure control through magnetic properties using an EM sensor”. *Journal of Magnetism and Magnetic Materials*, 490(2019), 165504.

[86] M. Jolfaei, J. Shen, A. Smith, L. Zhou, and C. Davis, “EM Sensor System for Characterisation of Advanced High Strength Strip Steels”, *Electromagnetic Non-Destructive Evaluation*, doi:10.3233/978-1-61499-836-5-49,2018.

[87] L. Zhou, R. Hall, C.L. Davis,” Measured and modelled low field relative permeability for dual phase steels at high temperature”, *J. Magn. Mater*. 475 (2019), 38–43.

[88] C.L. Davis, M. Strangwood, and A. Peyton "Overview of non-destructive evaluation of steel microstructures using multi frequency electromagnetic sensors", *Ironmaking and Steelmaking*, vol. 38, 2011.

[89] C.L. Davis, M. Papaelias, M. Strangwood, and A. Peyton, "Measurement of phase transformation in steels using electromagnetic sensors", *Ironmaking and Steel Making*, vol. 29, pp. 469-476, 2002.

[90] L. Zhou, “Non-Destructive Characterisation of Steel Microstructures Using Electromagnetic Sensors”, PhD thesis, University of Birmingham, p.238, 2015.

[91] J. Shen, L.Zhou,W.Jacobs,P.Hunt and C. Davis, **“**Real-time in-line steel microstructure control through magnetic properties using an EM sensor”, *Journal of Magnetism and Magnetic Materials*, Volume 490, 165504,2019.

[92] S.E. Krüger, M. Lord, and J.P. Mochalin, "Laser ultrasonic thickness measurements of very thick walls at high temperatures," *In Proceedings of AIN conference*, vol. 820, p.240-247, 2006.

[93] V.F. Hernandez, "Pulsed-electromagnet EMAT for high temperature applications," Ph.D. Thesis, The University of Warwick, 2011.

[94] K.S. Ho, D.R. Billson, and D.A. Hutchins, "Ultrasonic Lamb wave tomography using scanned EMATs and wavelet processing," *Non-destructive Testing and Evaluation*, vol. 22, no. 1, p. 19-34, 2007.

[95] G.S.Frankel, "Pitting Corrosion of Metals: A Review of the Critical Factors", ECS - The Electrochemical Society Journal of The Electrochemical Society, Volume 145, Number 6 *J. Electrochem. Soc.* 145 2186,1998.

[96] Q. Bai, Y. Bai, and W. Ruan, Flexible Pipes: Advances in Pipes and Pipelines, ISBN: 978-1-119-04126-9 ,2017.

[97] W. Luo, and J.L. Rose, "Guided wave thickness measurement with EMATs", *Insight*, 45 (11) 1–5, 2003.

[98] J. Johnson, K. Kim, S. Zhang, D. Wu, and X. Jiang, "High temperature acoustic emission sensing tests using a Yttrium calcium oxyborate sensor", *IEEE Transactions on Ultrasonics, Ferroelectrics, and Frequency Control*, vol. 61, no. 5, p. 805-814, 2014.

[99] E. Baziw, "Real-time seismic signal enhancement utilizing a hybrid Rao-Blackwellized particle filter and hidden Markov model filter," *IEEE Geoscience and Remote Sensing Letter*, vol. 2, no. 4, p. 418-422, 2005.

[100] M.F. Ali1, D.N.K. Jayakody, Y.A. Chursin, S. Afes, and S. Dmitry, "Recent Advances and Future Directions on Underwater Wireless Communications",27, pages1379–1412 ,2020.

[101] A. Palmeiro, M. Martin, I. Crowther, and M. Rhodes, "Underwater radio frequency communications", *In: proceedings of OCEANS, IEEE*, pp 1–8,2011.

[102] C. Gussen, P. Diniz, M. Campos, W.A. Martins, F.M. Costa, and J.N. Gois, "A survey of underwater wireless communication technologies", *J Commun Inf Sys*, 31(1):242–255,2016.

[103] M. J. Kaiser & S. Narra, "U.S. Gulf of Mexico pipeline activity statistics, trends and correlations",Pages 1-22,https://doi.org/10.1080/17445302.2018.1472517,2018.

[104] A.A. Cai, X. Qing, Z.N. Chen, B.K. Lok," Performance Assessment of Printed RFID Reader", Institute for Infocomm Research, Singapore. 117674 (2) , DOI: 10.1109/APS.2007.4395490,2007.

[105] Sensing and Monitoring Technologies for Mines and Hazardous Areas Monitoring and Prediction Technologies, Book ,2016.

[106] I. Vasilescu, D.K. Kotay, L.D. Rus, M. Dunbabin, and I.P. Corke, "Data Collection, Storage, and Retrieval with an Underwater Sensor Network", *In Proceedings of the 3rd international conference on Embedded networked sensor systems*, page154-165.https://doi.org/10.1145/1098918.1098936, 2005.

[107] M. Ho, S. El-Borgi, D. Patil and G. Song, "Inspection and monitoring systems subsea pipelines: A review paper", *Sage Journals*.Vol.19(2)606-645, https://doi.org/10.1177/1475921719837718,2020.

[108] A. Kumar, D. Parkash, and M.V. Kartikeyan, "Planer antennas for passive UHF RFID tag", *Progress in Electromagnetics Research B*, Vol.19, pp. 305-327,2010.

[109] G. Benelli, and A. Pozebon, "RFID Under Water: Technical Issues and Applications", DOI:10.5772/53934,2-13.

[110] S. Pais, and J.A. Symonds, "Data Storage on a RFID Tag for a Distributed System", *International Journal of UbiComp*, 2(2),doi: 10.5121/iju.2011.2203,2011.

[111] https://www.atlasrfidstore.com/rfid-insider/active-rfid-vs-passive-rfid/(accessed on 06 May 2020).

[112] K. Ahsan, S. Hanifa, and P. Kingston, "RFID Applications: An Introductory and Exploratory Study", *International Journal of Computer Science Issues*, Vol. 7, Issue 1, No. 3, 2010.

[113] D. Henrici, A. Kabzeva, T. Fleuren, and P. Müller, "Data Storage in RFID Systems", *Radio Frequency Identification Fundamentals and Applications Bringing Research to Practice*, Cristina Turcu (Ed.), ISBN: 978-953-7619-73-2, doi:10.5772/8002,2010.

[114] P.D. Chichi, and P. Kaur, "RFID technology and its applications: A review", *International Journal of Electronics, Communications & Instrumentation Engineering Research and Development(IJECIERD)*, ISSN 2249-684X, Vol.2, Issue 3, 109-120,2012.

[115] A.O. Ali, M.A. Aiyeoribe, and O.O. Lucky, "The Radio Frequency Identification Principles and Technical Impacts in Industrial Sectors", *AR Journal of Engineering and Technology,* Vol.1: Issue:1, ISSN Print: 2708-5155 | ISSN Online: 2708-5163, 2020.

[116] E. F. Terman, Radio Engineers Handbook. McGraw Hill, pages 785 – 786,1943.

[117] Y. Meiller, and S. Bureau, "Logistics Projects: How to Assess the Right System? The Case of RFID Solutions in Healthcare", *Americas Conference on Information Systems (AMCIS), Proceedings, AMCIS Proceedings*,547,2009.

[118] M.K. Htwe, M.M.Z. Htun, and M.H. Tun, “Design and Implementation of Bank Locker Security System Based On Fingerprint Sensing Circuit and RFID Reader”, *International journal of scientific & technology research*, Vol.4, Issue 07, ISSN 2277-8616 6, 2015.

[119] R. Parks, W. Yao, and C. Chu, “RFID Privacy Concerns: A Conceptual Analysis in the Healthcare Sector”, *In Proceedings of the 15th Americas Conference on Information Systems (AMCIS)*,06-09 ,2009.

[120] G. Benelli, A. Pozzebon, and G. Raguseo, “An RFID based system for the underwater tracking of pebbles on artificial coarse beaches”, *Sensor Technologies and Applications*, doi:10.1109/SENSORCOMM.52,2009.

[121] G. Benelli, D. Bertoni, and G. Sarti, “An analysis on the use of LF RFID for the tracking of different typologies of pebbles on beaches”, *IEEE International Conference on RFID-Technologies and Applications*, doi: 10.1109/RFID-TA.2011.6068673, 2011.

[122] A. Melski, L. Thoroe, T. Caus, and M. Schumann, “Beyond EPC – Insights from multiple RFID case studies on the storage of additional data on tag”, *International Conference on wireless Algorithms, Systems and Applications*, 281- 286 ,2007.

[123] P.Y. Luh, and Y. L. Chang, “Measurement of effective reading distance of UHF RFID passive Tags”, *Modern Mechanical Engineering*, 03(03), doi:10.4236/mme.2013.33016,2013.

[124] N .Sathappan, O.M. Tokhi, L. Penaluna, Z. Zhao , F .Duan, G .Shirkoohi, and A. Kaur, Development of an MFL Coil Sensor for Testing Pipes in Extreme Temperature Conditions, *Sensors*, Vol. 21 ,Issue 9 , doi:10.3390/s21093033,2021.

[125] M. L. Haas, and J.R. Miller, “Transforming heterogeneous data with database middleware: Beyond integration”, *Bulletin of the IEEE Computer Society Technical Committee on Data engineering*, 1-6 ,1997.

[126] (welding journal 2015 chuck hellier power generation mistras group,Inc Princeton junction NJNDT resource center/ www.nde.ed.org)/(accessed on 14 April 2022).

[127] (https://www.materialsperformance.com/articles/coating-linings/2021/03/researchers-say-corrosion-contributed-to-florida-sewage-spill)/(accessed on 09 February 2020).

[128] C`andid Reig, Mar´ıa-Dolores Cubells-Beltr´an and Diego Ram´ırez Mu˜noz, “Magnetic Field Sensors Based on Giant Magnetoresistance(GMR) Technology: Applications in Electrical Current Sensing”, *Sensors*, 9, 7919-7942; doi:10.3390/s91007919, 2009.

[129] https://news.energysage.com/saltwater-batteries-what-you-need-to-know/(accessed on 07 July 2021).

[130] British Standards Institution, “BS EN ISO 9934-3:2015” ,2015.

[131] H.Dong, J.Zhao ,W.qiang Zhao, M.Si, J.Y.Liu , "Study on the thermal characteristics of crude oil pipeline during its consecutive process from shutdown to restart". *Elsevier* ,Volume 14, 1004342019,2019.

[132] S. Mao, S. Gangopadhyay, N. Amin, E. Murdock. "NiMn-pinned spin valves with high pinning T field made by ion beam sputtering". *Appl. Phys. Lett.* 1996;**69** doi: 10.1063/1.117217. [CrossRef] [Google Scholar]

[133] M. Saito, N. Hasegawa, F. Koike, H. Seki, T. Kuriyama, "PtMn single and dual spin valves with synthetic ferrimagnet pinned layers". *J. Appl. Phys.* 1999;**85** doi: 10.1063/1.369145. [CrossRef] [Google Scholar]

[134] K.M. Lenssen, D. Adelerhof, H. Gassen, Kuiper A.E., Somers G.H., van Zon J.B.A. Robust giant magnetoresistance sensors. *Sens. Actuators A Phys.* 2000; **85**:1–8. doi: 10.1016/S0924-4247(00)00342-3. [CrossRef] [Google Scholar]

[135] C.Giebeler , Adelerhof D.J., Kuiper A.E.T., van Zon J.B.A., Oelgeschläger D., Schulz G. Robust GMR sensors for angle detection and rotation speed sensing. *Sens. Actuators A Phys.* 2001;**91**: 16–20. doi: 10.1016/S0924-4247(01)00510-6. [CrossRef] [Google Scholar]

[136] Prakash S., Pentek K. Reliability of PtMn-based spin valves. *IEEE Trans. Magn.* 2001;**37**: 1123–1131. doi: 10.1109/20.920487. [CrossRef] [Google Scholar]

[137] W. Yin, A.J. Peyton, M. Strangwood, C.L. Davis, "Exploring the relationship between ferrite fraction and morphology and the electromagnetic properties of steel"; Material Science; *Vol 51*. part5, 2004, p379-383.

[138] https://www.first4magnets.com/tech-centre-i61/information-and-articles-i70/alnico-magnet-information-i84/(accessed on 09 November 2019).

[139] TDK, 2013, Ferrites and Accessories, EPCOS, Data book

[140] https://www.homemade-circuits.com/lc-oscillator-circuit-how-it-works/(accessed on 04 September 2019).

[141] Paula Fraga-Lamas, Diego Noceda-Davila, Tiago M. Fernández-Caramés, Manuel A. Díaz-Bouza and Miguel Vilar-Montesinos, "Smart Pipe System for a Shipyard 4.0 Smart pipe system for a shipyard"

[142] https://www.offshore-mag.com/business-briefs/equipment engineering/article/16790839/seatooth-system-assesses-subsea-equipment-performance

Appendix A

Hall effect sensors are magnetic field-activated devices that work on the hall effect principle, which states that when a conductor or semiconductor with current flowing in one direction is applied perpendicular to a magnetic field, a voltage can be measured in a direction perpendicular to the current path [13]. The voltage induced in this way is known as the hall voltage.

The magnetostrictive sensor (MsS) is based on the magnetostrictive (Joule) and inverse magnetostrictive (Villari) concepts [24]. The magnetostrictive effect describes a slight change in the physical dimension or structure of ferromagnetic materials induced by an externally applied magnetic field.

Magnets lose their magnetic properties at high temperatures, and if they exceed the curie temperature, they lose their magnetic properties forever [139]. The magnetism decreases by a certain percentage with each rise in temperature, and this is known as the irreversible temperature coefficient [76].

Appendix B

The coding for the plot has been developed in Matlab as below for **Figure 4.33**.

```
z1=0.09388+55.718i;
z2=0.10714+111.43i;
z3=0.13365+222.87i;
z4=0.16016+334.31i;
z5=0.18666+445.75i;
z6=0.2137+557.18i;
z7=0.21361+559.53i;
z8=0.18702+447.62i;
z9=0.16042+335.72i;
z10=0.13382+223.81i;
z11=0.10723+111.90i;
z12=0.093932+55.95i;
```

```
real_z1=real(z1);
imag_z1=imag(z1);
real_z2=real(z2);
imag_z2=imag(z2);
real_z3=real(z3);
imag_z3=imag(z3);
real_z4=real(z4);
imag_z4=imag(z4);
real_z5=real(z5);
imag_z5=imag(z5);
real_z6=real(z6);
imag_z6=imag(z6);
real_z7=real(z7);
imag_z7=imag(z7);
real_z8=real(z8);
imag_z8=imag(z8);
real_z9=real(z9);
imag_z9=imag(z9);
real_z10=real(z10);
imag_z10=imag(z10);
real_z11=real(z11);
imag_z11=imag(z11);
real_z12=real(z12);
imag_z12=imag(z12);
plot(real_z1,imag_z1,'*',real_z2,imag_z2,'*',real_z3,imag_z3,'*',real_z4,imag_z4,'*',
real_z5,imag_z5,'*',real_z6,imag_z6,'*',real_z7,imag_z7,'*',real_z8,imag_z8,'*',
real_z9,imag_z9,'*',real_z10,imag_z10,'*',real_z11,imag_z11,'*',real_z12,imag_z12,'*');
```